THESIS

HIGH EFFICIENCY AIR DELIVERY SYSTEM FOR SOLID OXIDE FUEL CELL POWER GENERATION

Submitted by

Lars Jared-Brian Mitchel

Department of Mechanical Engineering

In partial fulfillment of the requirements

For the Degree of Master of Science

Colorado State University

Fort Collins, Colorado

Fall 2024

Master's Committee:

Advisor: Todd M. Bandhauer

Bret C. Windom
James Cale

ABSTRACT

HIGH EFFICIENCY AIR DELIVERY SYSTEM FOR SOLID OXIDE FUEL CELL POWER GENERATION

Distributed power generation systems can be used in the electric grid to reduce peak loads, raise power quality, and reduce/eliminate transmission losses. One distributed energy system with distinct advantages is a Solid Oxide Fuel Cell (SOFC) integrated with an Internal Combustion Engine (ICE) which has the capability to operate at electric efficiencies as high as 70%. This research aimed to produce and test a high efficiency air delivery system that supports the SOFC-ICE to generate power on the scale of 80 kW. The air balance of plant (BOP) system utilized low speed scroll-type rotating compressors and brazed plate and frame heat exchangers for efficient preheating. The scroll compressors were modeled in GT-Suite and the remaining air BOP system was modeled with thermodynamic and heat transfer equations. Then testing was done on the compressors and heat exchangers to validate the model so that the air BOP system performance could be accurately predicted within a range of conditions. Both compressors were run from a range of 20 g/s to 60 g/s with the heat through the system being swept from 100°C to 600°C which yielded compressor efficiencies over 60% and heat exchanger effectiveness over 0.90. The validated model was then used to make predictions about system performance at on and off-design conditions.

ACKNOWLEDGEMENTS

The first person I would like to acknowledge is Dr. Todd Bandhauer. Thank you for taking a chance on a kid who wanted to do grad school and run at the same time. Getting to work in this lab and experience engineering has had helped me see where my passion lies and given me a future I am genuinely excited about. Getting to talk to you about the industry and work through what I want to be is something I could not have figured out without you. I am also thankful for our discussions about sports when we had the time and hearing about some stories from back in the day in Ames.

Secondly, I could have never achieved or even begun to think about taking on graduate school without the help of Shane Garland. Thank you for all the help, Shane. Teaching me how to cut piping/insulation, code thermodynamic equations, and run full scale testing on a system I still do not completely understand how it works. Getting to work under you the past couple of years has taught me so much applicable knowledge that I would have never gained without your assistance. Your impact on me as an engineer cannot be overstated. Additionally, I loved getting to work for someone who also ran in college and will miss our talks about race results after we got through all the engineering topics for the day. Keep grinding on the bike!

I would also like to extend my thanks to everyone at the REACH Co-Lab. Getting to work with you all has been such a pleasure and made the sometimes-mundane parts of grad school not an issue for me. Fred and Victor, getting to sit by you two during this journey has been some of the most fun memories I have from college. I really enjoyed what I did at the Powerhouse, but I always knew that even if work got arduous, I had you two to keep my spirits up, complain about random topics, or joke around about working for the federal government.

Victor, I cannot wait for you to show me around Puerto Rico and Fred, I hope you know that I will be meeting you in Alaska sometime to catch some big fish.

I could not recognize my time here at CSU without thanking my teammates on the Cross Country and Track & Field team. Getting to compete here was a dream come true and I was right that I would meet some lifelong friends through running for the rams, although the jury is still out on Bedard (or "Brian" as I know him). Coach Hart, thank you for always believing in me and for going out of your way to make memories for this team. To Kelly, thank you for thinking the same way I do, coming up with nicknames for runners, and buying me lunch a couple times. Jacob, thank you for welcoming me to this team and supporting me throughout my entire time here. Brock, thanks for running slower to keep me company and for laughing at all the movie quotes. I never regretted a single mile I got to run with you, and I am glad that now we can just surf together instead. Mooney, thanks for being my older brother in Fort Collins. You have taught me so much about perseverance, competitive-spirit, and why I run. Getting to spend thousands of miles with you (some of which I was ahead so don't forget about those) was my favorite part about running at this school. Also, take care of Chris for me. I know he is a lot, but I truly believe in him.

I would also like to acknowledge my family. Mom and Dad, thank you for raising such a curious kid, who just had to know how everything worked. Those questions that you let me ask led me here and I really believe I can make a difference now. Mom thanks for the unconditional love while documenting the whole journey through photos, videos, and nice long hugs. Dad thank you for the dawn patrol sessions, answering my questions (usually) with thoughtful intent, and all the hiya hiyas, I never missed a single one. Finn, thanks for being the best hype man I have ever seen. Your constant joy and energy for life is contagious and can't think of a time we

didn’t spend smiling together. Alekos, thank you for being such a competitor and comedian at the same time. The competitive drive that we share is something I’ll always cherish, the mutual intent of wanting to beat each other no matter the cost raised a pretty good runner. Elin, thank you for being someone I could always lean on. Whenever I talk to you about my thoughts or feelings, I always felt very heard and understood. Keep climbing rocks dude!

To everyone mentioned above, I hope you all know how much your support meant to me throughout this process. I never felt alone during this trek, and it is due to the relationships I have with all of you and the people that you are. So, one last grand thank you to you all and you can now refer to me as Lars “Master of ME” Mitchel.

TABLE OF CONTENTS

LIST OF TABLES

LIST OF FIGURES

NOMENCLATURE

Variable	Description	Units
A	Area of heat exchanger	m^2
C	Heat capacity rate	kJ s^{-1} K^{-1}
D	Diameter	m
f	Friction factor	-
g	Acceleration due to gravity	m s^{-2}
$\bar{h}$	Convective heat transfer coefficient	W K^{-1} m^{-2}
h	Enthalpy	kJ kg^{-1}
k	Conductive heat transfer coefficient	W K^{-1} m^{-1}
L	Length of heat exchanger	m
$\dot{m}$	Mass flow rate of air	kg s^{-1}
NTU	Number of transfer units	-
$\overline{Nu}$	Nusselt number	-
P	Pressure	kPa
Pr	Prandtl number	-
q	Heat transferred	kW
Re	Reynolds number	-
u	Air velocity	m s^{-1}
U	Overall heat transfer coefficient	W K^{-1} m^{-1}
W	Work	kW

Ra	Rayleigh number	-
Cp	Specific heat	kJ kg^{-1} K^{-1}
T	Temperature	°C
$\dot{Q}$	Heat transfer	kJ
t	Thickness	m
R	Universal gas constant	kJ kg^{-1} K^{-1}
Greek Symbols		
Δ	Difference	-
η	Efficiency	%
ε	Effectiveness	-
μ	Dynamic viscosity	Pa s
ρ	Density	kg m^{-3}
Subscripts		
air	Air in the system	
C	Compressor	
ch	Channel	
h	Hydraulic	
HX	Heat exchanger	
s	Isentropic process	
w	Wall	
r	Ratio	

CHAPTER 1. INTRODUCTION

1.1 Background

The energy grid is changing drastically as electrical generation moves away from fossil fuels and towards renewable technologies. A consequence of this shift is a more transient energy demand that can benefit greatly from localized power generation. Figure 1-1 shows what is called the "duck curve" which is a way to illustrate how renewable energy has a peak generation in the middle of the day that could lead to overgeneration but has much less power generation during nightly hours when the demand is much higher.

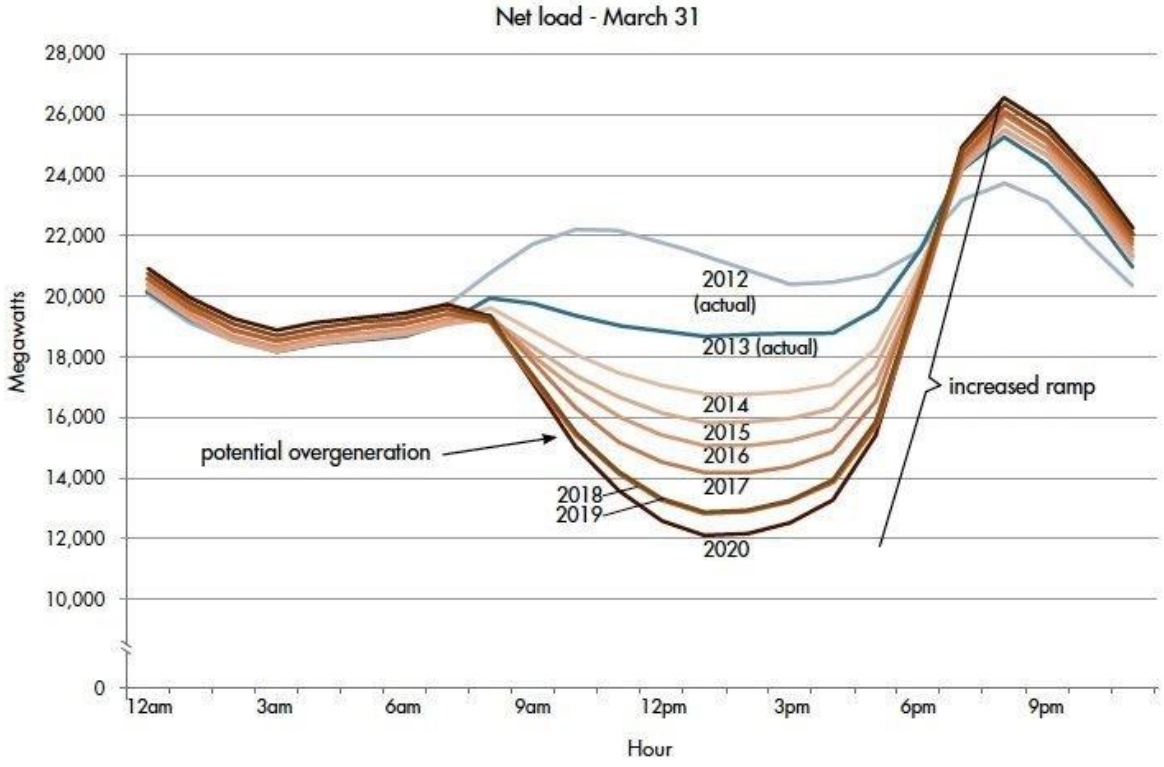

Figure 1-1. The "Duck Curve" shows areas of potential over and under generation [71].

Some of the most promising systems to complement renewable energy are SOFC based. These SOFC systems on their own offer low emissions, long-term stability, and are relatively low

cost [1–4]. However, by having SOFCs combined with an ICE, high efficiencies at a much lower complexity can be achieved [5–9]. This makes the SOFC-ICE system an ideal candidate for distributed power generation to complement renewable energy.

The SOFC-ICE system developed for this research is novel because of many factors that are yet to be addressed in research: it is metal supported rather than ceramic, the stacks are pressurized for higher efficiency, an intermediate temperature is used rather than high temperature, an ICE is present to boost the power output, and the full-scale system was constructed to be ran harmoniously rather than having certain aspects of the project predicted. Figure 1-2 gives an overview of the main system and operating principles.

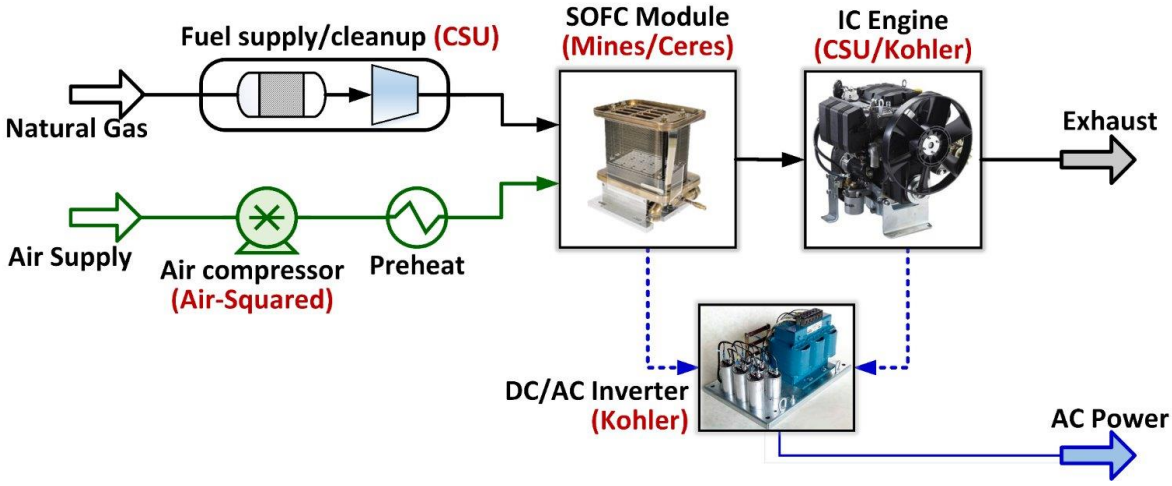

Figure 1-2. Full facility key components diagram.

For this system to reach a high efficiency, precise BOP systems were used to support the operation of both the SOFC and ICE. An efficient way of delivering the air for this system is utilizing scroll-type rotating machinery to meet the air flow, temperature, and pressure requirements. Several facets of scroll compressors are advantageous: high efficiency, small number of moving parts, and low level of noises/vibrations [10]. For preheating the air in the system, brazed plate and frame heat exchangers were utilized to maximize efficiency on getting the air up to temperature for the SOFC. The scroll compressors and heat exchangers represent the

major components of the air BOP system and are vital components of the overall system to be efficient.

For the SOFC-ICE system to operate effectively, certain temperature and pressure requirements of the air being fed to the SOFC are necessary to maintain. The air at the inlet of the SOFC stacks needs to be above a temperature of 540°C for efficient electrical-chemical power generation to take place. The pressure of this air must be at least 300 kPa. This elevated pressure is what allows for this system to be at lower temperatures. By having the air pressurized in the SOFC, more power can be generated due to the increase in fuel density.

The air BOP system that is required to achieve these conditions is made up of four key components: two scroll-type compressors, and two unique brazed plate and frame heat exchangers (the Anode Tail Gas Cooler and Air Preheater). First, air at 101 kPa is fed into the two scroll compressors where it is pressurized to 320 kPa to then be fed into the HXs for heating. In the ATG Cooler, tail gas from the SOFC is used for primary heating of the air. Following this, the air is then heated more in the AP where air exhaust from the SOFC is on the opposing side. This HX does the final heating of the air such that at the inlet of the SOFC, the air is conditioned to meet the requirements of 540°C and 300kPa for optimal SOFC-ICE power generation.

1.2 Research Objectives

The power generation method of SOFCs is not a newer technology, but having a full scale SOFC-ICE system is something yet to be done. The main objective of this research is to explore the most efficient way to deliver the air for the SOFC at this full-scale system. In previous research, these systems have had different requirements depending on the integration of gas turbines (GT) or ICEs, pressurizing the stacks, and the temperature that is needed for operation. Therefore, the air BOP of this SOFC-ICE system has a novel makeup and has unique parameters that are

attempting to be hit. The targets for the compressor modeling were to evaluate the most efficient way to run the compressors at three unique mass flow rates: 33 g/s, 66 g/s, and 100 g/s. These three points were selected because they represent 1/3, 2/3, and 3/3 of full flow. If the SOFC were to operate at part load it would still be necessary to operate the compressors and maximize efficiency thus these points were selected. The compressor model was also run on a mass flow sweep of 20% to 120% to find outlet conditions to be input into the thermodynamic model. The targets for the thermodynamic model were to evaluate the inlet temperature and pressure at the SOFC stacks. The temperature requirement is 540°C and the pressure cutoff is 300 kPa, respectively. A sweep of the air mass flow rate from 20% to 120% of full flow was done in the thermodynamic model to see if/when these conditions are met. If either the temperature or pressure requirements were not met or overshot, analysis was done to see how much extra power will be needed to meet these conditions and how this affects the efficiency of the overall system. These goals were set to explore the best way of maximizing efficiency on the air delivery for SOFC-ICE to keep the system efficient and a competitive power generation method.

1.3 Thesis Organization

The following sections outline the motivation for this research, the system performance modeling, test facility, and results/discussion for this air BOP study. Chapter two provides a review of the research already conducted on SOFC hybrid systems and reveals the gap that is being filled with this project. Chapter three describes the two models generated: one through GT-Suite to help analyze performance of the scroll compressors and the other through Engineering Equation Solver to describe the heat transfer taking place in the system/two HEXs being utilized. Chapter four outlines the test facility that was constructed to test the compressors, heat exchangers, and overall air BOP system. Chapter five will show the results of the study: validation on both models that

were generated, the test results from the physical project, and a discussion on the conditions of the air for the SOFC. Chapter six will draw the final conclusions from this study on the power that was saved from optimization, any additional power needed for additional preheating, and recommendations for future research.

CHAPTER 2. LITERATURE REVIEW

To understand how this power generation is possible and why it is being pursued in this manner, it is necessary to review the primary components and competitor systems for fuel cell-based power generation. The following sections will review: SOFC power generation, integrated systems with SOFC focusing on GT coupling, and principles behind an ICE hybrid system. Each of these systems carries unique challenges and require specific BOP for the power generation to take place.

2.1 SOFC Power Generation

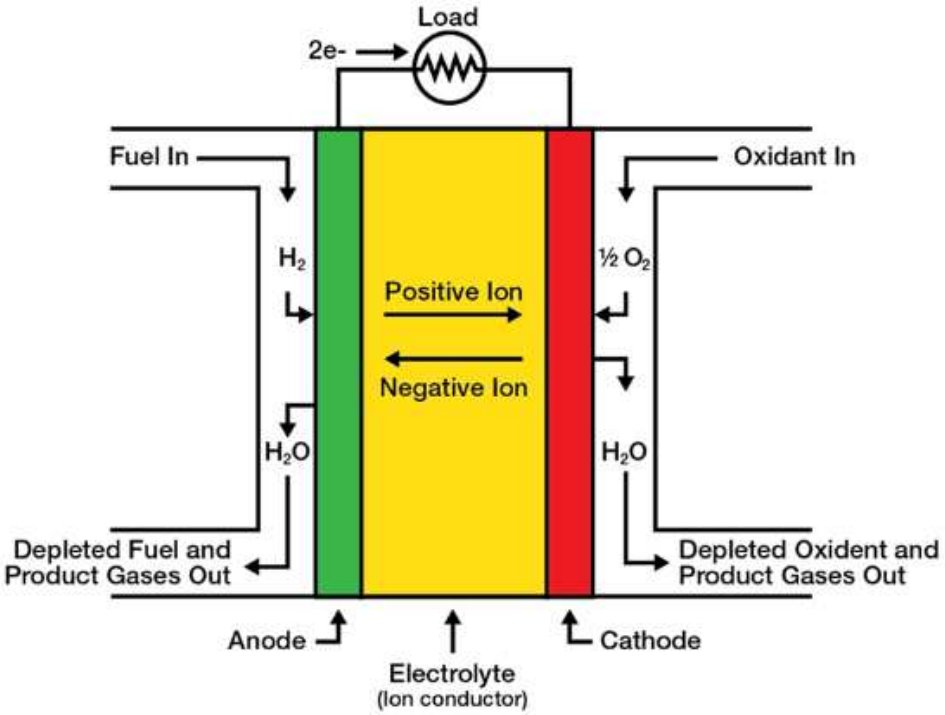

Figure 2-3. The working principle of how solid oxide fuel cells operate [72].

SOFCs are a much more sustainable approach towards localized power generation in contrast to typical engine gensets that burns natural gas at an efficiency around 35% [4]. A ceramic structure encloses a solid electrolyte between a cathode and an anode [11,12]. An oxidant, most

commonly air, is delivered to the cathode while on the anode side fuel is delivered. This allows for the fuel and air to diffuse to the electrolyte. Once the reactions take place, free electrons are created that can be transported using an external circuit to produce electricity [4,11,12].

SOFCs carry many advantages over other power generation methods. SOFC power generation has much more fuel flexibility being able to use hydrogen, natural gas, and biogas for the anode side while PEMs require hydrogen to operate [13]. SOFCs have the potential to operate at extremely high efficiency, with one study operating at an electrical efficiency of 85% [4]. However, high efficiency is achieved by increasing the number of stacks which drastically increases the cost and, as a result, applications have operated at around 60% for this class of power generation (100kW-200kW). This efficiency is far higher than that of coal power plants while also minimizing the environmental footprint since SOFCs usually use natural gas and do not combust the fuel but rather utilize a chemical reaction to produce power [4].

2.2 SOFC Hybrid Systems

Power generation methods through SOFCs can have a boosted efficiency if they are integrated to take advantage of the exhaust gases [14]. Researchers have focused on two primary hybrid systems: Gas Turbine hybrid systems and Internal Combustion Engine hybrid systems [15,16]. The following sections review these higher efficiency systems.

2.2.1 SOFC GT Hybrid Systems

Although SOFCs operate at a high efficiency, this can be increased significantly when these systems take advantage of the high operating temperatures [14]. One of the most researched systems is combining a SOFC with a GT for additional power generation, resulting in higher efficiency.

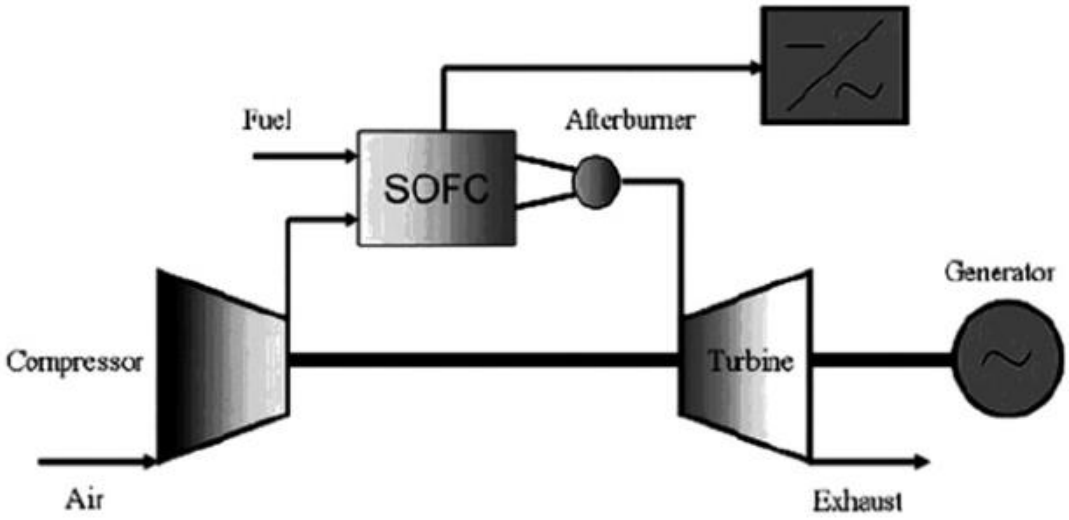

Figure 2-4. SOFC combined with a Gas Turbine power generation system diagram [73].

The working principle is a Brayton Cycle for a direct thermal coupling scheme. High temperature, non-utilized fuel from the SOFC product gases is used as fuel and combusted. This high temperature gas is then used to operate a GT which creates AC power and drives the air compressor [14].

Few studies have constructed the proposed system; however, Mitsubishi Heavy Industries created a 200kW SOFC-GT system that operated at an electrical efficiency of 52% [17]. While models of the system have shown efficiencies exceeding 70%, this demonstration proved to have physical and control issues that were not considered while modeling [18].

A primary issue is that these systems have is a high efficiency when operating at the design point, but once that condition is not met, the system's efficiency degrades quickly [19]. This reveals a big issue with the GT system because the design point window is quite narrow. GTs have a narrow operating window due to the operating maps of the compressors and this causes a SOFC-GT system to fall off the design point frequently [19]. Having the GT coupled to the compressor, as shown in Figure 2-4, means that the condition of the GT directly affects the compressor and thus the intake of air to the SOFC [20]. Since the SOFC-GT system has a very precise operating

range, this requires intricate control of the system [20]. Not only does this cause trouble within the actual running of the system but also inevitably leads to higher costs.

2.2.2 SOFC Engine Hybrid Systems

The complications of GT systems have lead researchers toward alternative ways of utilizing SOFC tail-gas. A proposed system that does this effectively is replacing the GT with a more flexible ICE. The air supply for the ICE can be decoupled while still combusting the gases from the SOFC. This process shows promise to be a more robust solution for sustainable power generation [21].

Primary challenges of GT-based systems have been how much the efficiency decreases away from their design points. Studies agree that to achieve above a 60% electrical efficiency, the turbomachinery *must* be operating at its design point [5]. ICE integration allows for simpler control, and its decoupled nature allows for the BOP to stay at design conditions even if the ICE is not operating at a steady state level. This decoupling is actualized by bypassing the fuel directly into the ICE [5]. The supplementary nature of the ICE increases the system's efficient load range which means much better response to the SOFC as well as demanding turbomachinery parts that have stricter bounds of operation [5].

Additionally, SOFC-ICE systems only require the BOP to maintain sufficient pressure in the system instead of a GT method that relies on power being generated by the BOP to generate electrical output [5]. This allows the system to be less sensitive to ambient temperature and pressure variations [5]. By having an ICE integration method, the overall system construction and operation becomes more robust and feasible for higher scale adoption.

2.2.3 Current Research in SOFC Hybrid Systems

Many different integration methods have been attempted to maximize the technology behind SOFC-ICE systems. Research has been done on the air compression intake for SOFCs, lower temperature stacks in tandem with higher temperature stacks, and improving robustness of the system [22–24].

Williams et al. [25] brought in a different stance on the air compression process being separated into two stages to lower the air inlet temperature of the heat exchangers and better improve the use of the exhaust heat from the SOFC. However, the inlet air temperature would also decrease which, in the incorrect setting, will lower the efficiency of the SOFC [25]. This research concluded on finding the process to not be applicable in an industry setting.

Chiang et al. [26] proposed a system that included having lower temperature SOFC before a higher temperature SOFC. By having these SOFCs in series, the simulation concluded that this combined efficiency would be slightly higher than having a sole elevated temperature SOFC. Having a more diverse temperature range readily available means the preheating process would only be required at the lower temperature end and the exhaust off the lower temperature SOFC can be used to lower costs of preheat for the higher temperature stack. Although this process seems promising, the addition of an entire new stack (for a very marginal gain in efficiency) is not cost effective when this is scaled to a larger application [26]. The cost would not be competitive enough for this power generation method to be adopted.

Halinen et al. [1] constructed a SOFC that was tested with simulated grid activity to see the effectiveness of the power production. Using only a high temperature SOFC for power generation, they were able to achieve a 60% DC electrical efficiency [1]. When the experiment shifted towards AC and a more grid-oriented application, the electrical efficiency dropped to 43%.

These results were found with a standalone SOFC, meaning without any supporting BOP. In application, the BOP would draw down these efficiency points, but the study did not account for this [27,28]. The conclusions of the study reveal the underestimation of the conversion difficulties, such as electrical efficiencies of trivial things like long wiring connections, and poor response with demand [1].

Towards a complete and operational SOFC-ICE system, few systems have been researched [7]. System feasibility analysis has been done to show that for a 100kW class system, an ICE integration was superior to a GT option [8]. Choi et al. [7] conducted experimental testing within a simulation setup to research the design points that are most ideal for this system. By creating a simulation of the SOFC, they tested the actual performance of an ICE as if it were in a complete system. They effectively tested the performance and production of an SOFC-ICE system and achieved a 59.0% electrical efficiency, a 15.5% improvement on the standalone SOFC system they had modeled [7]. This system used a lower temperature stack, but the lack of pressurizing the SOFC could be the reason why the efficiency failed to reach 70% electrical efficiency.

The concerns holding back the adoption of SOFC-ICE systems are the lack of robustness and excessive costs [29]. To combat this, Reddy et al. [8] reviewed the development of metal supported SOFCs being applicable for intermediate temperature stacks. The standard choice of ceramic is due to the high temperatures in SOFCs [30,31]. Although the ceramic can withstand the heat, it is a brittle material that makes SOFCs sensitive to vibrations [8,30,31]. Pressurized SOFCs can operate at intermediate temperatures to allow for a metal supported option. This not only brings down cost, but also makes the SOFCs much more robust [8]. By utilizing an intermediate temperature SOFC, costs will be saved on fuel preheat, heat exchangers, and BOP because heat intensive material selection is no longer required [32–35].

2.2.4 Gaps in Current Research in SOFC Hybrid Systems

This research strives to fill the gaps remaining in physical testing of the SOFC-ICE system at scale. SOFCs show great promise in their ability for power generation at a lower cost and could be a great complement to other renewable energy technologies [5,36–38]. Studies have constructed SOFC-GT power generation systems that boost the efficiency of those SOFCs, however, the high cost and intense complexity of these systems keep them from being more feasible for larger scale application [20,39,40]. Researchers have shifted toward SOFC-ICE systems with the relevant research shown in Table 2-1. Hailen et al. [1], Choi et al. [7], Chuahy et al. [5], and Burbank et al. [19] developed simulations of these SOFC-ICE systems, finding that the ICE method resulted in a more practical and higher efficiency system than previously researched. Williams et al. [25], Reddy et al. [8], and Kumar et al. [21] demonstrated the capabilities behind pressurized SOFCs, and the ability of them to bring the temperature and cost down. Araki et al. [17] validated working efficiencies with these intermediate temperature SOFCs. Despite the advances of each of these studies, a system which combines the research behind lower temperature, pressurized SOFCs with ICEs has yet to be developed and is the basis of this study [2,3,6,9,41].

Table 2-1. Comparison table of previous research to this study.

	Metal Supported	**Pressurized**	**Intermediate Temperature**	**ICE Hybrid**	**Full Scale Lab Study**
Williams et al.		X			
Reddy et al.	X	X	X		
Araki et al.			X	X	
Halinen et al.				X	
Choi et al.		X		X	
Chuahy et al.				X	X
Burbank et al.				X	
Kumar et al.		X	X		
This study	X	X	X	X	X

This research strives to develop this SOFC-ICE system, fully at scale. Once the system is constructed and ready for testing, it is hypothesized that testing will show a 70% electrical efficiency in a power generation system that can enable cleaner energy solutions for the future.

2.3 Air BOP Systems for SOFC-ICE Power Generation

2.3.1 Scroll Compressors

Scroll compressors are being utilized in the system for the following reasons: they are low noise and low vibration, they are able to operate oil free, the control of this type of device is much simpler, and they can achieve high efficiencies at the PR and air mass flow rate needed in this system which high efficiency air compression helps boost the overall system efficiency by a non-trivial margin [42–44].

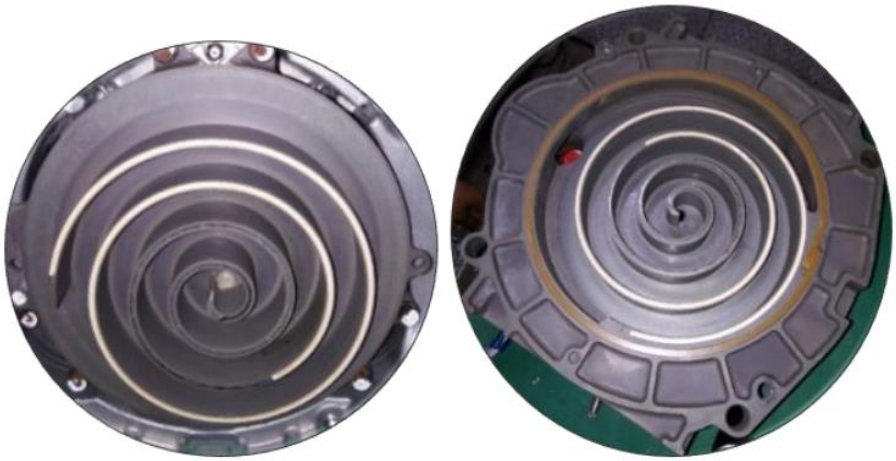

Figure 2-5. Picture of what the scrolls within a scroll compressor with the orbiting scroll on the left and stationary scroll on the right [74].

Scroll compressors can operate with low noise and vibration due to the much lower speeds that they need to be run at when compared to other types of compressors [45,46]. This allows for a more robust system and less noise pollution in the location of this power generation set [47,48]. Scroll compressors can operate without the use of oil. This makes it such that there is no leakage from the compressor of oil into the air stream which could easily foul the SOFC and lead to damage of the sensitive stacks [49]. The control on scroll compressors has high operational reliability, which makes control over the system simpler, efficient, and predictable [45,46,50]. Along with this, these scroll devices can attain a much higher efficiency than their centrifugal counterparts,

which would operate at an efficiency range around 45-50% [49]. By having these scroll compressors operating at high efficiency, 55-65%, it saves on energy used for the air delivery which is the most energy intensive part of the overall system and therefore boosts the efficiency greatly [51–53]. Combining these characteristics, literature has shown that scroll compressors have potential as a solution for air BOP of SOFC systems [54].

2.3.2 Brazed Plate and Frame Heat Exchangers

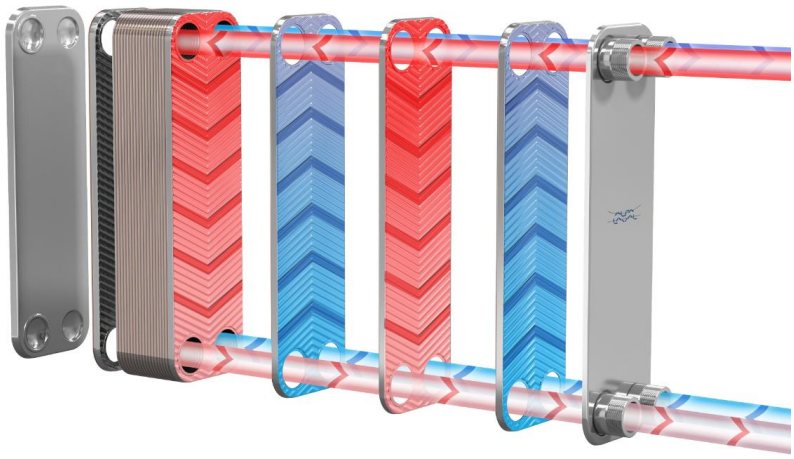

Figure 2-6. Brazed plate and frame exploded view [75].

Other critical components include the heat exchangers which maintain inlet stack temperature [55–57]. To reduce cost and keep the system efficiency high, compact brazed plate and frame heat exchangers (BPHEs) are implemented to utilize the heat of the exhaust air for inlet air preheating [58,59]. Brazed plate and frame heat exchangers are being used because of the higher operating temperatures which would melt the gaskets on other types of heat exchangers [60]. These types of heat exchangers can achieve high effectiveness to allow for ample preheating for the SOFC requirements [61].

2.4 Research Needs for an Air BOP System to Support SOFC-ICE Power Generation

Literature has shown that when it comes to full-scale facility models being made for the air delivery system, research is lacking. Having a model of the air compression, preheating, and delivery is something that is novel to research and vital to any SOFC power generation system. In tandem with this, having a full system constructed is another gap within research. By having a full system to run through testing, the full system model is not only able to be made but also to be validated such that the modeling could be used to find areas of improvement. By having this unique full system model validated, the operation of the compressors can be optimized to save power at different levels of flow to maximize efficiency. Also, this model can be used to see when conditions are or are not met during different cases of flow when running the system at part up to full load. All this helps to find ways to save power and run the compressors in an optimal fashion such that they still hit the flow and pressure requirements but while consuming the least amount of power and ensure heat and pressure requirements for SOFC functionality are met.

2.5 Focus of Current Investigation

It is shown through the previous literature that optimization on the air BOP system can help boost the overall efficiency of SOFC-ICE power generation system.

By having the compressors operating to pressurize the air to the SOFC, the energy density of the system is increased and therefore, less SOFC is needed. The SOFC represents the most expensive part of the system make-up, and by pressurizing this air into the chemical process within the SOFC, a much more cost-effective system is made due to not needing as large of a SOFC to still hit the power output necessary.

The lower temperature that is being explored within this research is driven by a materials decision. By running at a lower temperature, 600°C versus high temperature systems that operate at 1000°C, the air BOP system can be constructed of metal rather than ceramic. The lower temperature is driven more so by a materials choice as the metal supports are more robust along with a more cost-effective approach to generating this system.

For this system to reach a high efficiency, precise BOP systems are used to support the operation of both the SOFC and ICE. An efficient way of delivering the air for this system is utilizing scroll-type rotating machinery to meet the air flow, temperature, and pressure requirements. Several facets of scroll compressors are advantageous: high efficiency, small number of moving parts, and low level of noises/vibrations [10,62]. Also, due to the lower speeds of these devices variable speed drives can be used to have high performance control and more controllability because of the wide operating range when compared to centrifugal compressors [62]. Combining these characteristics, literature has shown that scroll compressors have potential as a solution for air BOP of SOFC systems [54]. Characterizing the compressor in different flow capacities is essential for maximizing the compressor and system efficiency [63]. Other critical components include the heat exchangers which maintain inlet stack temperature. To keep the system efficiency high, compact brazed plate and frame heat exchangers were implemented to utilize the heat of the exhaust air for inlet air preheating [58,59].

The purpose of this research is to model and experimentally confirm the proposed air BOP systems function at relevant scale which will help prove the full system can achieve the target efficiency [64,65]. This was done through first modeling the thermodynamic system within the air BOP. This includes generating a model within GT-Suite of the scroll compressors to see characteristics of the flow through the compressors at different speeds, pressures, and

temperatures. The second part of this was thermodynamic modeling within the heat exchangers and throughout the system to ensure pressure and temperature of the air when it is delivered to the SOFC stacks.

From the compressor modeling, the optimal way of running the compressors was studied. By having a system model of the amount of pressure drop and flow needed, the operation of the compressors can be varied and find the minimum amount of power needed to meet these requirements. With the compressor optimization done, the thermodynamic model was used to see if the temperature and pressure of the air, through the rest of the system, is adequate for the SOFC to generate power from. A turn down analysis was included in this study because of the importance for electrical generation systems to operate at lower loads. Typical gensets have turn down capability so that they can adjust based on load and react accordingly for a stable electrical grid. Modeling this SOFC-ICE at lower loads is necessary to ensure that it would be a robust solution for electrical power generation. Finally, these conclusions were then put into context of the overall system to see how the overall efficiency was affected. Either positively by optimizing the compressor operation and/or negatively by seeing if the air is not at the appropriate temperature or pressure which would then need additional compression or heating.

CHAPTER 3. SYSTEM PERFORMANCE MODELING

This chapter will describe the process used to generate both the thermodynamic model that is used to predict the performance of the heat exchangers and overall system that deliveries the air, and the compressor model that is used to predict the performance of the compressors at different speeds, flow rates, and pressure ratios. In addition to predicting the performance of the compressors, this model is also used to see the temperature of the outlet air to then be uploaded to the thermodynamic model to see if the final conditions of the air at the SOFC inlet are met for both temperature and pressure.

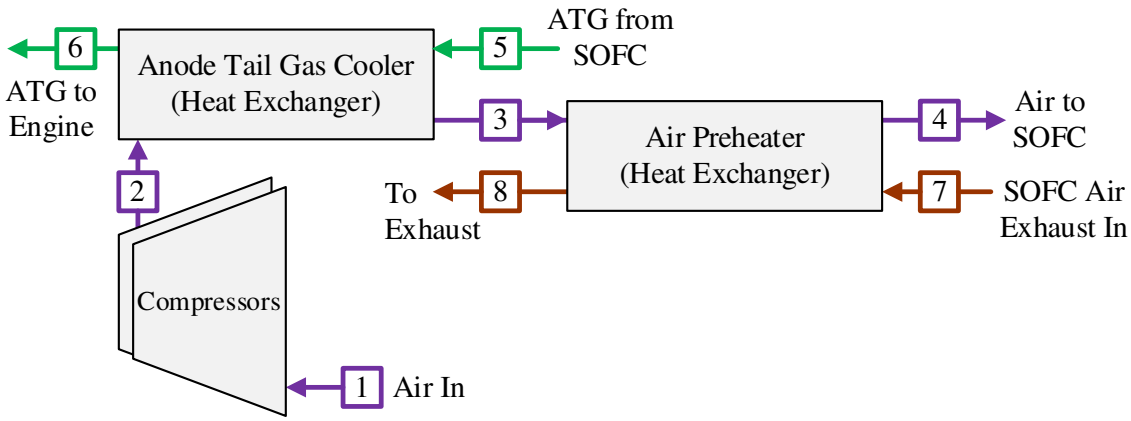

Figure 3-7. The different flow paths and interaction between fluids within the HEXs.

3.1 Thermodynamic System Modeling

This section will describe the thermodynamic modeling approach that was used to characterize both the Anode Tail Gas (ATG) Cooler and Air Preheater (AP) brazed plate and frame heat exchangers. It will also discuss the methods used to predict how the rest of the system (piping,

elbows, unions, etc.) affected the air flow and the conditions the air would be in by the time it is delivered to the SOFC.

The thermodynamic system model was written in EES. This software was used because it has preloaded tables to pull data on the conditions of fluids at certain pressures, temperatures, and states. Along with that, the software runs as a solver that can be utilized to find unknowns about fluids if given an appropriate number of equations and variables to solve.

3.1.1 Thermodynamic System Setup

The system model is based on the interaction between four key components shown in Figure 3-7: two heat exchangers (the ATG Cooler and the AP) and two scroll-type air compressors. The compressors first take in air that has been pressurized to 101 kPa and compresses it further (depending on the PR needed to be tested but it can range from 1.5-3.3). After these two compressors, the air is then fed firstly into the ATG Cooler where anode tail gas exhaust off the SOFC is counter-flowed as the hot fluid within this HX to raise the temperature of the air. After this initial heating, the air is then fed into the AP where the final preheating takes place. The hot fluid in this HX is air exhaust from the SOFC, flowing in a countercurrent method for maximum effectiveness. Upon leaving the AP, the air is then fed into the SOFC. There are also components that are present in the system, like elbows, that are accounted for in the full system model.

3.1.2 System Assumptions

Table 3-2. Assumptions made within the model for different fluid flows and initial temperatures and pressures.

	Temperature [°C]		Mass Flow [g/s]		Pressure [kPa]	
	Condition	Value	Condition	Value	Condition	Value
Anode Tail Gas	T[5] constant	276	Varies same scale as comp. flow	35	P[5] constant	294
SOFC Exhaust	T[7] constant	612	90% of comp. flow	90	P[7] constant	309
Ambient Air	T[1] constant	25	Matches comp. flow	100	P[1] constant	101

***value for when air flow into compressor is at 100 g/s**

The thermodynamic model was written in EES and utilizes 9 assumptions to solve equations that predict the behavior of the equipment as shown in Table 3-2. Models for the SOFC stacks are out of the scope of this research and therefore assumptions were made about the temperature and pressure requirements of the inlet and outlet gases. Specification sheets were provided by the stack manufacturer and the target temperatures and pressures are based off these values. The target inlet air temperature and pressure are 540°C and 300 kPa, respectively, while the outlet conditions are 612°C and 290 kPa. These values are set by the chemical makeup of the SOFC for highest efficiency performance and the operation of the stacks [48,66]. One of the key aspects of this model was to vary the mass flow rate of the air from 20% to 120% (where 100 g/s is the full flow or 100%). The ATG varies on the same scale as the air, meaning if the air flow is at 50% then the ATG flow would also be at 50% (i.e., 17.5 g/s). The variance in flow rate was performed to simulate startup conditions, but also part-load operation. The last major assumptions are the air temperature and pressure at the compressor inlet. The assumed inlet air temperature is 25°C and 101 kPa because that is the standard temperature and pressure of ambient air at sea level.

The following equations step through the thermodynamic relations that are used to solve for a state point within one of the heat exchangers. Appendix A gives more details and shows a sample calculation of this process being solved.

The first step is setting the mass flow rates that are being used in the solver. With this information and data from the GT-Suite model, the work by the compressor can be calculated and the corresponding temperatures.

$$\dot{m}_{exhaust} = 0.9 \times \dot{m}_{air} \tag{3.1}$$

$$\dot{W}_2 = \dot{m}_{air}(h_2 - h_1) \tag{3.2}$$

$$\dot{W}_{iso} = R \times T_{k1} \times \ln(\frac{P_2}{P_1}) \times \dot{m}_{air} \tag{3.3}$$

Being able to find the outlet enthalpy from knowing the power consumed (from the GT-Suite model), next the model starts to set parameters for the fluids inside the HXs and for the fluids that are flowing on either side of the plates. This is done through the following equations for both the air and tail gas in the ATG Cooler.

$$D_e = 2 \times Pressing_{depth} \tag{3.4}$$

$$\mu_{air} = \nu_{air} \times \rho_{air} \tag{3.5}$$

$$\mu_{tg} = \nu_{tg} \times \rho_{tg} \tag{3.6}$$

$$Re_{ch_{air}} = \frac{\dot{m}_{air} \times D_e}{Pressing_{depth}\,(w)\,\mu_{air}} \tag{3.7}$$

$$Re_{ch_{tg}} = \frac{\dot{m}_{tg} \times D_e}{Pressing_{depth}\,(w)\,\mu_{tg}} \tag{3.8}$$

$$C_{air} = \dot{m}_{air}(Cp_{air}) \tag{3.9}$$

$$C_{tg} = \dot{m}_{tg}(Cp_{tg}) \tag{3.10}$$

$$C_r = \frac{\min[C_{air}, C_{tg}]}{\max [C_{air}, C_{tg}]} \tag{3.11}$$

With the specific heat capacity, ratio, and Reynolds numbers calculated for both fluids, the maximum possible heat transfer can be found. Upon this solving, and knowing the inlet temperatures of both fluids, the final outlet temperatures can be found using the equations below.

$$q_{max} = C_{min}(T[15] - T[2]) \tag{3.12}$$

$$NTU = \frac{U \times ATG_{area}}{C_{min}} \tag{3.13}$$

$$\varepsilon = \frac{1 - \exp[-NTU(1 - C_r)]}{1 - C_r \exp[-NTU(1 - C_r)]} \tag{3.14}$$

$$q = q_{max} \times \varepsilon \tag{3.15}$$

$$q = C_{air}(T[3] - T[13]) \tag{3.16}$$

$$q = C_{tg}(T[5] - T[16]) \tag{3.17}$$

Additionally, cooling within the compressors needed to be accounted for as it impacts the air outlet temperature. Based off the air mass flow rate the following equations were developed to correct the outlet air enthalpy which is used with pressure to determine the outlet air temperature.

$$h_{2_{actual}} = h_2 + \frac{\dot{Q}_{cool}}{\dot{m}_{air}} \tag{3.18}$$

$$\dot{Q}_{cool} = \dot{m}_{glycol}(Cp_{glycol})(T_{out} - T_{in}) \tag{3.19}$$

The cooling heat duty, $\dot{Q}_{cool}$, was determined experimentally by measuring the temperature change, $T_{out} - T_{in}$, and flow rate of the coolant, $\dot{m}_{glycol}$, to find the specific heat, Cp_{glycol} , and calculate the value as shown in equation (3.19). Standard flow rate for the coolant through one

compressor is 3 L min-1 and a typical temperature difference would be around 7°C which yields a cooling duty of about 1.5 kW. Holding cooling duty at a constant value is a valid assumption because the flow rate of the glycol through the compressors is held constant at that 3 L min^{-1} value and thus yields a reasonably constant amount of cooling seen in the compressors. Tabel 3-3 shows how steady that cooling load in the compressor stayed at different air mass flow rates.

Table 3-3. Cooling load in the compressor at different air mass flow rates.

Air Mass Flow Rate (g/s)	Cooling Load (kW)	Glycol Flow (LPM)
33.3	1.48	3
66.6	1.51	3
100	1.53	3

3.1.3 Heat Exchanger Modeling

Next, the two HXs are modeled with the Effectiveness-NTU method. This method allows testing a range of inlet temperatures to calculate outlet temperatures under a variety of conditions. Since the two HXs have already been designed and installed the amount of heat transfer area is set this allows for outlet temperatures to be calculated. The most uncertain variable within these calculations is characterizing the convective heat transfer coefficient, $\overline{h}$. For the characterization of $\overline{h}$, the Wenzhe and Pega correlation was chosen to calculate the Nusselt number and, subsequently, the heat transfer coefficient [67,68].

$$\overline{Nu} = \frac{\bar{h} D_{\mathrm{h}}}{k} = 0.2913 (Re_{\mathrm{ch}}^{0.702}) \left(\frac{\mu}{\mu_{\mathrm{w}}}\right)^{0.14} (Pr^{\frac{1}{3}}) \tag{3.20}$$

The convective and conductive heat transfer coefficients are used to calculate the overall heat transfer coefficient where h_{f1} and h_{f2} represent the convective coefficient for the fluids which could be air or anode tail gas, t_{plate} is the thickness of the plate, and k_{plate} is the conductive coefficient for the plate.

$$U = \frac{1}{\left[\frac{1}{h_{f1}} + \frac{t_{plate}}{k_{plate}} + \frac{1}{h_{f2}}\right]} \tag{3.21}$$

Solving this equation solves for the overall heat transfer coefficient, U, which is mainly dependent on the convective coefficients.

The epsilon-NTU method can then be used to find the amount of heat transfer that would take place within the HEXs based on equations (3.22), (3.23), and (3.24).

$$NTU = \frac{UA}{C_{min}} \tag{3.22}$$

For counterflow HEXs where $C_r < 1$

$$\varepsilon = \frac{1 - \exp\left[-NTU(1 - C_r)\right]}{1 - C_r \exp\left[-NTU(1 - C_r)\right]} \tag{3.23}$$

$$\varepsilon = \frac{q}{q_{max}} \tag{3.24}$$

The HEXs were each discretized four times, where at each interval properties were recalculated based on the outlet temperature of the previous section.

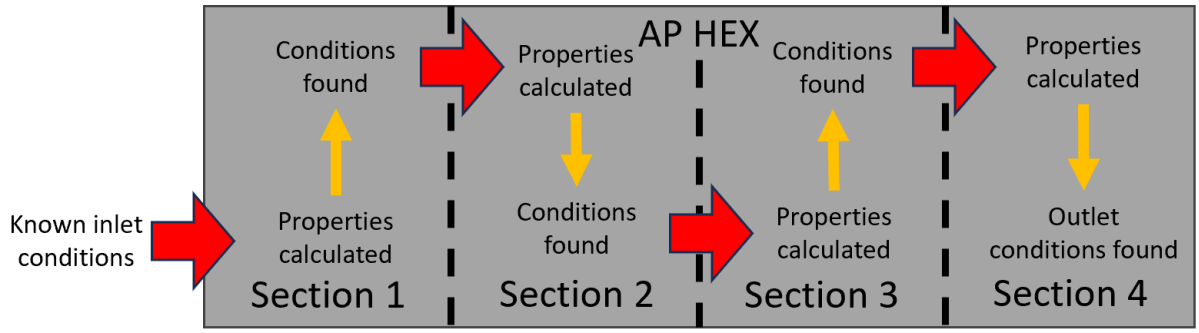

Figure 3-8. Discretization of the heat exchangers working principle.

3.1.4 Pressure Drop Modeling

The pressure drop through the system was calculated to ensure the air being delivered to the SOFC would meet specifications. The pipe diameters, pipe lengths, elbows, and constrictions were used to calculate the pressure drop through the piping network and Equation (3.25) shows the Neagu correlation which was used to calculate the pressure drop seen in the heat exchangers [69].

$$\Delta P_{\mathrm{ch}} = 4f\frac{\rho u^2}{2}\left(\frac{L}{D_{\mathrm{h}}}\right) \tag{3.25}$$

This calculation is to allow for seeing the different pressure drops that will be occurring during different levels of operation: anywhere between 20%-120% of full flow, varying levels of PR out of the compressors, and different amounts of heating in the air system.

To calculate the pressure drop in the piping the frictional factor of the system needs to be set based on the Reynolds number from the air flow, this calculation is shown in equation (3.26).

$$f_g = \frac{64}{Re_{air}} \tag{3.26}$$

Following this, major losses need to be accounted for based on this factor from equation (3.26), the amount of pipe length in the system, the pipe diameter that the air is flowing through, and the air speed within the facility.

$$h_{L_{major}} = f_g\left(\frac{P_{length}}{P_d}\right)\left(\frac{u_{air}^2}{2g}\right) \tag{3.27}$$

With the major losses calculated, the minor losses also need to be added for a full system model to be representative of the actual system. To do this, k-values for the components in the system were researched and applied so that the minor losses could be calculated utilizing the following equations.

$$K_{tot} = (N_e k_e) + (N_u k_u) + (N_{bv} k_{bv}) + (N_t k_t) + (N_{cv} k_{cv}) \tag{3.28}$$

$$h_{L_{minor}} = K_{tot}(\frac{u_{air}^2}{2g}) \tag{3.29}$$

Both the major and minor losses are then used to find the overall pressure drop that will occur in the system. This modeling is vital for predicting accurate delivery pressure to the SOFC stacks and allows for seeing this prediction not only at standard conditions but also part-load, start-up, and off design conditions as well. The following equation represents the overall system pressure drop that will occur.

$$\Delta P_{pipes} = (h_{L_{minor}} + h_{L_{major}}) \tag{3.30}$$

Table 3-4 shows how the total pressure drop seen in the system is broken down between the drop seen in the heat exchangers, major losses, and minor losses throughout the system.

Table 3-4. Total pressure drop seen in the system broken down by components.

Mass Flow	Pressure Drop (kPa)				Total ΔP
Rate (g/s)	ATG Cooler	AP	Major Losses	Minor Losses	(kPa)
33.3	0.62	0.65	1.17	0.08	2.52
66.6	2.63	2.77	5.02	0.36	10.78
100	4.79	5.03	9.12	0.66	19.60

3.1.5 Heat Loss Modeling

Additionally, equations were developed to account for heat loss that occurs throughout the system before data is collected. Thermocouples are placed throughout for temperature readings, but these readings are not directly at the outlets/inlets of the heat exchangers or other components. Therefore, there is a certain amount of heat loss that occurs before the air reaches the thermocouples and the temperature is reported. A thermal circuit was developed to calculate this

heat loss. The thermal circuit included resistance from convection from the fluid temperature to the inner wall of the pipe, resistance from conduction through the pipe, resistance from conduction through the insulation, and resistance from natural convection acting around the insulation. The Dittus-Boelter [70] equation was used to find the convective heat transfer coefficient for the flow inside the pipe (for cooling in this application).

$$\overline{Nu} = \frac{\bar{h}D_{\mathrm{h}}}{k} = 0.023Re^{\frac{4}{5}}Pr^{0.3} \tag{3.31}$$

Then, the Churchill and Chu [70] equation was used to solve for the heat transfer coefficient that is representative of the natural convection that is taking place on the outside of the insulation.

$$\overline{Nu} = \frac{\bar{h}D_{\mathrm{h}}}{k} = \left[0.6 + \frac{0.387Ra_{\mathrm{D}}^{\frac{1}{6}}}{\left(1 + \frac{0.559^{\frac{9}{16}}}{Pr}\right)^{\frac{8}{27}}}\right]^2 \tag{3.32}$$

These heat loss equations can now accurately predict temperatures for the air throughout the system at varying conditions. These predictions can account for scenarios in which the ambient temperature is changing, the air mass flow rate is varying, and the amount of piping that the air is traveling through before analysis needs to take place.

The following table shows an example of what a section of piping might have as attributes that are accounted for in both the pressure drop and heat loss calculations

Table 3-5. Specifications of the sections of piping in the system.

Pipe length	Pipe diameter	# of elbows	# of tees	# of unions	Insulation thickness
123”	2.067”	5	3	2	1”
75”	2.067”	6	2	1	1”
259”	2.067”	4	2	2	1”

3.2 Compressor Modeling

The software being used for the compressor modeling is GT-Suite. This industry standard modeling software can accurately generate performance maps and predict performance of turbomachinery devices based on test data. This software was selected because it can make accurate predictions at those variable conditions that need to be tested for at that start-up, part load, and full load conditions.

The data collected on the respective compressors needs to have corrected conditions to account for varying parameters such as: ambient temperature, humidity, and ambient pressure. Data is collected at steady state points during testing as the raw values. These tests last two minutes and the average value during this test is taken as the value for the respective parameter, i.e. temperature or pressure. With these values collected the corrected values for speed and mass flow rate can be found using the following equations. To do this, a corrected air mass flow rate is used to generate the model of the compressor along with corrected speed to account for the parameters that were discussed earlier. The following two equations outline the process to take the raw speed and air mass flow rate and convert them into their corrected values.

$$Corrected\ Speed = \frac{Speed}{\sqrt{\frac{T}{T_{ref}}}} \tag{3.33}$$

$$\dot{m}_{corrected} = \dot{m}\sqrt{\frac{T}{T_{ref}}\left[\frac{P}{P_{ref}}\right]^{-1}} \tag{3.34}$$

Where the variable *speed* is the shaft speed of the compressors, in RPM and the variables T and P are the inlet temperature and pressure of the air going into the compressors. With these equations utilized it ensures that the compressor model generated is not dependent on the inlet flow conditions needing to be the same but is instead corrected for these differences.

Once the compressor model is generated, this can work in tandem with the thermodynamic system model to accurately predict the inlet conditions of the air at the inlet to the SOFC stacks with the power to do this prediction while varying to conditions that are not actually tested.

The following table lists out the tests that were conducted for the generation of the compressor model. Equations 3.33 and 3.34 were then used to correct the data that was collected, and it was uploaded to the software to generate models of the compressors.

Table 3-6. Testing matrix for the data that was inputted to generate the compressor models.

Speed	PR
430	1.5, 2.0, 2.5, 3.0, 3.3
130	1.5, 2.0, 2.5, 3.0, 3.3
1900	1.5, 2.0, 2.5, 3.0, 3.3

Blind testing was then conducted at different speeds than the ones used to generate the model. Then the model was run at these same speeds to see how accurately the model was predicting the performance of the compressors and the results were compared. These results are shown in further detail in chapter 5.

3.3 Turn-Down Analysis

This model was generated to be able to run a turn-down analysis on the system. This was necessary because at different varying conditions the SOFC stacks will still need air flow at the appropriate conditions to be operational. Three cases were selected to explore the most efficient way to operate the compressors while still meeting SOFC temperature and pressure requirements. The turn down ratio is set at 3:1 and therefore flow conditions were explored at 33.3 g s^{-1}, 66.6 g s^{-1}, and 100 g s^{-1} which represents 33.3% of full flow, 66% of full flow, and 100% of full flow

respectively. At each of these conditions, the compressor model was used to do a sweep of speeds for each individual compressor to determine the optimal speed in which the mass flow condition was met but with the least power consumed. With the optimal speeds set, the outlet air conditions from this model could then be set as the inlet conditions of the thermodynamic model to then explore what the air conditions will be at the inlet of the SOFC. Figure 3-9 shows the workflow of this process.

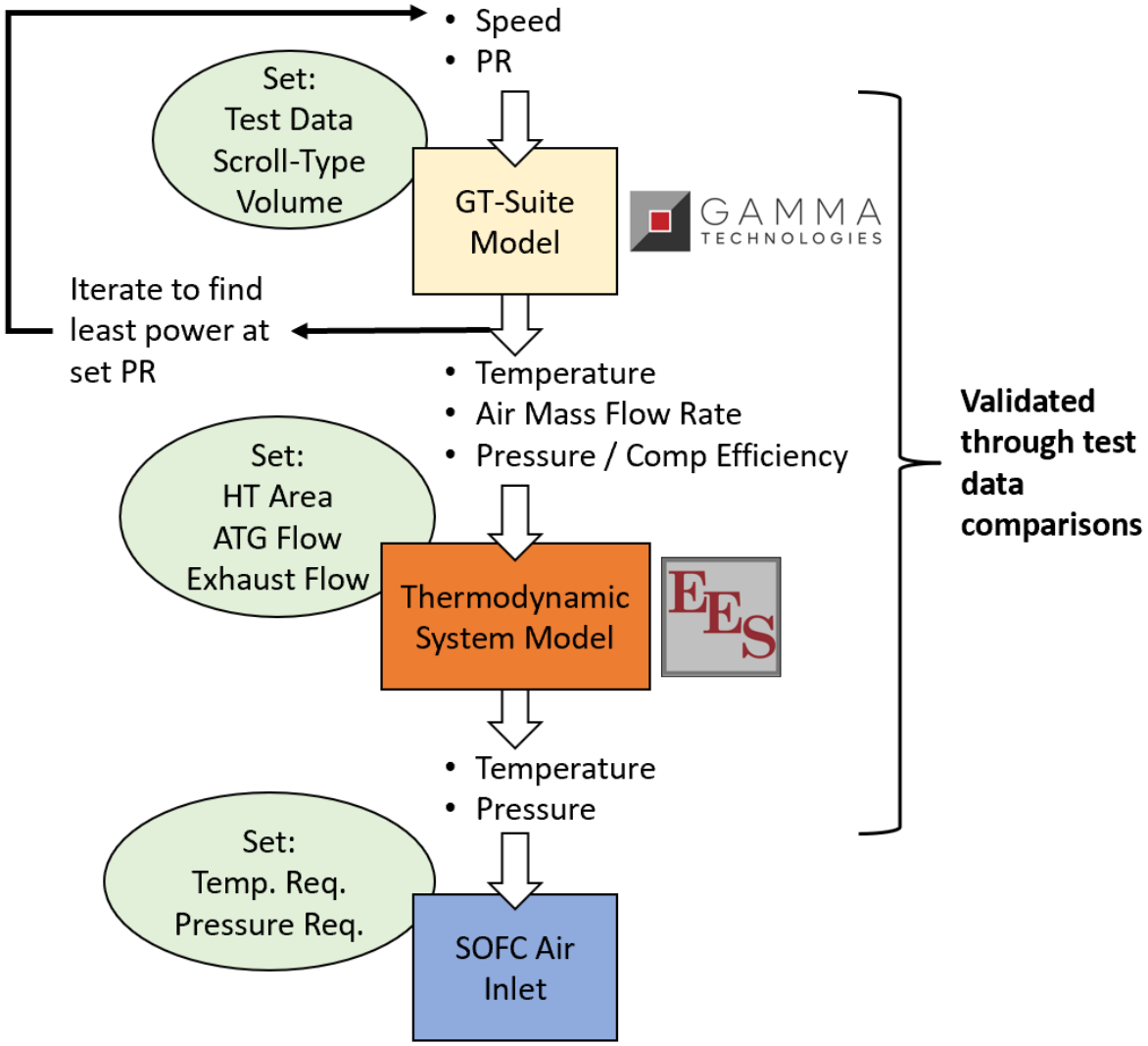

Figure 3-9. Workflow process of the modeling conducted in this study.

CHAPTER 4. TEST FACILITY

4.1 Full System Description

The test facility used during this study is part of a larger system currently under construction at Colorado State University as part of the ARPA-e INTEGRATE program to develop a >70% hybrid SOFC-ICE power generation system. The focus of this research is the modeling and testing of the components used to increase the temperature and pressure of the air supplied to the fuel cell.

The full system to generate electrical power through a SOFC-ICE system has many components. These components are necessary to deliver natural gas as the fuel to the anode side of the SOFC and air to the cathode side as well as support equipment for these processes. Natural gas is fed through a compressor and then preheated before being used in the SOFC. The SOFC does not consume all this fuel and unused tail gas is then mixed with air and combusted in the ICE for additional power generation. Both the SOFC and ICE generate DC power that is then converted into AC which is sent to the grid. On the air side, ambient air is fed into the scroll compressors, where it is pressurized to about 320 kPa. Following this, the air is sent through two different BPHEs to be preheated before the SOFC. The air exhaust from the SOFC is used to preheat the inlet air and then expanded in two expanders to recover some additional power. After this, the air is vented back to the ambient atmosphere outside the building.

The major components for the air BOP are the two scroll-type Air Squared (AS) compressors and two HXs: the ATG cooler and the AP. The expanders are not a part of this research due to manufacturing delays, thus the air BOP analysis will solely focus on the air delivery to the SOFC but not include results on the exhaust side performance.

4.2 Air BOP System Description

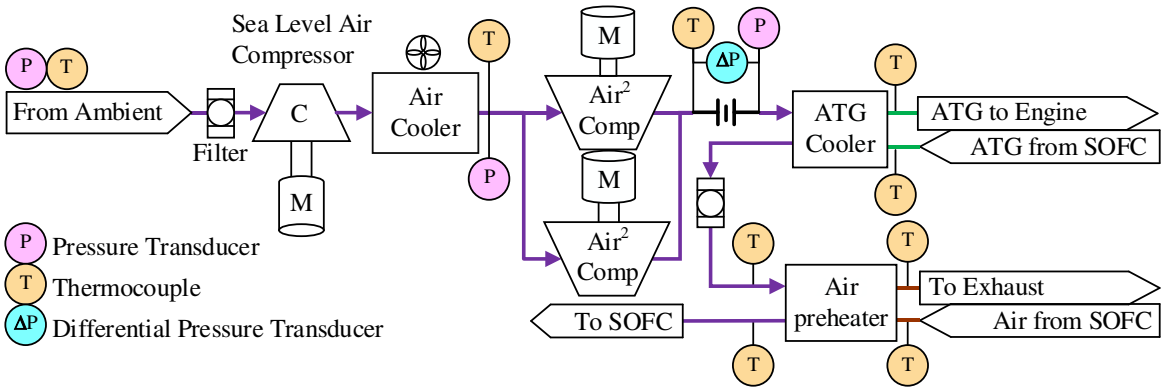

Figure 4-10. Schematic showing the air BOP system with all components and instruments.

The overall air BOP system contains more than just compressors and heat exchangers as shown in Figure 4-10. Air is taken from ambient and first put through a filter before reaching the sea-level air compressor. This compressor then compresses the air to 101 kPa, or approximately 1 atmosphere. Following this, the Air Cooler radiator heat exchanger cools the air back down closer to ambient conditions so that the air being fed into the AS compressors is at a standard pressure of 1 atmosphere and closer to a temperature that is representative of the ambient conditions. Then the AS compressors are fed in parallel to compress the air to the set PR. Following this the first BPHE is the ATG Cooler that uses the ATG to first heat up the air and then the AP does the final heating using the air exhaust from the SOFC. Throughout the system there are pressure transducers, thermocouples, and differential pressure transducers to record data on the conditions of the air throughout the system. Also seen throughout the makeup is filters to clean the air to ensure that delivery to the sensitive stacks does not foul the SOFC.

All these components make up the air BOP system to ensure that heated, pressurized, and clean air is delivered to the SOFC at the rate that is needed. More detailed specifications on these components will follow.

4.2.1 Sea Level Air Compressor

With the facility being at altitude of about 5,000 feet at Colorado State University in Fort Collins, CO the ambient pressure is around 84.4 kPa instead of a typical sea level pressure of 101 kPa. Therefore, it is necessary to have a compressor prior to our system analysis to ensure that the conditions being delivered are at that standard pressure of 101 kPa. The sea level compressor in this system is a screw compressor that is driven by a motor. A Variable Frequency Drive (VFD) device controls the speed of the device to ensure appropriate delivery. A LabView controller adjusts the VFD of this motor to make sure that the amount of air being pulled by the AS compressors is met and that the pressure seen at the intake of the AS compressors is at 101 kPa to meet standard pressure. Below in Figure 4-11 is a picture of this experimental set up of the motor that is driving the centrifugal compressor and that actual compressor. Additionally, the intake air filter is shown where ambient air is pulled into the system by the sea level air compressor to feed into the air BOP.

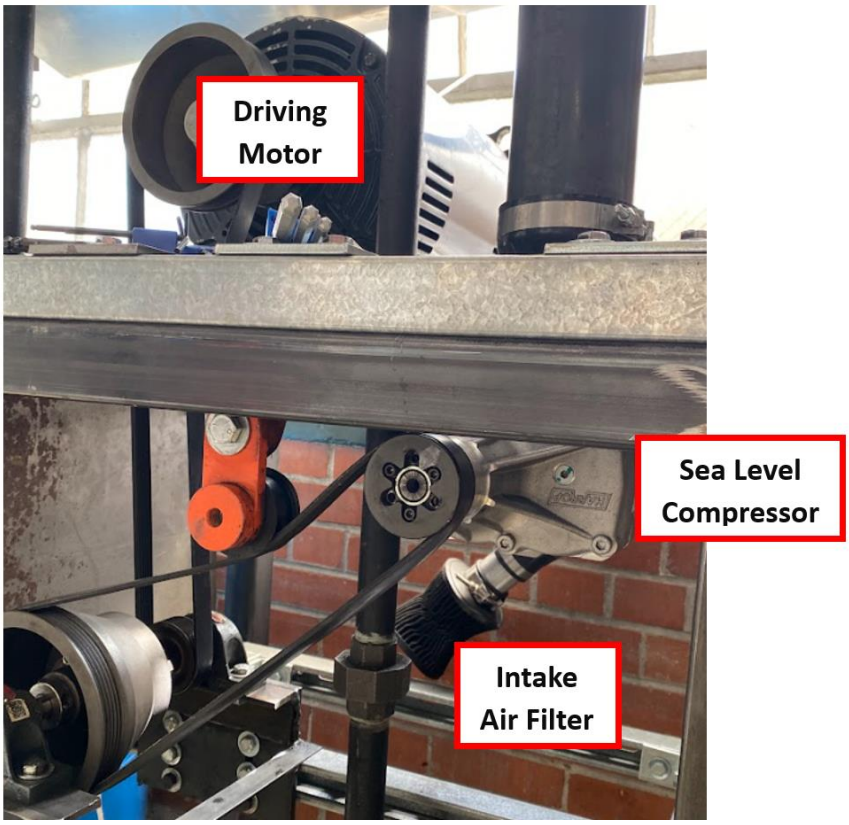

Figure 4-11. Annotated image of the sea level compressor and driving motor for the device.

4.2.2 Air Cooler

Following the initial compression from the sea level compressor, the air needs to be cooled back to ambient conditions. This is done using the Air Cooler heat exchanger in the system. The Air Cooler is a radiator type heat exchanger that has fans installed behind it to pull ambient air over the fins and cool the sea level compressed air back closer to ambient air temperature. A window directly behind the Air Cooler is opened during operation and the heat exchanger allows for ambient air to be pulled over the fins that are connected to the piping so that the air flowing through them can be cooled to the appropriate ambient temperature. Below is Figure 4-12 that shows this heat exchanger installed in the facility.

Figure 4-12. Annotated image of the Air Cooler heat exchanger.

It is important to have this heat exchanger installed because having the system feed to the AS compressors at ambient sea level conditions is the standard for research. Since the facility is not at sea level and instead altitude, it is necessary to have this pre-pressurization and cooling to meet that standard.

4.2.3 AS Scroll Compressors

The AS scroll type compressors are an essential part of the air BOP as they do the final air compression for the air to be delivered at the correct pressure to the SOFC to operate efficiently. The scroll compressors were produced by Air Squared to the specifications listed in Table 4-6 with a nominal air mass flow rate of 60 g/s and a 3.2 PR. These specifications were used in the generation of the system model in GT-Suite as set parameters from the manufacturers.

Table 4-7. Detailed specifications on the scroll compressors from Air Squared.

Scroll type compressors		
Volume ratio	2.26	
Suction volume	1633.8 cc	
Coolant fluid	Propylene Glycol	
Mass	~401 lbs (w/o coolant)	
Connection	2” NPT	
Electrical Specifications		
Nominal speed	1800 RPM	
Frequency	60 Hz	
Capacity	15 Hp	
Nominal voltage	460V AC	230V AC
Continuous rated line current	17.4 A	34.8 A

The compressors are controlled by motors that are connected to their own individual VFDs. These VFDs are connected to a LabView system that can control the speed to hit a set PR. The system also has the capability to control the compressors to a set speed, but the main controller has the speed vary to achieve the PR that is set in the system.

Scroll compressors were chosen for this application because of their high efficiency and simplicity of control. With the overall system needing to stay extremely efficient, scroll compressors higher efficiency help to achieve this. Additionally, having a more reliable control of the air flow and pressure ensures that the overall system can have steady operation which leads to higher efficiencies. These devices and respective motors are shown in Figure 4-13.

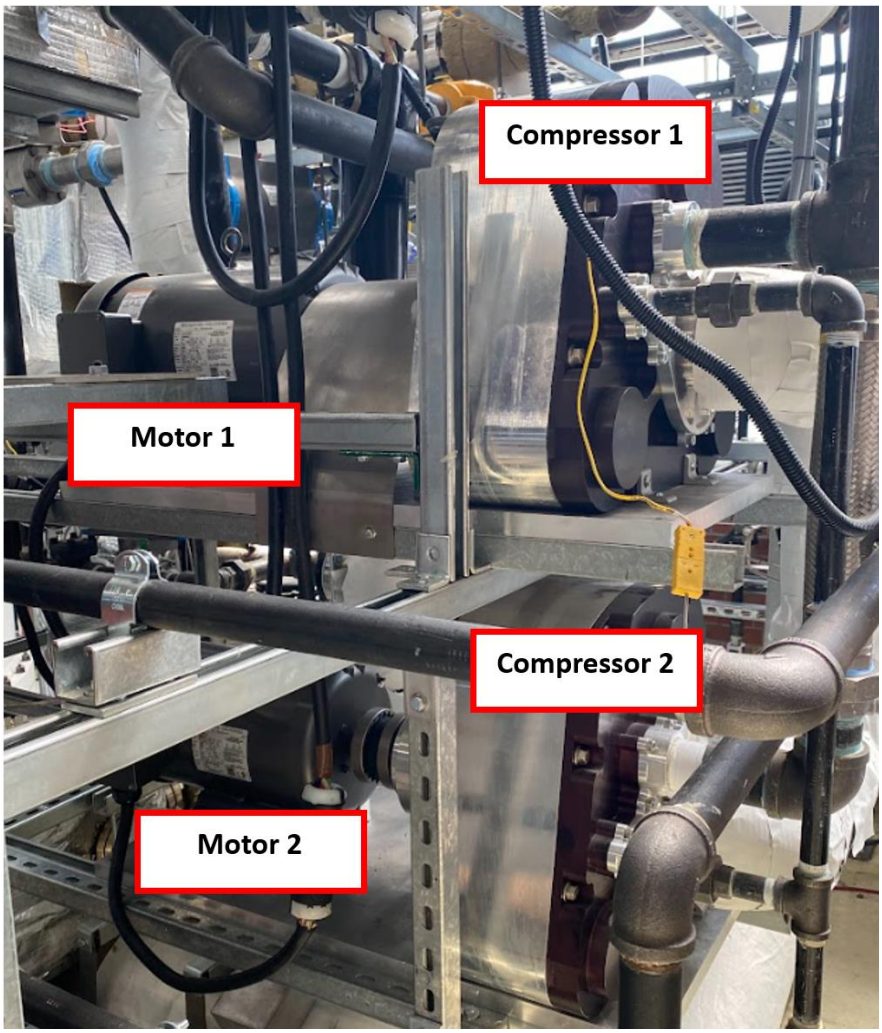

Figure 4-13. Scroll compressors and their respective motors that drive them.

4.2.4 ATG Cooler Heat Exchanger

The ATG heat exchanger does the first round of preheating the air prior to it being delivered to the SOFC. It does this by taking advantage of the hot tail gas that comes off the anode side of the SOFC. This exhaust anode tail gas leaving the stacks reaches the ATG cooler at a temperature of about 276 °C. The air, due to compression from the AS compressors, reaches this point at an already elevated temperature of about 134°C. Once both fluids have reached the ATG Cooler and flowed through their respective plates, the ATG leaves at a temperature of about 233.7°C while the air will be heated up to about 181.8 °C. This preheating gets the air up to a higher temperature so

that the following heat exchanger, the AP, can do the final preheating to get the air up to temperature for effective SOFC power generation. (The temperatures outlined in this section assume that the system is running at full load where the air mass flow rate is 100 g/s at a PR of 3.2).

The ATG Cooler is a brazed plate and frame heat exchanger and the makeup of one of these devices is broken down in Figure 4-14. Brazed connections are used because of the high operating temperatures and the known operating conditions which means that the size of these devices does not need to be variable as the amount of heat transfer that needs to take place is known.

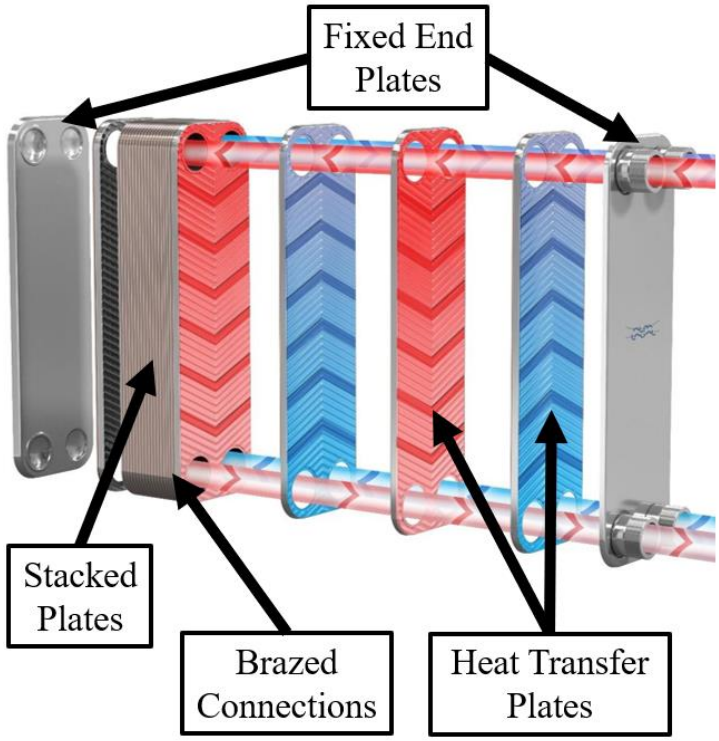

Figure 4-14. Breakdown image of brazed plate and frame heat exchanger design.

The exact specifications of the ATG Cooler are found in Table 4-7. These specifications are provided by the manufacturers of the equipment and are utilized in the thermodynamic model to solve the heat transfer equations to solve for outlet temperatures based on varying parameters such as: air mass flow rate, PR from the AS compressors, and heater load.

Table 4-8. Detailed specifications on the ATG Cooler heat exchanger.

ATG Cooler brazed plate and frame heat exchanger		
	Hot	Cold
Number of channels	28	29
Number of plates	60	
Length	613 mm	
Width	186 mm	
Height	158 mm	
Weight	32.51 kg	
Heat transfer area	5.292 m^2	
Plate material	Alloy625	
Solder	Ni	
Connection type	2” NPT	
Flow set-up	Countercurrent	

This heat exchanger was selected because of the high effectiveness reported from testing by the manufacturers and Figure 4-15 shows the ATG Cooler in the actual test facility. The heat exchanger is wrapped in insulation along with all the piping leading up to/from the component to reduce the amount of heat loss while the fluids are traveling throughout the system and for safety reasons to keep anyone from being burnt by hot piping. Figure 4-16 shows the ATG Cooler before insulation was added with labels to show the inlet and outlets for the respective fluids.

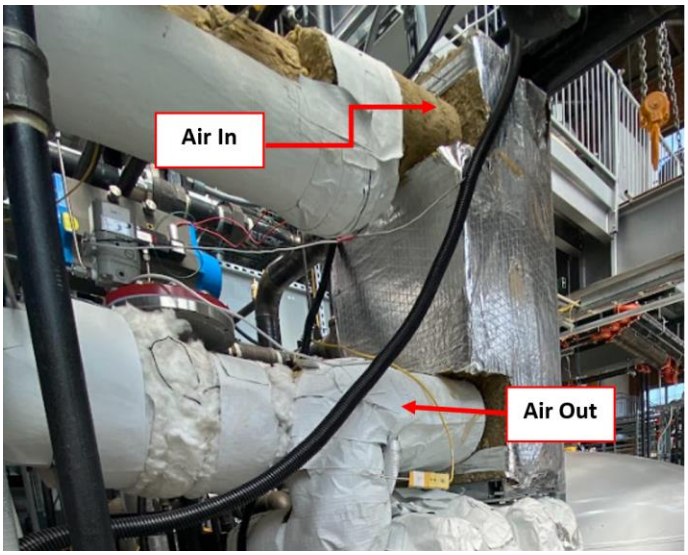

Figure 4-15. Image of the ATG Cooler installed in the facility wrapped in insulation to reduce the amount of heat loss while the fluids flow through the system.

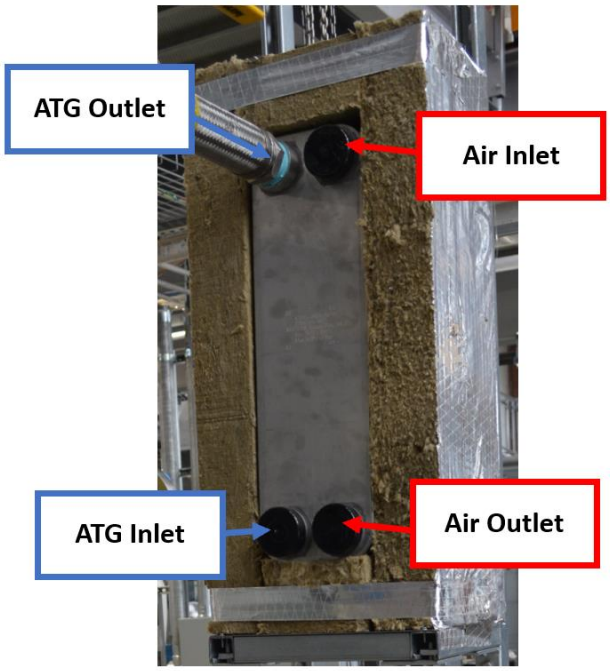

Figure 4-16. ATG Cooler without insulation with labels showing the inlet and outlet connections for the respective fluids.

4.2.5 Air Preheater Heat Exchanger

The Air Preheater does the final preheating prior to its arrival at the SOFC stacks. It achieves this by using the exhaust air coming from the cathode side of the SOFC stacks. This exhaust reaches the AP at about 612°C while the air is up to about 181.1°C due to the initial heating from the ATG Cooler. With this HX being slightly larger than the ATG Cooler it can achieve a higher effectiveness and get the air temperature of the inlet air closer to the exhaust inlet temperature. The exhaust gas leaves the preheater at about 304.4°C while the inlet air gets all the way up to 542.8°C. This AP can achieve the final heating load for the air to be conditioned properly before the SOFC stacks but there is also an inline heater available following this AP that can help to boost this inlet temperature (the temperatures outlined in this section assume that the system is running at full load where the air mass flow rate is 100 g/s at a PR of 3.2). This inline heater will

be necessary during start-up to provide the initial heating of the SOFCs before they are hot enough to generate power.

The AP is a brazed plate and frame heat exchanger (the same as the ATG Cooler) that is of a set construction due to those brazed connections. The break-down of how this component operates can be referred to above in Figure 4-14. The exact specifications of the AP are found in Table 4-8. These specifications were provided by the manufacturers of the AP and were reported with precision. Therefore, these dimensions and knowns are taken advantage of in the thermodynamic model and are essential for the heat transfer equations to solve properly and predict outlet temperatures/pressures at the SOFC inlet.

Table 4-9. Specifications on the Air Preheater heat exchanger construction.

Air Preheater brazed plate and frame heat exchanger		
	Hot	Cold
Number of channels	35	36
Number of plates	74	
Length	613 mm	
Width	186 mm	
Height	191.6 mm	
Weight	38.48 kg	
Heat transfer area	6.615 m^2	
Plate material	Alloy625	
Solder	Ni	
Connection type	2” NPT	
Flow set-up	Countercurrent	

This type of heat exchanger was selected due to the high effectiveness that it can achieve. This helps the system to consume less power and get to a higher efficiency by utilizing the heat from that exhaust air gas. The following image, Figure 4-17 shows a picture of the AP installed in the facility.

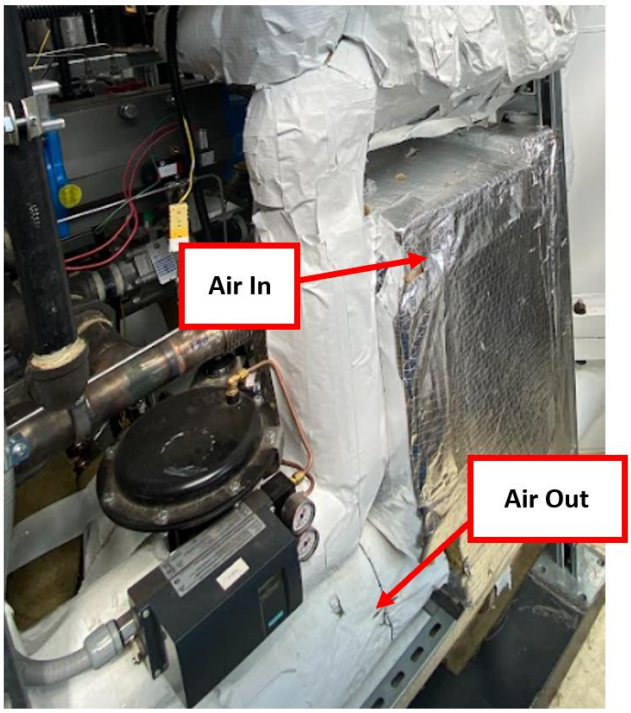

Figure 4-17. The Air Preheater heat exchanger installed in the facility.

This HX is also wrapped in insulation for the same reasoning as the ATG Cooler: to preserve as much heat as possible from being lost to ambient conditions and for the sake of safety to keep from the high temperatures impacting anyone who would work in that area. The following figure shows the HX without any insulation and labels the inlets/outlets for each respective fluid.

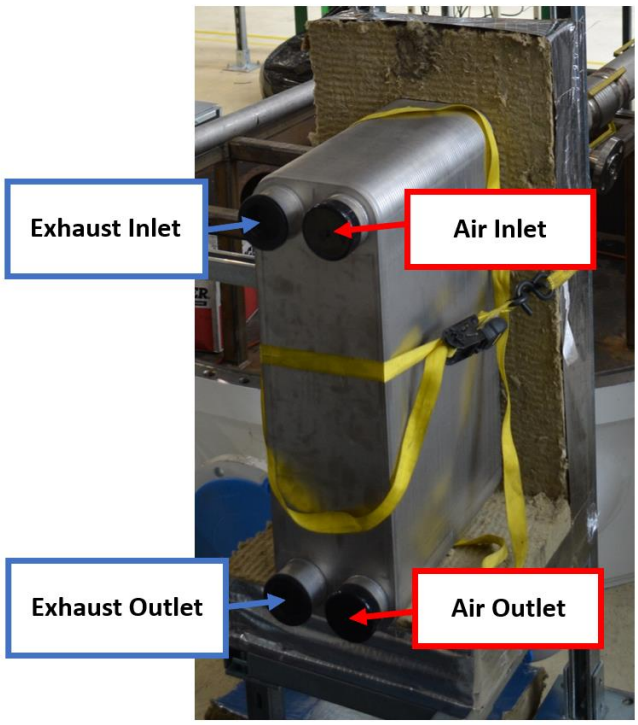

Figure 4-18. AP HX before wrapped in insulation with connections labeled for flows.

There are cases in which the preheating system of both the ATG Cooler and AP fail to get the air up to the appropriate temperature at the SOFC inlet. These scenarios are explored more in the following sections but during operation where this occurs, the inline heater that is in the system for start-up can be turned on, but this does lower the overall system efficiency.

4.2.6 Data Acquisition Equipment

Throughout the system there are data acquisition components to collect information on the air flow regarding parameters such as: temperature, pressure, and mass flow rate. There are several instrument types in the facility including thermocouples, pressure transducers, and power meters. K-type thermocouples with an associated uncertainty of ±0.75% are used for temperature readings, pressure transducers have an uncertainty of ±0.25%, and differential pressure transducers have an uncertainty of ±0.5%. The power meter that is used to measure electrical power has an uncertainty

of ±0.5%, respectively. These instruments are used for system monitoring and data analysis as well as uncertainty calculations for the test data.

Temperature and pressure readings are taken before and after the AS compressors for data analysis. The air then passes through an orifice plate where the differential pressure is measured to calculate the mass flow rate. After this process, the air flows through two heat exchangers for preheating prior to entering the SOFC. ATG, which is an exhaust gas coming off the SOFC, is used to heat the air in the ATG cooler heat exchanger. Then, air exhaust from the SOFC is used for heating the air in the AP heat exchanger. Temperature readings are taken on the inlet and outlet side of the heat exchangers to characterize their performance. However, the thermocouples are not directly at these outlets/inlets and therefore a heat loss calculation must be performed to account for the distance from the thermocouples to the outlets. Table 4-9 outlines how far these thermocouples are from the respective HXs.

Table 4-10. Distances for the thermocouples at the outlets/inlets of the HXs and the associated heat loss for each.

	AP	Heat Loss (°C)	Air Flow (g/s)
Hot Inlet	23”	-3.3	100
Hot Outlet	8”	+0.8	100
Cool Inlet	87”	-17.9	100
Cool Outlet	59”	+12.5	100

These methods of collecting data represent the results that are presented in this research. Error to account for the uncertainty of the devices is included in all the following figures. The locations of all these specific devices can be seen in Figure 4-10 in respect to the other components that are discussed in this section. For a more detailed look at the exact system make-up refer to the piping and instrumentation diagram (P&ID) in Appendix B.

4.2.7 Supporting Equipment

This section will outline details on the rest of the supporting equipment in the system including things such as: pipe size and length, filters, and valves.

Most of the piping that the air is running through in the system is carbon steel, 2” NPT connected pipe. This size was selected due to the flow requirements and lower pressure drop that is seen of pipes at this diameter. Most of the piping for the air system is wrapped in 2” thick fiberglass insulation to reduce the amount of heat loss and keep the air temperature as high as possible while traveling throughout the facility. Much of this piping was cut onsite using a pipe threader device that can cut the pipes down to the length needed and thread the ends of the pipe for connections to take place. The pipe connections are a plethora of carbon steel elbows, unions, and tees. Figure 4-19 shows a picture of most of the air BOP piping that was generated for this system.

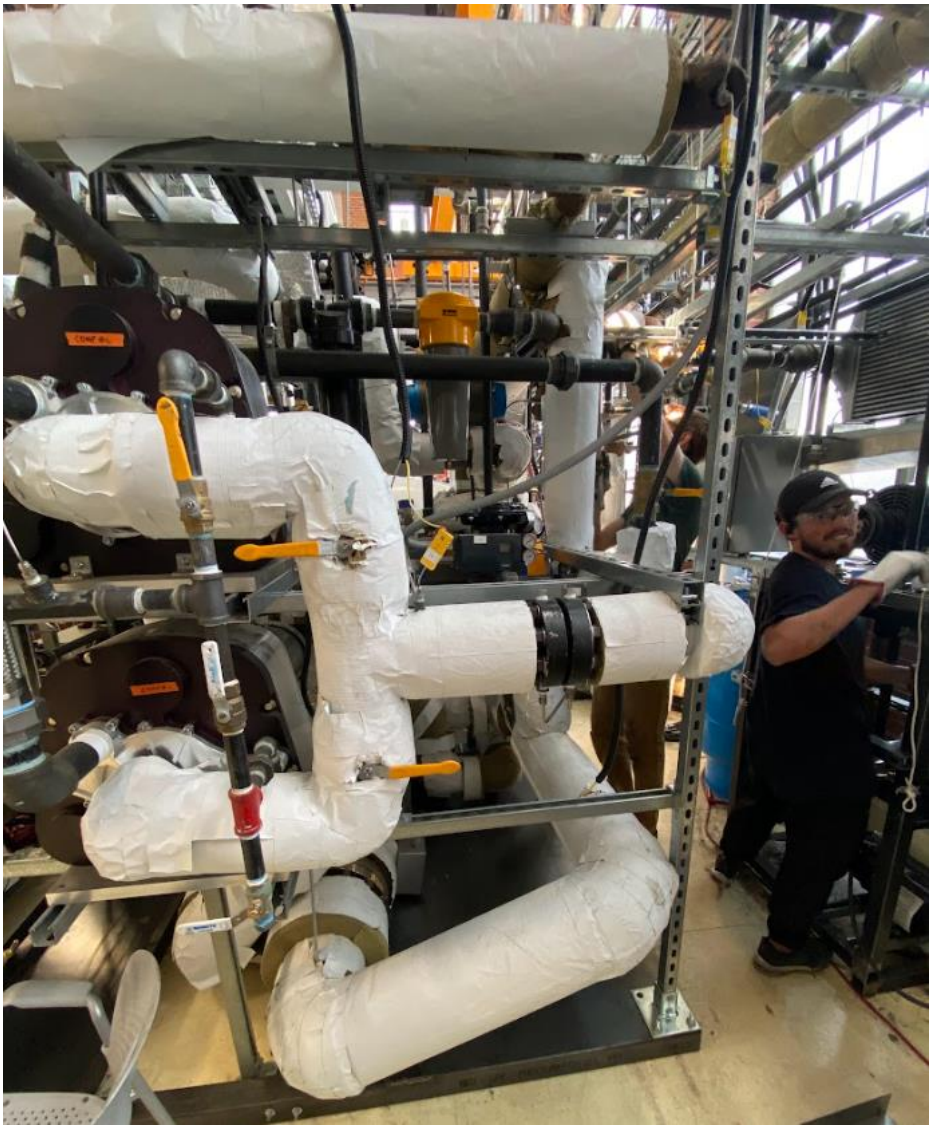

Figure 4-19. Most of the piping for the air BOP wrapped in white insulation to keep from heat loss occurring.

The system also has two distinct filters included. Prior to the air reaching the AS compressors they travel through an oil separator filter and an activated carbon filter. These devices are to ensure that an oil leakage in the sea level compressor or impurities in the piping leading to the compressor are cleaned out. The SOFC stacks are sensitive to fouling therefore these filters help to keep the air stream as pure as possible. There are more additional filters further down the

air streamline that lie between the ATG Cooler and the AP. These act as the final pass of cleaning the air before its use in power generation. However, these filters cause very high pressure drop due to their high flow coefficient and therefore there is a bypass line available for these filters. The testing results shown in this research utilized that bypass line around the second set of filters to mitigate the large pressure drop that was being seen. Below is Figure 4-20 that shows the two filters in the system prior to the AS compressors.

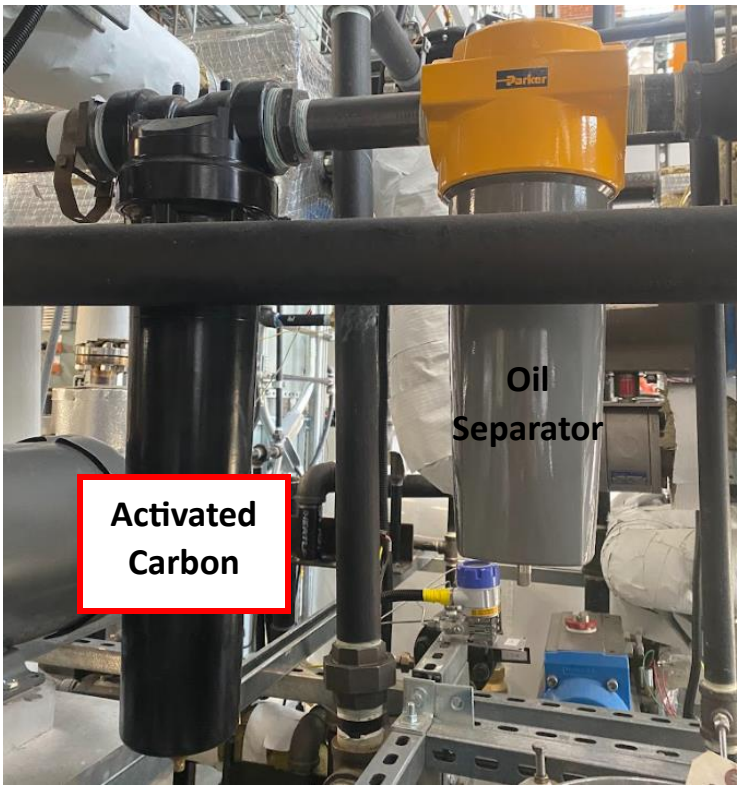

Figure 4-20. The oil separator and activated carbon air filters.

Throughout the system are multiple valves to help control the air flow within the system. For completely closing and opening section, ball valves are utilized and can be seen in Figure 4-19 as the yellow handles that are close to the AS compressors. For controlling the flow, a couple of Proportional Control Valves (PCV) are put throughout the system. These PCVs are gate type valves that can open to a proportional amount between 0%-100%. This allows the operator to

control the Cv through the valve to help build pressure in the system or constrict the amount of flow that is seen. Along with the PCVs there is also a Back Pressure Regulator (BPR) towards the end of the air system. The purpose of the BPR is to help the system build pressure as it acts as a regulator between the system pressure and ambient pressure on the exhaust line. Both the PCVs and BPR are controlled through LabView. It can take in live data and adjust the positioning of these devices based on a set pressure that the operator can specify. The controller automatically adjusts the devices to meet the set point. All these devices act as the makeup of the air BOP system and are accounted for in the modeling of the system that was discussed earlier in this research.

CHAPTER 5. RESULTS AND DISCUSSION

This section of the paper will go over the results from the modeling, testing, and resulting optimization. Validation on both the compressor and thermodynamic modeling will be shown along with the occurring results for the 3:1 turn ratio that was explored. With the modeling validated predictions can be made about the system, and these results will be discussed in detail about how the air BOP affects the overall efficiency of the SOFC-ICE system.

5.1 Compressor and HX Testing

Testing was conducted on each compressor individually to collect data to be uploaded to the GT-Suite compressor model. These scroll compressors were tested in the facility that was described in Chapter 4 which can be referred to see the system setup. PR and speed were varied to get ample enough data to generate this model.

Testing was also conducted on the AP heat exchanger to validate the thermodynamic modeling that was researched. The effectiveness of the AP was compared to that of the model at a variety of inlet temperatures for both the cool side and hot side of the HX while holding the pressures and mass flow rates constant. Capabilities to vary the inlet temperatures of the AP are possible and due to the very similar construction of the AP to the ATG Cooler, it is assumed that since the modeling is the same for both devices, if it is validated for the AP, it can be applied to the ATG Cooler.

5.1.1 Compressor Testing

The initial compressor testing was conducted by having the mass flow rate incrementally increase until the compressors reached max speed at a constant outlet pressure of 320 kPa. Figure 5-21 is a graph showing the effect of mass flow rate on efficiency. The total efficiency is the

isentropic work divided by the total measured electrical power. The isentropic efficiency is determined by correcting the air outlet temperature based on the internal cooling from the glycol.

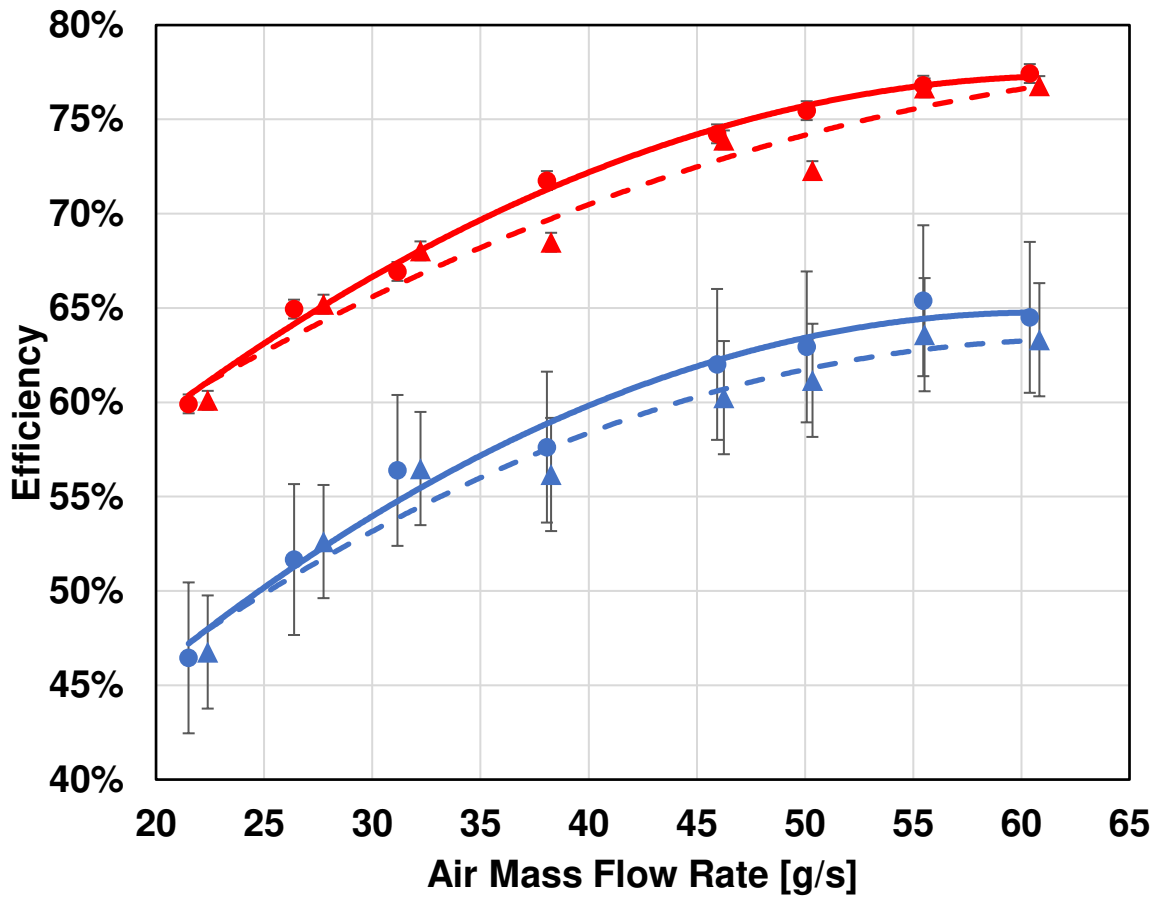

Figure 5-21. Isentropic and total efficiencies for the two AS scroll compressors.

This graph shows that there is about a 10% gap between the compressor's isentropic efficiency and total efficiency. This gap is representative of losses that are occurring within the compressors during operation and could be attributed to bearing, electrical or fluidic losses. Actions that can be taken to reduce this gap are implementing extremely precise bearings, high efficiency electrical circuits, and effective lubrication. Compressor 1 is reporting higher efficiency than compressor 2 because of better manufacturing practices leading to more efficient compression. Alignment is better between the motor and scroll device on Compressor 1 which

could be leading to less losses and the tolerances between the scroll and housing are different within the device which leads to better compression and increased isentropic and total efficiency.

Another sweep of tests was performed to collect data on the compressors at a wider range of speeds and pressure ratios to generate the compressor maps shown in Figure 5-22. Five different tests were run for each compressor where the speed was set at 1000 RPM, 1300 RPM, 1600 RPM, 1800 RPM, and 2100 RPM. While at a constant speed, the pressure ratio varied at five different points: 1.5, 2.0, 2.5, 3.0, and 3.3. These speeds were selected because they represent the lowest speed the compressors can be run at for low power output SOFC operation, and the highest speed rated for the motors that are driving the compressors. The pressure ratio increments were set to explore the range of operating points where a pressure ratio of 3.3 is the max pressure ratio that the compressors will be run at during full system operation.

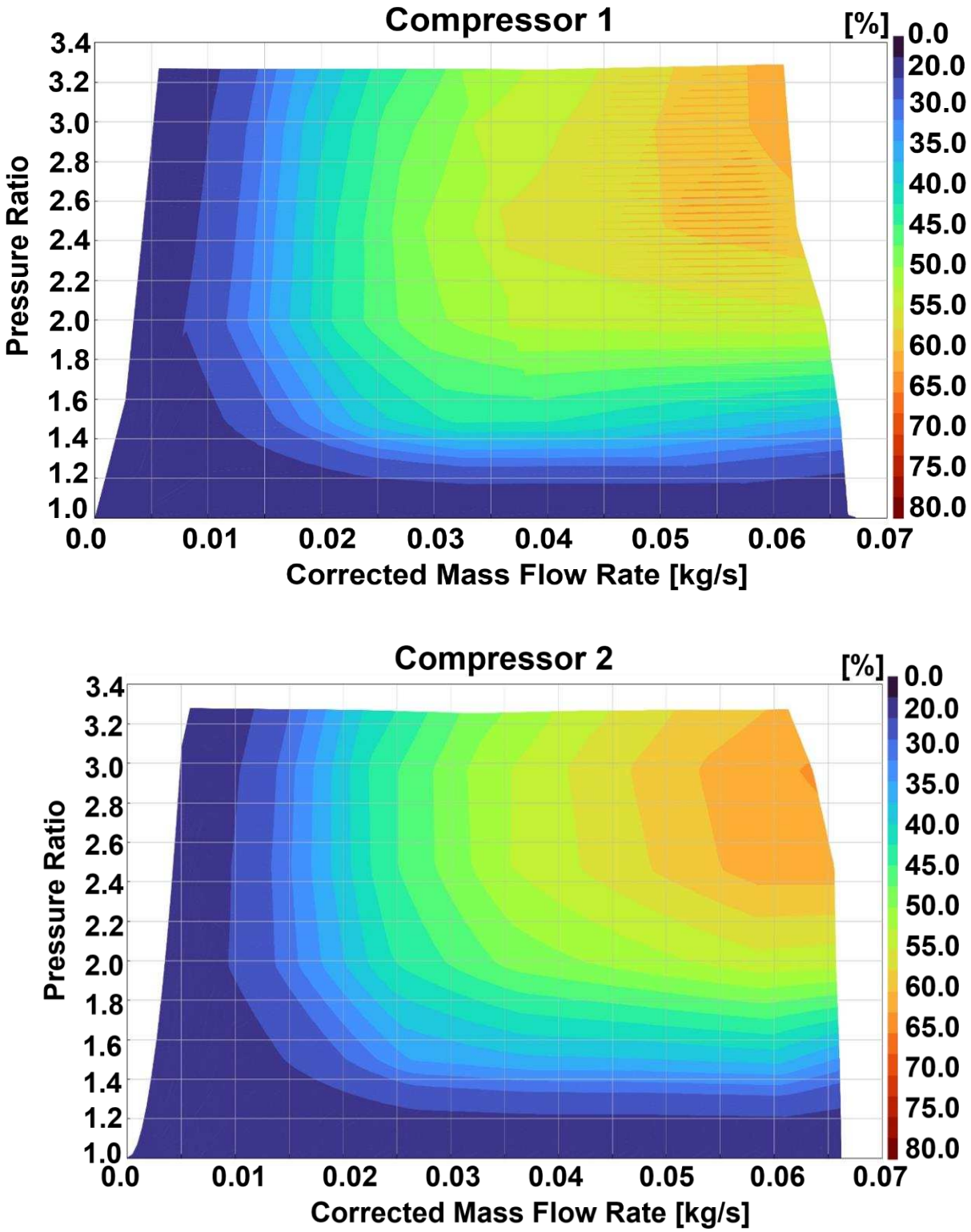

Figure 5-22. Compressor maps.

As shown in Figure 5-22, compressor 1 and compressor 2 achieve maximum efficiencies of 67.8% and 65.1%, respectively. This result is like Figure 5-21 where compressor 2 has a lower efficiency by 2.5% because of manufacturing differences between the two units. The modeling optimization discussed in Chapter 3 uses these maps to sweep through different conditions to see how to get the required PR at the least amount of power based on these maps generated. Optimization is necessary to see this tradeoff between speed, efficiency, and PR with not just the operation of one compressor but both as they have unique operation.

5.1.2 AP Testing

The AP HX was tested through utilizing the inline heater that is in the system to simulate hot exhaust that would be from the SOFC. The outlet heater temperature was varied from 300°C to 600°C to see how it affected the effectiveness of the HX. The outlet pressure of the compressors was held at 300 kPa with the mass flow rate held at 33 g/s. The glycol flow rate was held steady at 3 LPM through the compressor to hold the outlet temperature out of the compressor as consistent as possible. The operator would wait for a steady state before taking a test point. Steady state was indicated by the system temperature not changing more than 2°C over the course of a fifteen-minute span. The test points would record data for two minutes and the results shown are an average throughout this two-minute span. Figure 5-23 shows the results of this testing where the corrected data is the results of the test once corrections were made for heat loss utilizing the equations that were discussed in Chapter 3.

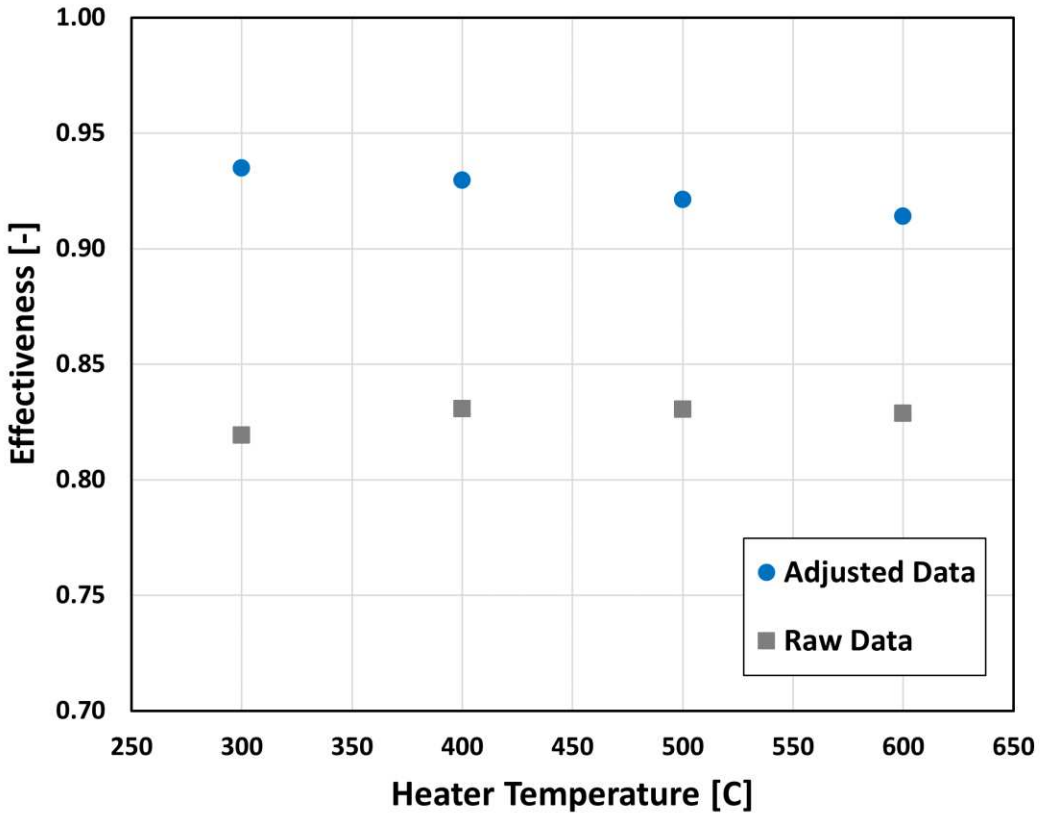

Figure 5-23. AP effectiveness at varying inlet temperatures for the hot side.

This graph shows that there is a large amount of heat loss that is affecting the system and causing the effectiveness of the HX to not be as high as they could. The thermocouple locations for the temperatures needed in this calculation are far from the AP location and thus this heat loss correction is necessary to see the true effectiveness of the AP. The effectiveness goes down slightly as higher temperatures are run through the HX and this could be caused by the larger temperature difference between the two fluids requires more HT area to stay at a higher effectiveness, which because the AP is not variable in size, a lower effectiveness is reported.

5.2 Modeling Validation

This section will outline the methods and results of the models that were generated for this research. It will go through the validation of the compressor model based on the power

consumption and outlet temperatures. Then it will show the validation of the thermodynamic modeling based on the effectiveness results from testing as compared to the actual model.

5.2.1 Compressor Modeling Validation

The validation of the compressor model required comparison between test data and model outputs for both temperature and power at speeds that are different than were used to generate the compressor models. Having sufficiently high temperatures is necessary for efficient SOFC operation; therefore, temperature was selected as a factor to be explored using modeling. Power was selected because validation of the model's capacity to predict power consumption is needed to draw conclusions on saving power. Table 11 shows the speeds and PRs that were explored for the validation of the compressor modeling.

Table 5-11. Blind testing parameters for the validation of the compressor modeling.

Speed	PR
1000	1.5, 2.0, 2.5, 3.0, 3.3
1600	1.5, 2.0, 2.5, 3.0, 3.3
2200	1.5, 2.0, 2.5, 3.0, 3.3

Pressure was not included because the pressure ratio is a set parameter and therefore it is assumed that both the actual and modeled compressors would be meeting the pressure (i.e., pressure ratio) that they are set to. The model for compressor 1 was on average within 5.25% for the predicted power and 5.23% for the outlet temperature. For compressor 2, it was on average within 3.97% for the predicted power and 3.30% for the outlet temperature. As seen in Figure 5-24, consistent overprediction of power consumption was made by the model in most operating conditions.

Error bars are included for the measured power in Figure 5-24 but is only ±0.5% and is too small to see. Meanwhile, the modeled outlet temperature was more evenly distributed. These validated compressor models were used to optimize performance over a range of conditions while

ensuring the SOFC requirements are met by using the outlet conditions from the compressor model as the inlet conditions for the thermodynamic model. The model could be off because of not considering the pressure loss in the actual system before data is collected, ambient temperature changes between test days, and intake pressure differences due to imperfect operation of the sea level compressor in maintaining 101 kPa.

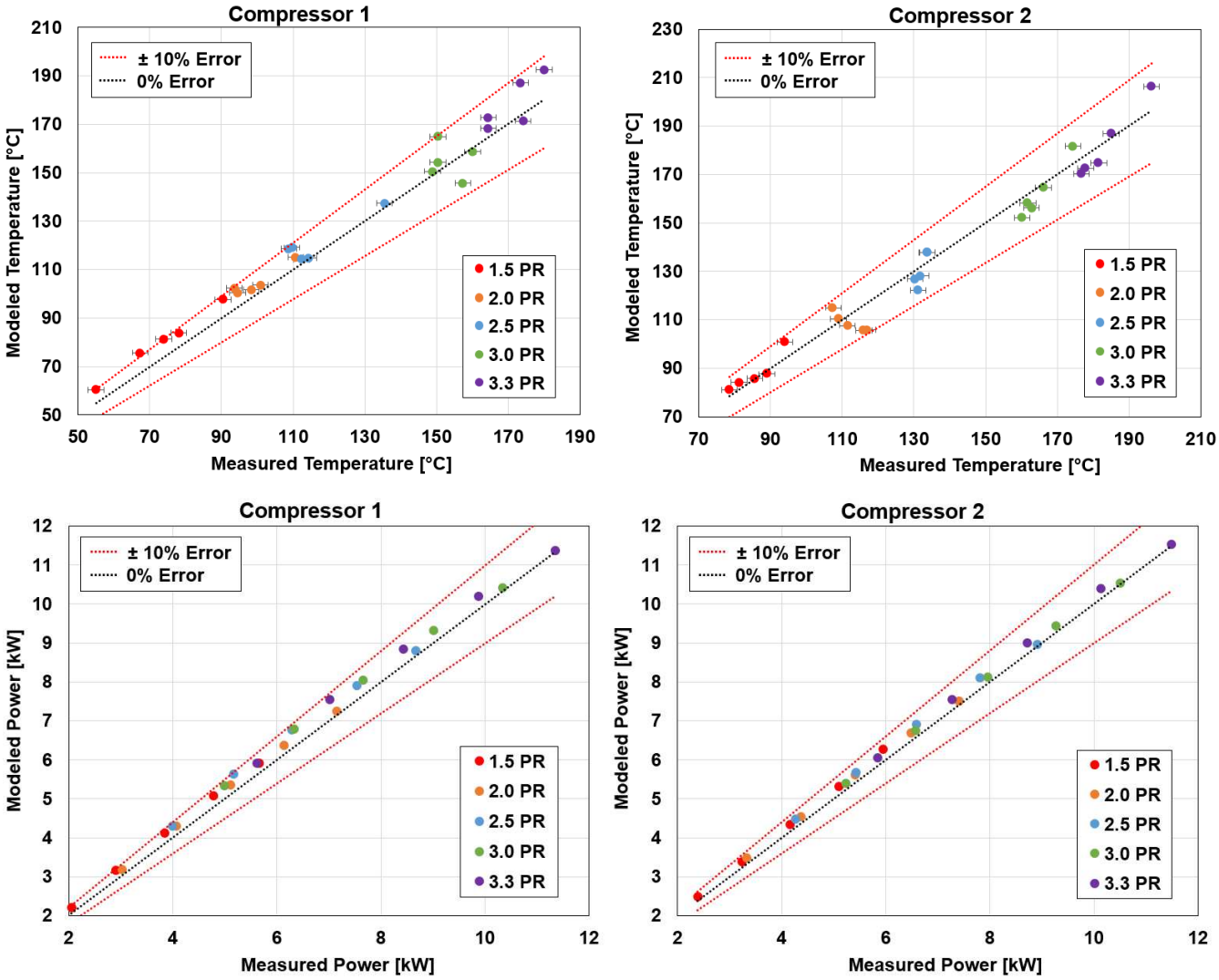

Figure 5-24. Validation graphs for modeling compressor power and outlet temperature.

5.2.2 HX Modeling Validation

To verify the accuracy of the thermodynamic model outputs, the model and experimental data were compared. To start, the temperature was compared between the actual system and the modeling system at a variety of inlet temperatures. The model had an average difference of 1.26% for the air temperature out of the AP when compared with test data and retained an average difference of 1.30% for the exhaust temperature leaving the AP.

Next, the heat exchanger effectiveness was compared between the model and test data as shown in Table 5-10. The effectiveness comparison encapsulates more details about the flow in the system and model and is therefore a parameter that was used to validate the model in terms of temperature calculation. The model consistently reported higher effectiveness than the testing but stayed within 0.362% when compared with the test data results. One reason for the higher reporting of the effectiveness from the model could be that the model does not account for contact resistance or radiation present in the heat loss. Another factor could be fouling that may be present in the physical system but is not represented in the modeling of the heat exchanger.

Table 5-12. Heat exchanger modeling shows good correlation to test data.

	Effectiveness		
Heater Temp [°C]	***Model***	***Data***	***% Difference***
300	0.954	0.935 ± 0.042	0.503% ± 1.85%
400	0.939	0.930 ± 0.041	0.241% ± 3.05%
500	0.933	0.921 ± 0.041	0.324% ± 2.69%
600	0.928	0.914 ± 0.040	0.380% ± 2.35%

5.2.3 System Modeling Validation

There are two parts of the full system model that need to be validated: the heat loss calculation for the locations of the thermocouples along with the full system pressure drop modeling.

To validate the heat loss calculation that is included in the thermodynamic model of the system, test data was compared to the model at a variety of temperatures from testing where the temperature was ramped from 300°C to 600°C while holding all other parameters constant. The heat loss from the test data is between two thermocouples that have no components between them and just piping/connections and modeled as the same setup. Figure 5-25 shows the results of this comparison where the model was on average off by 4.11% ± 1.5%.

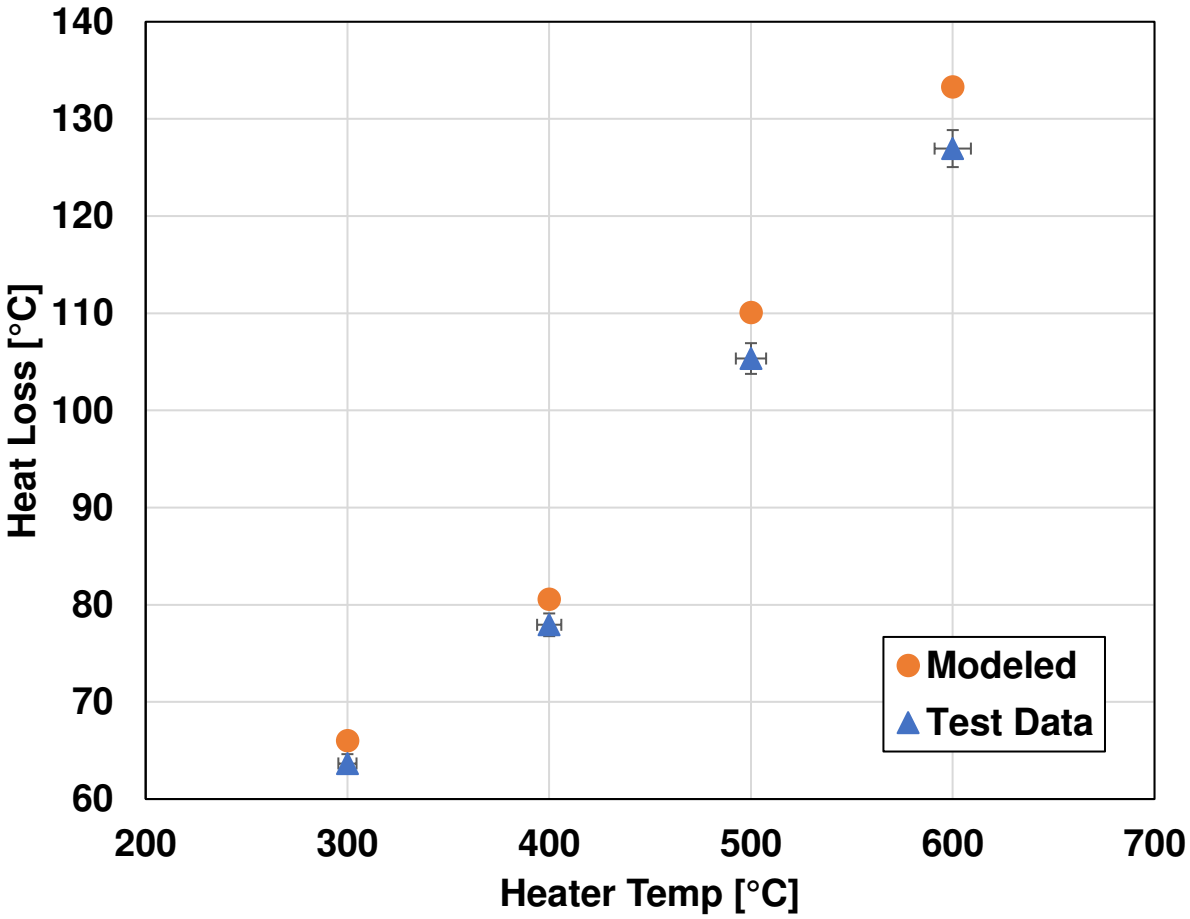

Figure 5-25. Heat loss modeling shows good correlation with test data.

To validate the pressure loss modeling for the entire system, test data was compared with the model outputs at a variety of air mass flow rates. Flow rate was selected as the independent

variable for this analysis because the pressure drop is a much stronger function of the air mass flow rate rather than the temperature of the air in the system.

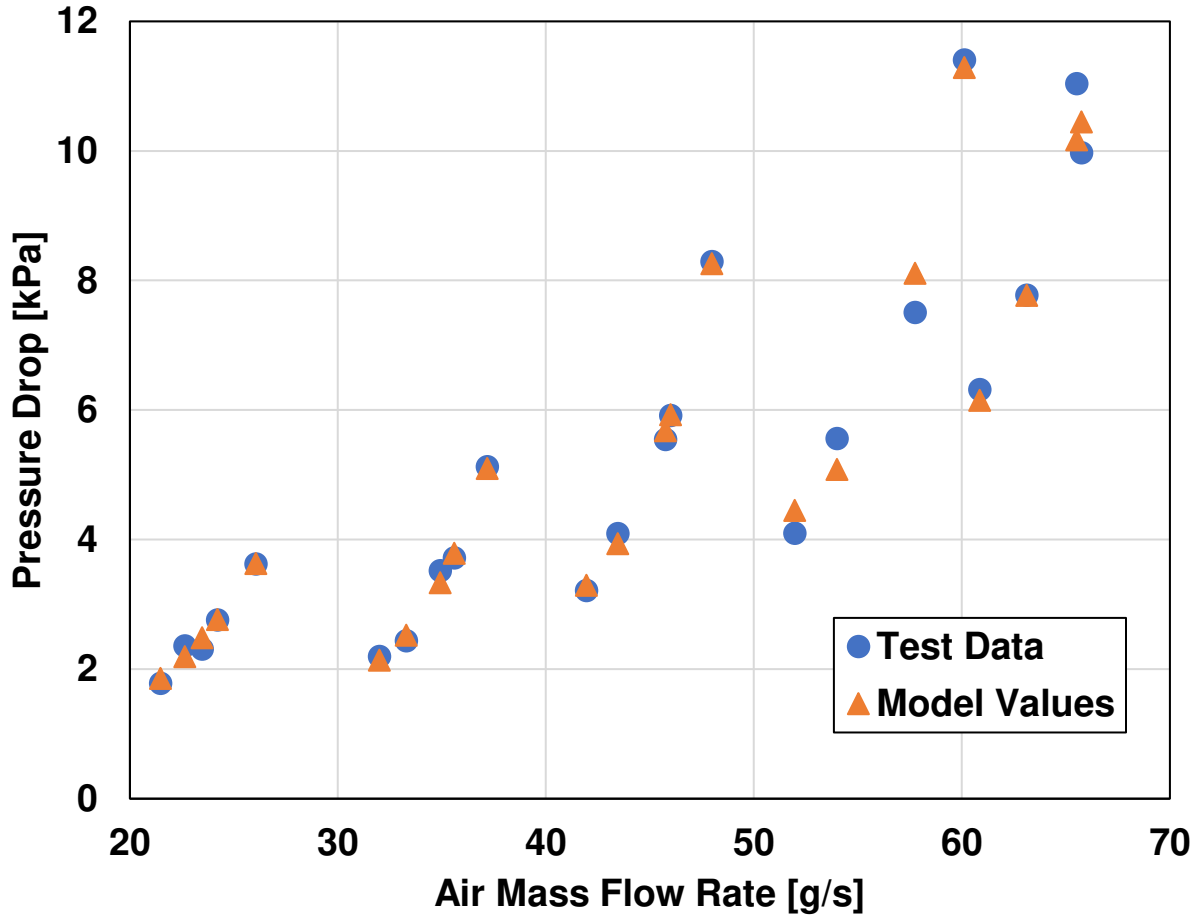

Figure 5-26. Pressure drop validation for thermodynamic modeling.

Figure 5-26 shows the results of comparing test data to the model at a variety of air mass flow rates. The pressure drop modeling had an average error of 3.73% compared with the test results (which retain error bars due to the instrumentation error but are too small to be seen in Figure 5-26) which indicates a strong correlation.

However, the modeling points at higher flow retain higher error because the more turbulent flow is less predictable, and the correlation has more uncertainty. The increasing air mass flow rate increases the Reynolds number. At 30 g s-1 a Reynolds number of 11,266 is reported versus at 50

g s-1 the Reynolds number is at 20,348. Thus, the Neagu correlation that is used, reports more error associated with at these Reynolds numbers above 15,000 [69].

5.3 Predictive Modeling

This section will review the predictive modeling that was conducted for the three cases of interest. Since a turn down ratio of 3:1 was selected, the three cases are 33 g/s, 66 g/s, and 100 g/s as these flow rates represent 33%, 66%, and 100% of full flow, respectively. These three cases are indicative of the startup process (33 g/s), part load operation for a lower class of power generation (66 g/s), and full load power generation (100 g/s).

This review will first go over the compressor predictive modeling and optimization. Then, based on the results from this modeling, the output conditions will be uploaded to the thermodynamic model to see how the temperature and pressure perform. Based on this model the results can then be used to further optimize the compressor operation and thus feed back into the thermodynamic model to see final conditions of the air at optimized operation to see if the temperature and pressure meet specification.

5.3.1 Compressor Optimization

Within the context of this research, there are two unique scroll compressors in the test facility that are available to assist with air delivery. During this research, the term “non-optimized” refers to running the compressors in parallel with an equal amount of speed and therefore air mass flow through them. For example, if the 66 g/s case was being explored, the non-optimized way of running the compressors would be running both so that compressor 1 would be delivering 33 g/s of air at the set PR and, likewise, compressor 2 would be running to also hit 33 g/s of air mass flow rate at that same set PR.

Following this, the optimized way of running the compressors utilizes the GT-Suite models that were generated and finds the most efficient way of delivering the required amount of air flow at the appropriate air mass flow rate and PR by stepping through different speeds and compressor operation.

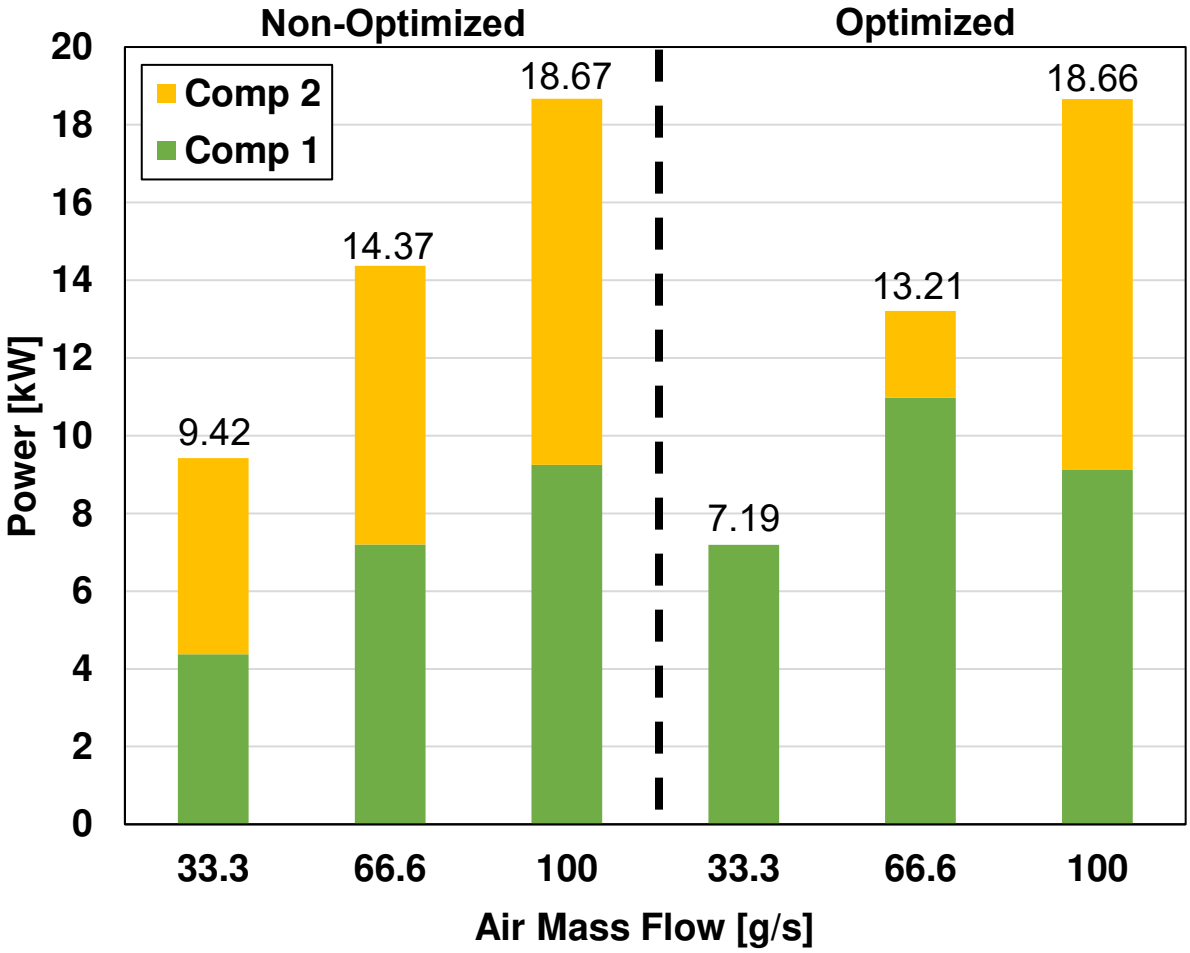

Figure 5-27. Graph showing the power saved from the compressors by running them at optimized versus non-optimized operation.

By running through different compressor speeds at each of the cases, optimized compressor operation was found to save 2.23 kW for the 33.3% case, 1.16 kW for the 66.6% case, and 0.01 kW for the 100% case. This is because the two compressors have slightly different performances over their range of operating conditions. With compressor 1 being higher efficiency, it was seen that the optimal operation runs compressor 1 at a higher load because it can pressurize more air at the same level of power consumption as compressor 2. As seen in Figure 5-27, the optimal way to run the 33.3% case is to solely run compressor 1 to take advantage of it hitting a higher efficiency island rather than having both compressors operating at a lower efficiency and therefore consuming more power. Operation within the higher cases (66.6% and 100%) requires both compressors, however, compressor 1 should take a larger load due to its higher efficiency in a wider range of flows. For case 3 there is not much room for optimization because to hit the high flow of 100 g/s, both compressors are running at full speed but there was still some room for improvement on taking advantage of the higher efficiency of compressor 1 over compressor 2. Figure 5-28 shows the results of splitting this load between the two different compressors and optimizing the operation as seen on the compressor maps.

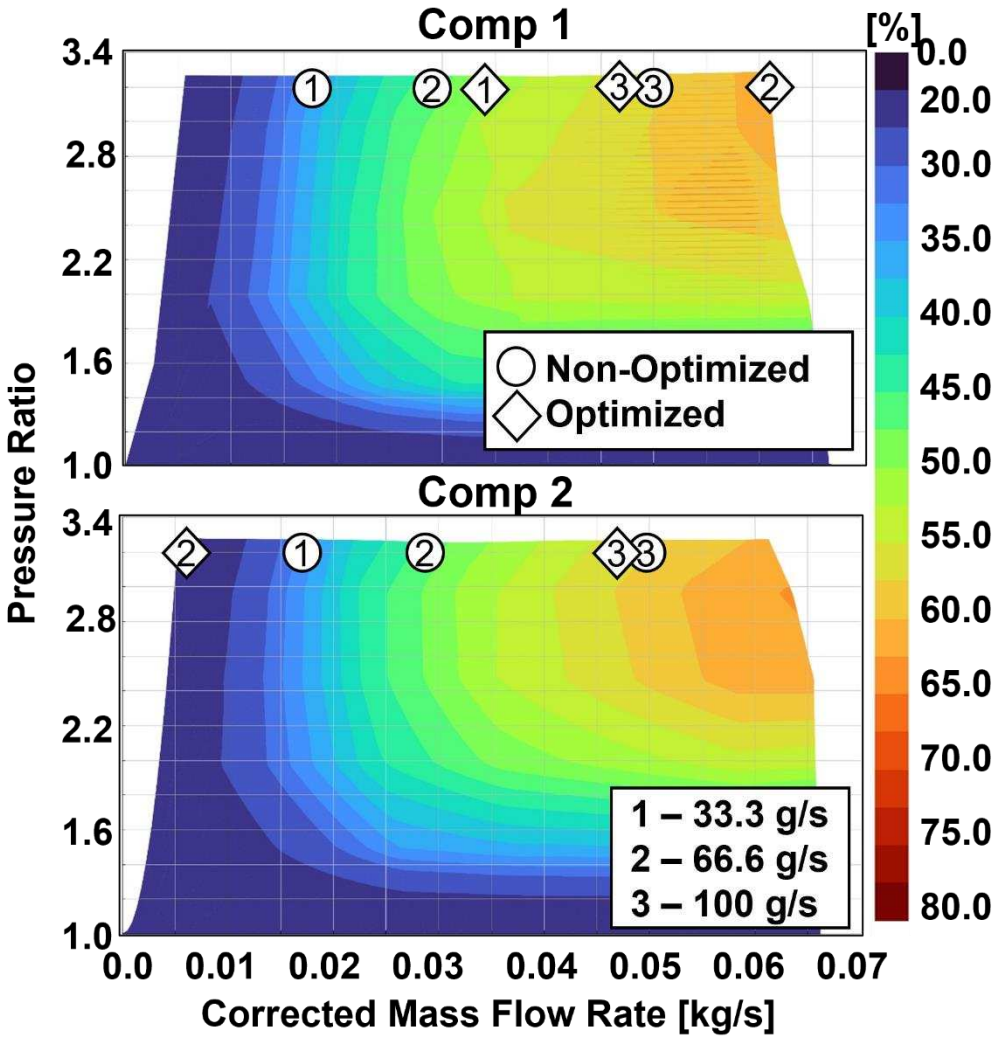

Figure 5-28. Operating points on the compressor maps for non-optimized and optimized compressor settings.

This image does not have an optimized operation point for compressor 2 at case 1 because the optimized condition for that scenario would be to just run compressor 1 for that load as it can deliver enough air flow at a much higher efficiency than running the compressors in parallel.

5.3.2 Pressure Drop Optimization

The next optimization was taking advantage of the predictive modeling of the pressure drop that will be seen in the system. Currently, the system just sets the PR at 3.2 for the compressors

but this is not necessary as the pressure drop modeling can show a more precise number for what the PR should be set at to hit 300 kPa at the SOFC inlet.

By knowing the desired outlet pressure, the operation of the compressor can be optimized. The model was then used to see the compressor power requirement to maintain 300 kPa at different flow rates. Figure 5-29 and 5-30 outlines the results of running the compressors to have an outlet pressure held at 320 kPa (or a pressure ratio of 3.2) versus running the compressors at variable outlet pressure to just ensure that the SOFC inlet meets the necessary 300 kPa based off the modeled pressure drop.

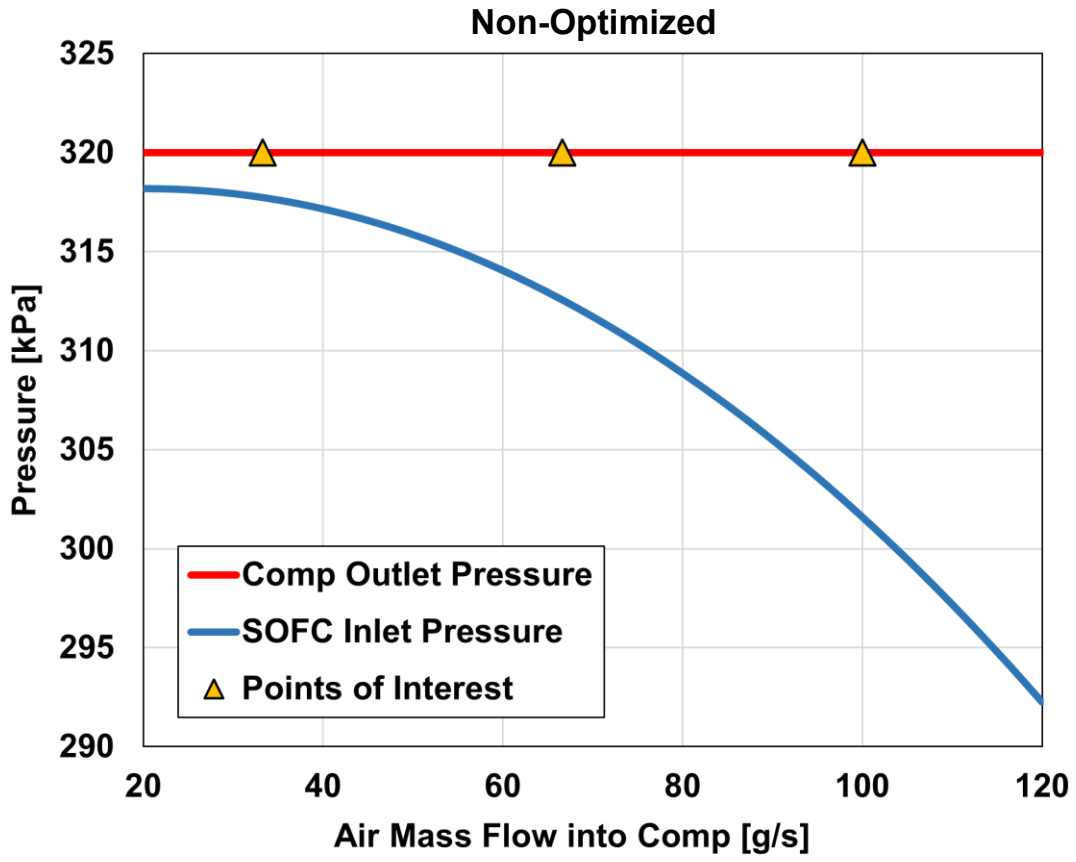

Figure 5-29. Pressure from non-optimized compressor operation.

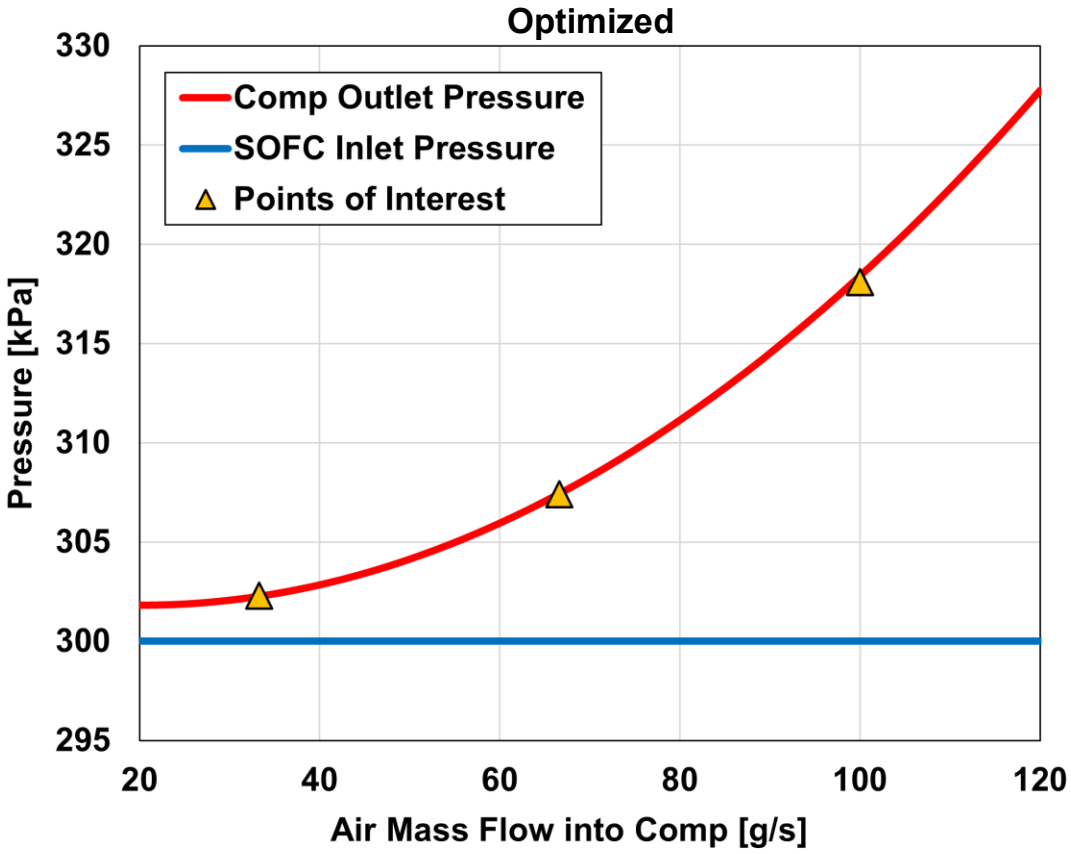

Figure 5-30. Pressure from optimized compressor operation.

An outlet pressure of 320 kPa is not necessary until flow is at about 104 g/s. Therefore, power optimization can be achieved by enabling the compressors to run dynamically according to predicted pressure drop instead of at a constant 320kPa outlet. Figure 5-31 shows the results from optimizing both the compressor speed and pressure drop. The adjusted parameters were found to save 2.67 kW for the 33.3% case (0.44 kw compared to the GT-Suite optimized operation), 1.51 kW for the 66.6% case (0.35 kw compared to the GT-Suite optimized operation), and 0.1 kW for the 100% case (0.09 kw compared to the GT-Suite optimized operation). By having the compressors operate at lower pressure ratios, less power is necessary to do the compression. More power savings is seen at the lower flows because there is a lower pressure drop and therefore the

compressors can be run at a lower pressure ratio (3.03 versus 3.2) while at the higher flow case the pressure drop is already 3.18 as compared to the original of 3.2.

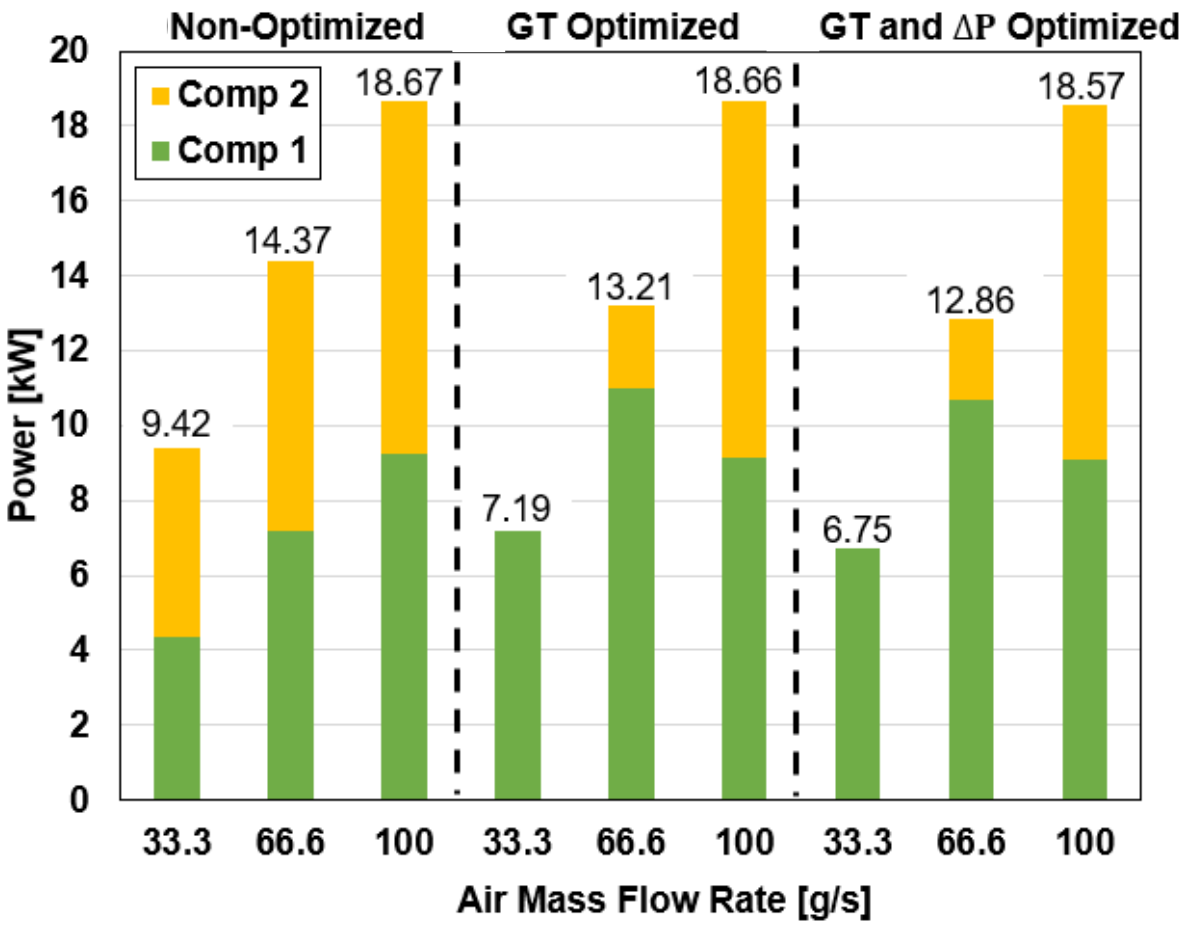

Figure 5-31. Graph showing the power saved from optimizing both the compressor operation and pressure drop predictive modeling.

These two layers of optimization help to save even more power than if the system was just to have the compressors set at a PR of 3.2 as per the original plan. Figure 5-32 shows all the operation points as they sit on the compressor performance maps. The only difference between the GT Optimized points and the GT & ΔP points are that the latter have lower PR but are at the same corrected mass flow rate line.

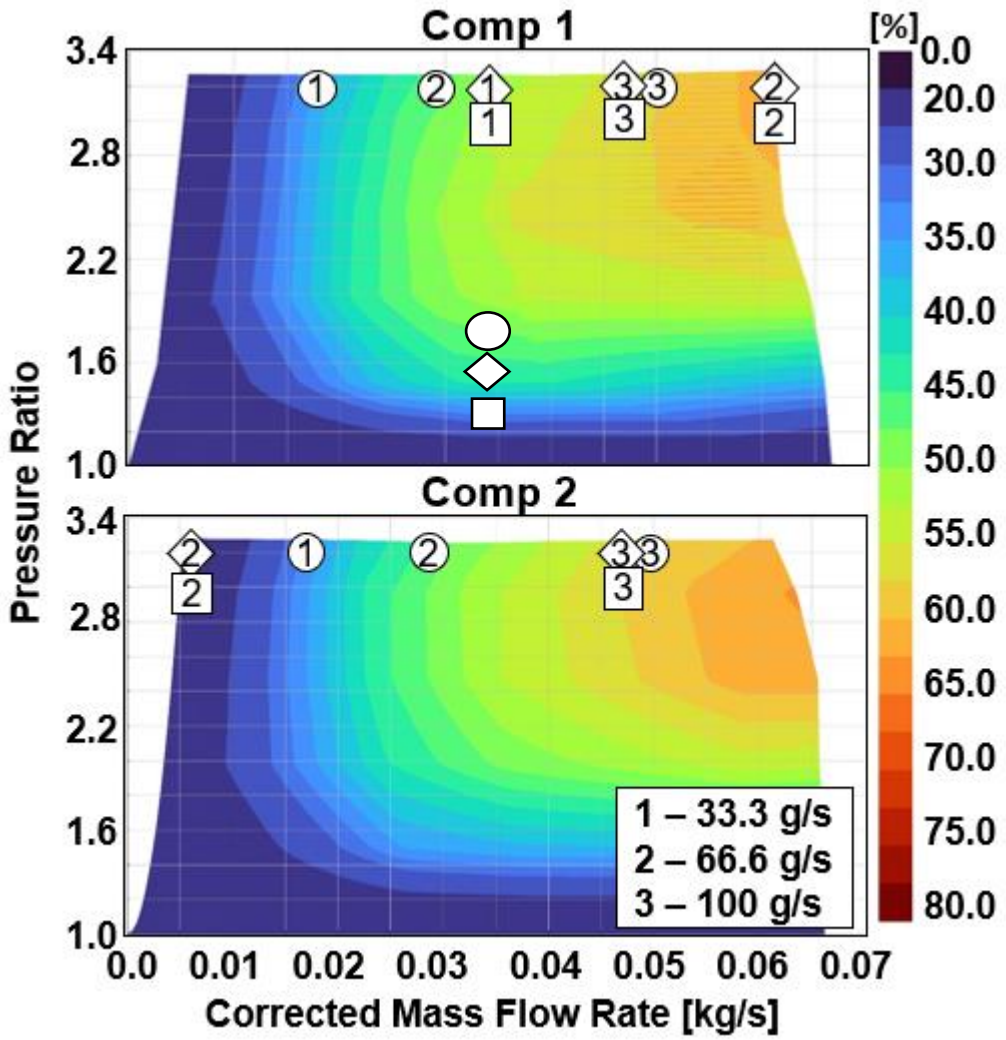

Figure 5-32. Compressor maps with state points listed for non-optimized operation, GT-optimized operation, and GT & ΔP optimized operation.

This helps to illustrate how the pressure drop optimization is more efficient because it can keep the operation on the same efficiency island but at a lower PR which will require less power and then in turn make the system more efficient.

By running at this optimized case, the overall system efficiency is improved and can be quantified based off an assumption that the cases linearly impact the amount of power output seen from the SOFC. For the 33.3% case the SOFC would produce 26.64 kW of output power. Thus, at 33.3% the previous optimization would save 2.67 kW which would in turn be a 10.02% boost in

system efficiency. This is because the lower flow rate means lower power output which in turn means that this 2.67 kW saved is a much higher ratio than if operation was at 80 kW. For the 66.6% case the optimization has a 2.38% boost in system efficiency and finally for the 100% case it can raise it by only 0.13%.

5.3.3 Temperature Modeling Results

The results to explore are how the temperature of the air varies at the SOFC inlet at these different flow rates. The thermodynamic model is utilized to see how the temperature of the air varies based on the air mass flow rate and how this will impact the overall system efficiency.

For the SOFC to operate efficiently it needs air to be delivered at an elevated temperature of at least 540°C. Figure 5-33 shows the results of that delivered air temperature based on the varying air mass flow rate. Included on this graph is a line for the air temperature out of the AP to illustrate the amount of heat loss that is present as this is the last heating element before the air reaches the SOFC. Additionally, there is a line to represent the amount of heater power that is necessary for the heater to be turned on and used to meet that SOFC inlet temperature requirement.

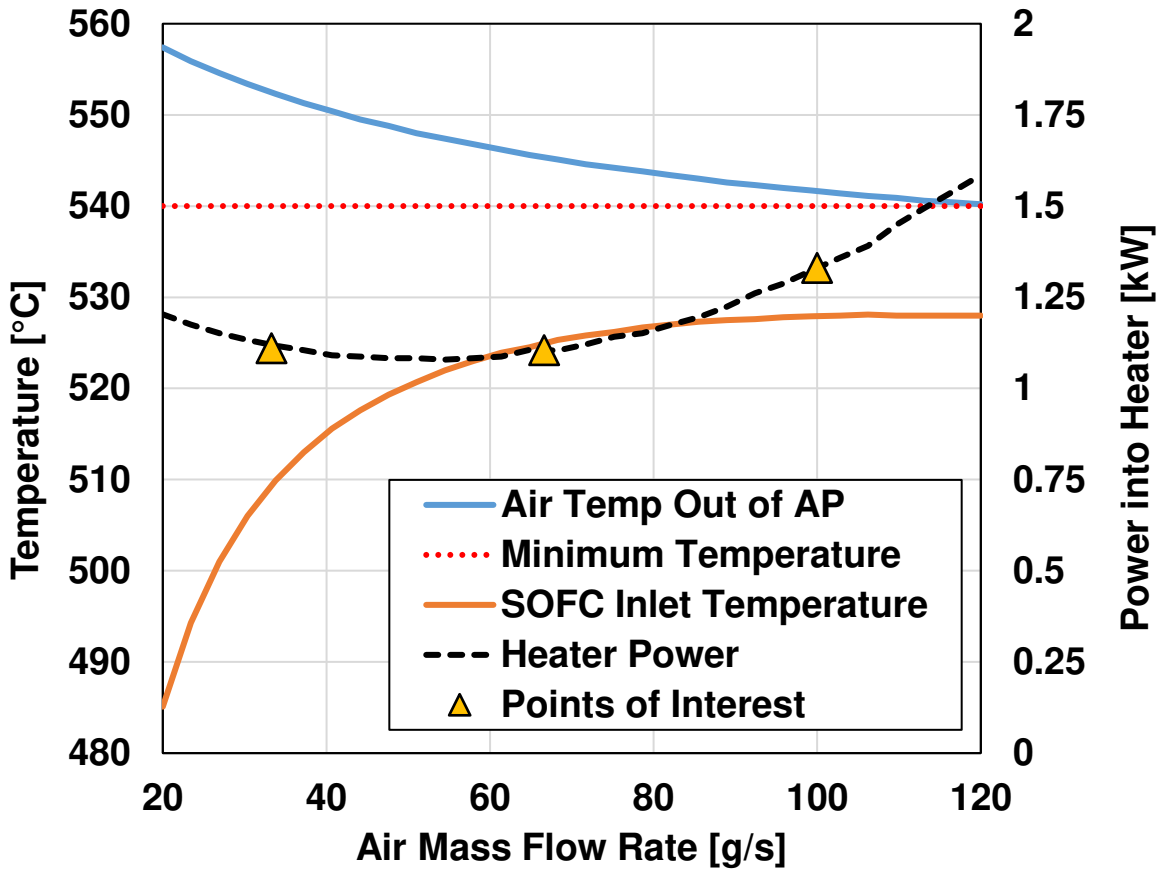

Figure 5-33. SOFC inlet air temperature at a variety of flow rates and the power into the heater needed to achieve the minimum temperature for the SOFC.

These results show that due to the high heat losses in the piping the air temperature into the SOFC never achieves the 540°C requirement despite leaving the AP above this specification. One method to increase this SOFC inlet temperature would be to operate the compressors at a lower efficiency island because this would cause the temperature out of the compressors to increase. Although this does increase the temperature slightly, about 10°C, it is not enough to meet the required temperature at the SOFC inlet and would require an additional 1.4 kW of power input. Another option to increase the compressor outlet temperature would be to decrease the glycol flow in the compressors, while still maintaining the cooling needed for the compressors to maintain clearances and maintain durability. Again, this method fails to reach the inlet temperature

requirement at the SOFC inlet. The main reason that both these methods fail is because the air mass flow rate is the dominating factor controlling the temperature.

These methods can help to increase the outlet temperature out of the compressors, but the air mass flow rate has a stronger effect on the heat transfer inside the heat exchangers. Although the air is going into these heat exchangers at a slightly higher temperature, the heat transfer that takes place is the dominating factor for increasing the air temperature, not the outlet air temperature from the compressors. Since these methods cannot meet the heating requirement, an inline heater will be used to increase the temperature above the limit. However, the use of this heater means additional power input into the system which lowers the overall efficiency due to the electrical heat load. In a nominal case where the power output from the stacks is 80 kW, this extra 1.3 kW of power for the inline heater would lower the overall system efficiency by 1.63%. This effect gets worse at lower flow conditions because the SOFC produces less power, so the inline heater power takes up a higher percentage. At 1/3 flow, the inline heater power needed for heating is 1.13 kW, but the SOFC is only producing 26.67 kW meaning that this would lower the overall system efficiency by 4.24%. The heater power has a parabolic shape due to the tradeoff between heat loss and mass flow rate. At lower flows, more power is needed because of the large gap between the inlet temperature and the minimum temperature. At higher flows, more power is needed because the flow rate is much higher, even though the gap between the inlet temperature and minimum temperature is much smaller. The points around 55 g/s have the least heater power because those points have a balance between temperature lift required and mass flow rate.

CHAPTER 6. CONCLUSIONS

The air BOP system for SOFC power generation is a vital component to allow the system to operate at high efficiency. Using novel scroll compressors and high effectiveness, compact brazed plate heat exchangers, an effective air BOP system can be developed to meet the requirements for SOFC operation.

The compressor modeling was on average off 4.61% for the power and 4.27% for the outlet temperature based on test data. The thermodynamic performance model in this study was accurate within 1.26% for the air and 1.30% for the exhaust based on results from testing. Using an optimized plan for compressor operation, on average across all three cases 1.43 kW of power can be saved to boost the overall system efficiency (assuming an output of 80 kW from the SOFC) by 1.78%. Under all flow conditions between 20% to 120% of air flow, the temperature requirement is not met but an inline electric heater will be used, which will lower the efficiency of the overall system on average (assuming a proportional output from the SOFC to the air mass flow rate) of 2.69%.

The system suffers from high amounts of heat loss due to the amount of piping that the air must travel through before being able to reach the SOFC stacks. Being able to reroute the piping to lower this amount of distance would help to keep the air temperature seen at the SOFC stacks comparable to that of the temperature seen out of the AP. Increasing the size of the HX would help but with them both already showing effectiveness above 0.90, this would not be a cost-effective solution compared to that of decreasing the distance of piping. Another change which could help is increasing the amount of insulation present in the system. Having thicker insulation would keep the air temperature in the piping to stay more consistent while it travels throughout the full system. Currently, the simplest solution is to operate the inline heater to help make up for the temperature

loss that is being seen. Although this does lower the overall system efficiency, this effect is somewhat offset by the efficiency that is saved through the optimized compressor operation and pressure drop.

6.1 Future Work

There are still some areas of this research that should be explored further to help fully encapsulate the air BOP system for SOFC power generation. There are as follows:

- The full air BOP system includes expanders to recover some power from the pressurized air exhaust leaving the SOFC stacks. A similar analysis should be conducted to that of the compressors for this system to see how the operation of these expanders will impact the system's efficiency. Upon delivery, a model can be generated from test data and added into the thermodynamic model that was built for this research. This would give a better understanding of how the air BOP performance impacts the overall system efficiency of SOFC power generation.
- Testing of the ATG Cooler HX to verify the thermodynamic modeling of it should take place. Although the model was validated through testing of AP and the ATG Cooler and AP are the same minus the AP being slightly taller, it would still be better practice to do individual testing of the ATG Cooler to validate the thermodynamic model completely. A comparison between the test data effectiveness of the ATG Cooler as compared to the model at a variety of inlet temperatures (the same testing and validation method of the AP) could take place to verify that the AP modeling aligns with the ATG Cooler modeling.
- Finally, full system testing should take place to show how the full air BOP system operates in conjunction while all the components are operating. Testing where both

compressors are operating at a PR of 3.2 with high speed, both the ATG Cooler and AP have the hot fluids to preheat the air are present, the SOFC is on and taking in the air, and having the hot and pressurize exhaust air flowing both through the AP and expanders. By having test data on the full system operation, modeling can be validated, predictive cases can be executed, and overall system efficiency can be seen without any simulation necessary. Having a full system operating is the most thorough way of validating the research presented here as well as future research that this paper recommends.

- For the full air BOP that includes the expanders some additional analysis should be conducted. A sensitivity study should be done to see the tradeoffs between: how much power can be saved running the compressors efficiently at as low a pressure as possible versus having over-pressurization to allow the expanders to recuperate more energy efficiently, how much the pressurization effects the power output/efficiency of the SOFC to see how much power can be saved either at the front end on the compressor operation or through recuperation of the expanders, and how well the expanders operate to see if initial cost of over pressurization is worth the input power because of how well the expanders recuperate that energy or if this does not help system efficiency. In tandem with this would also include some testing on the SOFC itself, does delivering a higher inlet pressure lead to a higher outlet pressure or does it stay steady regardless of the air pressure on the inlet side? Generating maps for the expanders will be necessary to see where these efficiency tradeoffs are as well as finding the sensitivity of the SOFC to these pressure changes which will likely need to be conducted through testing. Sweeping through different

inlet pressures of the air intake to the SOFC to see how it affects performance will give context on the most optimal way to run the full air BOP system.

REFERENCES

[1] Halinen M, Rautanen M, Saarinen J, Pennanen J, Pohjoranta A, Kiviaho J, et al. Performance of a 10 kW SOFC Demonstration Unit. ECS Trans 2011;35:113–20. https://doi.org/10.1149/1.3569985.

[2] Araki T, Ohba T, Takezawa S, Onda K, Sakaki Y. Cycle analysis of planar SOFC power generation with serial connection of low and high temperature SOFCs. J Power Sources 2006;158:52–9. https://doi.org/10.1016/j.jpowsour.2005.09.003.

[3] Fuel Cell Handbook (Seventh Edition). 2004.

[4] Baldi F, Wang L, Pérez-Fortes M, Maréchal F. A cogeneration system based on solid oxide and proton exchange membrane fuel cells with hybrid storage for off-grid applications. Front Energy Res 2019;6. https://doi.org/10.3389/fenrg.2018.00139.

[5] D.F. Chuahy F, Kokjohn SL. Solid oxide fuel cell and advanced combustion engine combined cycle: A pathway to 70% electrical efficiency. Appl Energy 2019;235:391–408. https://doi.org/10.1016/j.apenergy.2018.10.132.

[6] Braun RJ. High Efficiency, Low Cost & Robust Hybrid SOFC/ICE Engine Power Generator. Golden, Colorado: 2019.

[7] Choi W, Kim J, Kim Y, Song HH. Solid oxide fuel cell operation in a solid oxide fuel cell–internal combustion engine hybrid system and the design point performance of the hybrid system. Appl Energy 2019;254. https://doi.org/10.1016/j.apenergy.2019.113681.

[8] Reddy MJ, Svensson JE, Froitzheim J. Evaluating candidate materials for balance of plant components in SOFC: Oxidation and Cr evaporation properties. Corros Sci 2021;190. https://doi.org/10.1016/j.corsci.2021.109671.

[9] Park SH, Lee YD, Ahn KY. Performance analysis of an SOFC/HCCI engine hybrid system: System simulation and thermo-economic comparison. Int J Hydrogen Energy 2014;39:1799–810. https://doi.org/10.1016/j.ijhydene.2013.10.171.

[10] Blunier B, Cirrincione G, Hervé Y, Miraoui A. A new analytical and dynamical model of a scroll compressor with experimental validation. International Journal of Refrigeration 2009;32:874–91. https://doi.org/10.1016/j.ijrefrig.2008.11.009.

[11] Ji Z, Miao XY. Overall scheme design of a closed solid oxide fuel cell hybrid engine for ships. Energy Convers Manag 2024;314. https://doi.org/10.1016/j.enconman.2024.118682.

[12] Griffiths I, Wang R, Ling-Chin J, Paul Roskilly A. Solid oxide fuel cells with integrated direct air carbon capture: A techno-economic study. Energy Convers Manag 2024;315. https://doi.org/10.1016/j.enconman.2024.118739.

[13] Singh M, Zappa D, Comini E. Solid oxide fuel cell: Decade of progress, future perspectives and challenges. Int J Hydrogen Energy 2021;46:27643–74. https://doi.org/10.1016/j.ijhydene.2021.06.020.

[14] Zhang X, Chan SH, Li G, Ho HK, Li J, Feng Z. A review of integration strategies for solid oxide fuel cells. J Power Sources 2010;195:685–702. https://doi.org/10.1016/j.jpowsour.2009.07.045.

[15] Colón Rodríguez J, Harun NF, Zhou N, Sabolsky E, Tucker D. SYSTEM ANALYSIS OF A 100KW INTERNAL COMBUSTION ENGINE (ICE) SOLID OXIDE FUEL CELL (SOFC) HYBRID CONFIGURATION. 2020.

[16] Xu Z, Zhang Y, Hou S, Gao B, Gao J. Cold start control of solid oxide fuel cell-internal combustion engine system. 2021 5th CAA International Conference on Vehicular Control and Intelligence, CVCI 2021, Institute of Electrical and Electronics Engineers Inc.; 2021. https://doi.org/10.1109/CVCI54083.2021.9661170.

[17] 2008 Fuel Cell Seminar calls for papers. Fuel Cells Bulletin 2008;2008:11. https://doi.org/10.1016/S1464-2859(08)70070-1.

[18] Buonomano A, Calise F, d'Accadia MD, Palombo A, Vicidomini M. Hybrid solid oxide fuel cells-gas turbine systems for combined heat and power: A review. Appl Energy 2015;156:32–85. https://doi.org/10.1016/j.apenergy.2015.06.027.

[19] Burbank W, Witmer DD, Holcomb F. Model of a novel pressurized solid oxide fuel cell gas turbine hybrid engine. J Power Sources 2009;193:656–64. https://doi.org/10.1016/j.jpowsour.2009.04.004.

[20] Harun NF, Tucker D, Adams TA. Technical challenges in operating an SOFC in fuel flexible gas turbine hybrid systems: Coupling effects of cathode air mass flow. Appl Energy 2017;190:852–67. https://doi.org/10.1016/j.apenergy.2016.12.160.

[21] Kumar P, Singh O. A review of solid oxide fuel cell based hybrid cycles. Int J Energy Res 2022;46:8560–89. https://doi.org/10.1002/er.7766.

[22] Verda V, Calí Quaglia M. Solid oxide fuel cell systems for distributed power generation and cogeneration. Int J Hydrogen Energy 2008;33:2087–96. https://doi.org/10.1016/j.ijhydene.2008.01.046.

[23] Subhashini PVCK, Rajesh K V.D. Manufacturing method of BSCF cathode for low-temperature solid oxide fuel cell-A review. Mater Today Proc 2022. https://doi.org/10.1016/j.matpr.2022.04.653.

[24] Vichard L, Steiner NY, Zerhouni N, Hissel D. Hybrid fuel cell system degradation modeling methods: A comprehensive review. J Power Sources 2021;506. https://doi.org/10.1016/j.jpowsour.2021.230071.

[25] Williams GJ, Siddle A, Pointon K. DESIGN OPTIMISATION OF A HYBRID SOLID OXIDE FUEL CELL & GAS TURBINE POWER GENERATION SYSTEM. 2001.

[26] Chiang H-WD, Hsu C-N, Huang W-B, Lee C-H, Huang W-P, Hong W-T. Design and Performance Study of a Solid Oxide Fuel Cell and Gas Turbine Hybrid System Applied in Combined Cooling, Heating, and Power System. Journal of Energy Engineering 2012;138:205–14. https://doi.org/10.1061/(asce)ey.1943-7897.0000078.

[27] Abouemara K, Shahbaz M, Mckay G, Al-Ansari T. The review of power generation from integrated biomass gasification and solid oxide fuel cells: current status and future directions. Fuel 2024;360. https://doi.org/10.1016/j.fuel.2023.130511.

[28] Rahimipetroudi I, Omer A, Hwan Park S, Haeng Hur J, Won Lee D, Rashid K, et al. Efficient 5 kW-class solid oxide fuel cell (SOFC) hotbox design with off gas integration for power generation. Appl Therm Eng 2024;249. https://doi.org/10.1016/j.applthermaleng.2024.123459.

[29] Braun R, Floerchinger G, Wahlstrom D, Sullivan NP, Vincent T, Danforth R, et al. Development of a High-Efficiency, Low-Cost Hybrid SOFC/Internal Combustion Engine Power Generator. ECS Trans 2021;103:221–30. https://doi.org/10.1149/10301.0221ecst.

[30] Wu D, Ren H, Huang X, Ge W, Xie T, Tian Z, et al. Strengthening functional properties and competitive crystallization behavior of La2O3-BaO-CaO-Al2O3-B2O3-SiO2 glass-ceramic for solid oxide fuel cells: Agglomeration effect of rare-earth oxide. J Non Cryst Solids 2024;632. https://doi.org/10.1016/j.jnoncrysol.2024.122933.

[31] Opakhai S, Kuterbekov K, Zeinulla Z, Atamurotov F. Development and investigation of a porous metal-ceramic substrate for solid oxide fuel cells. International Journal of Thermofluids 2024;22. https://doi.org/10.1016/j.ijft.2024.100663.

[32] Sanna C, Squizzato E, Costamagna P, Holtappels P, Glisenti A. Electrochemical study of symmetrical intermediate temperature - solid oxide fuel cells based on La0.6Sr0.4MnO3 / Ce0.9Gd0.1O1.95 for operation in direct methane / air. Electrochim Acta 2022;409. https://doi.org/10.1016/j.electacta.2022.139939.

[33] Bagherisereshki E, Tran J, Lei F, AuYeung N. Investigation into SrO/SrCO3 for high temperature thermochemical energy storage. Solar Energy 2018;160:85–93. https://doi.org/10.1016/j.solener.2017.11.073.

[34] Gandiglio M, Lanzini A, Leone P, Santarelli M, Borchiellini R. Thermoeconomic analysis of large solid oxide fuel cell plants: Atmospheric vs. pressurized performance. Energy 2013;55:142–55. https://doi.org/10.1016/j.energy.2013.03.059.

[35] Lee YD, Ahn KY, Morosuk T, Tsatsaronis G. Exergetic and exergoeconomic evaluation of an SOFC-Engine hybrid power generation system. Energy 2018;145:810–22. https://doi.org/10.1016/j.energy.2017.12.102.

[36] Su Z, Yang L, Zhao N. Multi-criteria assessment of an environmentally-friendly scheme integrating solid oxide fuel cell hybrid power and renewable energy auxiliary supply. J Clean Prod 2022;369. https://doi.org/10.1016/j.jclepro.2022.133410.

[37] Liu F, Gao Y, Li J, Wei T, Ye Z, Zhang T, et al. Direct ethanol solid oxide fuel cells integrated with internal reforming for renewable power generation. Sep Purif Technol 2022;298. https://doi.org/10.1016/j.seppur.2022.121678.

[38] Calise F, Cappiello FL, Cimmino L, Dentice d'Accadia M, Vicidomini M. Renewable smart energy network: A thermoeconomic comparison between conventional lithium-ion batteries and reversible solid oxide fuel cells. Renew Energy 2023;214:74–95. https://doi.org/10.1016/j.renene.2023.05.090.

[39] Chen D, Serbin S, Washchilenko N, Burunsuz K. Parameter evaluation for a hybrid marine system combining solid oxide fuel cells and overexpanded steam-injected gas turbine. International Journal of Thermofluids 2024;21. https://doi.org/10.1016/j.ijft.2024.100565.

[40] Huang Z, You H, Chen D, Hu B, Liu C, Xiao Y, et al. Thermodynamic, economic, and environmental analyses and multi-objective optimization of a CCHP system based on solid oxide fuel cell and gas turbine hybrid power cycle. Fuel 2024;368. https://doi.org/10.1016/j.fuel.2024.131649.

[41] Welaya YMA, Mosleh M, Ammar NR. Thermodynamic analysis of a combined gas turbine power plant with a solid oxide fuel cell for marine applications. International Journal of Naval Architecture and Ocean Engineering 2013;5:529–45. https://doi.org/10.2478/IJNAOE-2013-0151.

[42] Cho M, Kim Y, Ho Song H. Solid oxide fuel cell–internal combustion engine hybrid system utilizing an internal combustion engine for anode off-gas recirculation, external reforming, and additional power generation. Appl Energy 2022;328. https://doi.org/10.1016/j.apenergy.2022.120146.

[43] Choi W, Song HH. Composition-considered Woschni heat transfer correlation: Findings from the analysis of over-expected engine heat losses in a solid oxide fuel cell–internal combustion engine hybrid system. Energy 2020;203. https://doi.org/10.1016/j.energy.2020.117851.

[44] Kim J, Kim Y, Choi W, Ahn KY, Song HH. Analysis on the operating performance of 5-kW class solid oxide fuel cell-internal combustion engine hybrid system using spark-assisted ignition. Appl Energy 2020;260. https://doi.org/10.1016/j.apenergy.2019.114231.

[45] Yuanyang Z, Liansheng L, Jiang S, Wei Z, Pengcheng S. Research on oil-free air scroll compressor with high speed in 30 kW fuel cell. n.d.

[46] Zhao Y, Li L, Wu H, Shu P. Theoretical and experimental studies of water injection scroll compressor in automotive fuel cell systems. Energy Convers Manag 2005;46:1379–92. https://doi.org/10.1016/j.enconman.2004.08.006.

[47] Braun RJ, Reznicek E, Cadigan C, Sullivan NP, Danforth R, Bandhauer TM, et al. Development of a Novel High Efficiency, Low Cost Hybrid SOFC/Internal Combustion

Engine Power Generator. ECS Trans 2019;91:355–60. https://doi.org/10.1149/09101.0355ecst.

[48] Cadigan C, Chmura C, Floerchinger G, Frankl P, Hunt S, Jensen S, et al. Performance characterization of metal-supported solid-oxide fuel cell stacks at elevated pressure. J Power Sources 2023;573. https://doi.org/10.1016/j.jpowsour.2023.233083.

[49] Wang J, Han Y, Pan S, Wang Z, Cui D, Geng M. Design and development of an oil-free double-scroll air compressor used in a PEM fuel cell system. Renew Energy 2022;199:840–51. https://doi.org/10.1016/j.renene.2022.08.154.

[50] Wang J, Song Y, Jiang X, Cui D, Qu Y. An analytical model of claw rotor profiles and working process model with the mixing process for claw vacuum pumps. Vacuum 2015;114:66–77. https://doi.org/10.1016/j.vacuum.2014.12.029.

[51] He F, Zhu F, Xu K, Xu Y, Liu D, Yang G, et al. A highly oxygen reduction reaction active and CO2 durable high-entropy cathode for solid oxide fuel cells. Appl Catal B 2024;355. https://doi.org/10.1016/j.apcatb.2024.124175.

[52] Chen Y, Fan Y, Lee S, Hackett G, Abernathy H, Gerdes K, et al. Interface and grain boundary degradation in LSM-YSZ composite Solid Oxide Fuel Cell cathodes operated in humidified air. J Power Sources 2019;438. https://doi.org/10.1016/j.jpowsour.2019.227043.

[53] Liu Y, Deng X, Huang D, Fu M, Tao Z. Manipulating cathode composition to enhance performance of proton-conducting solid oxide fuel cells through indium doping. Int J Hydrogen Energy 2024;78:363–7. https://doi.org/10.1016/j.ijhydene.2024.06.299.

[54] Blunier B, Miraoui A. Modelling of fuel cells using multi-domain VHDL-AMS language. J Power Sources 2008;177:434–50. https://doi.org/10.1016/j.jpowsour.2007.11.002.

[55] Wu B, Luo Y, Feng Y, Zhu C, Yang P. Design and thermodynamic analysis of solid oxide fuel cells–internal combustion engine combined cycle system based on Two-Stage waste heat preheating and EGR. Fuel 2023;342. https://doi.org/10.1016/j.fuel.2023.127817.

[56] Mei S, Jian J, Zhang X, Liu Y, Zhu Y, Wang S. Layout design and performance evaluation of hydrogen-fueled solid oxide fuel cell power generation system. Energy Convers Manag 2023;293. https://doi.org/10.1016/j.enconman.2023.117495.

[57] Ouyang T, Zhao Z, Wang Z, Zhang M, Liu B. A high-efficiency scheme for waste heat harvesting of solid oxide fuel cell integrated homogeneous charge compression ignition engine. Energy 2021;229. https://doi.org/10.1016/j.energy.2021.120720.

[58] Prabhakara RB, Sunden B, Das SK. An experimental and theoretical investigation of the effect of flow maldistribution on the thermal performance of plate heat exchangers. J Heat Transfer 2005;127:332–43. https://doi.org/10.1115/1.1860568.

[59] Tuo H, Hrnjak P. Effect of the header pressure drop induced flow maldistribution on the microchannel evaporator performance. International Journal of Refrigeration 2013;36:2176–86. https://doi.org/10.1016/j.ijrefrig.2013.06.002.

[60] Jafari A, Sadeghianjahromi A, Wang CC. Experimental and numerical investigation of brazed plate heat exchangers – A new approach. Appl Therm Eng 2022;200. https://doi.org/10.1016/j.applthermaleng.2021.117694.

[61] Gullapalli VS. Modeling of brazed plate heat exchangers for ORC systems. Energy Procedia, vol. 129, Elsevier Ltd; 2017, p. 443–50. https://doi.org/10.1016/j.egypro.2017.09.207.

[62] Blunier B, Pucci M, Cirrincione M, Cirrincione G, Miraoui A. A scroll compressor with a high-performance sensorless induction motor drive for the air management of a PEMFC system for automotive applications. IEEE Trans Veh Technol 2008;57:3413–27. https://doi.org/10.1109/TVT.2008.919618.

[63] Guth T, Atakan B. Semi-empirical model of a variable speed scroll compressor for R-290 with the focus on compressor efficiencies and transferability. International Journal of Refrigeration 2023;146:483–99. https://doi.org/10.1016/j.ijrefrig.2022.10.024.

[64] Qiu W, Rayasam SH, Shaver GM, Rimstidt T, Van Alstine DG, Graziano M. Modeling and Robust Coordinated Control of Turbocharged Natural Gas Engine with Genset Application. IFAC-PapersOnLine, vol. 55, Elsevier B.V.; 2022, p. 39–44. https://doi.org/10.1016/j.ifacol.2022.10.259.

[65] Dolovai P, Joergl HP, Hirzinger J. H ∞ Controller Design for Speed Control of a Natural Gas Engine. n.d.

[66] Boushehri C, Cadigan C, Chmura C, Floerchinger G, Sullivan NP, Braun RJ, et al. Experimental validation of model predictive control for solid oxide fuel cells. J Power Sources 2023;579. https://doi.org/10.1016/j.jpowsour.2023.233271.

[67] Li W, Hrnjak P. Single-phase flow distribution in plate heat exchangers: Experiments and models. International Journal of Refrigeration 2021;126:45–56. https://doi.org/10.1016/j.ijrefrig.2021.01.026.

[68] Li W, Hrnjak P. Compensating for the end-plate effect on heat transfer in brazed plate heat exchangers. International Journal of Refrigeration 2021;126:99–108. https://doi.org/10.1016/j.ijrefrig.2021.01.019.

[69] Neagu AA, Koncsag CI, Barbulescu A, Botez E. Estimation of pressure drop in gasket plate heat exchangers. Ovidius University Annals of Chemistry 2016;27:62–72. https://doi.org/10.1515/auoc-2016-0011.

[70] Dewitt DP, Bergman TL, Lavine AS, Incropera FP. Heat and MassTransfer 7th-Incropera-Dewitt n.d.

[71] Jones-Albertus B. Confronting the Duck Curve: How to Address Over-Generation of Solar Energy. Office of Energy Efficiency and Renewable Energy 2017.

[72] Mahboob S. Revisiting the mechanism of solid oxide fuel cells (SOFC's); its difficulties and probable new mechanism. vol. 12. 2023.

[73] Chinda P, Brault P. The hybrid solid oxide fuel cell (SOFC) and gas turbine (GT) systems steady state modeling. Int J Hydrogen Energy 2012;37:9237–48. https://doi.org/10.1016/j.ijhydene.2012.03.005.

[74] Zhang Q, Feng J, Wen J, Peng X, Events H/, Html Zhang / Orderlit, et al. Study on the Scroll Compressors Used in the Air and Hydrogen Cycles of FCVs by CFD Modeling. 2018.

[75] Halonen P. Brazed Vs Gasketed Heat Exchangers. Adwatec 2021.

APPENDIX A. SAMPLE CALCULATIONS

The following appendix shows sample hand calculations for validation on the EES evaluation of thermodynamic calculations, heat transfer correlations, and the test data.

A.1. Basic Flow Setting Calculations

The initial calculations show the flow setting conditions for the fluids within the heat exchanger. Parameters are set in Table A-1 for known or set values. Based off of these knowns, certain properties were calculated that were needed for the thermodynamic analysis to be solved about the amount of heat transfer present in the ATG HEX.

A.2. Heat Exchanger Thermodynamic Calculations

The following calculations represent the correlations and equations that were utilized to find the amount of heat transfer that was present in the two HEXs. Based off of values found in the preceding section and implementing researched correlations, outlet temperatures could be predicted by knowing the air mass flow rate, inlet temperatures, and size of the HEX. This sample calculation represents one section (of four) of the ATG Cooler HEX. The same calculation was ran four times for each HEX, but only one point is shown in the following sample for the sake of simplicity and brevity.

A.3. Heat Exchanger Pressure Drop Calculation

Next is a sample calculation of the method that was used to determine the amount of pressure drop that was occurring in the respective heat exchangers. Certain parameters, such as using single-phase air and Reynolds number, gave way to the researched correlation that was used to calculate this pressure drop. The sample shows the calculation for the pressure drop in the ATG Cooler, but the same calculation was ran for the AP as well.

A.4. Full System Pressure Drop Calculation

Next, the full system pressure drop was modeled based on the amount of piping, number of components, and flow path that the air was actually traveling in. Flow coefficients were found for each of the components and researched correlations were utilized based on the Reynolds number of the air in the system. This calculation shows the full method used for the system pressure drop that was found to occur.

A.5. Heat Loss Calculation

Finally, the calculation is done to show how the heat loss that was present in the system was modeled into this research. The thermocouples that were collecting data on the temperatures present were not at the direct locations that they are modeled at in methods. Therefore, a correction was calculated to see how much heat loss (or gain, depending on flow direction) was present to then be adjusted for in the calculations of things such as: efficiency, PR, and heating requirements. The following sample calculation shows a full method for a single thermocouple based on the parameters in Table A-1. This calculation changes based on things such as: air mass flow rate, distance of the thermocouple to the component, and temperature of the air in the piping.

Table A-1. Input parameters for solving.

Parameter	Value	Units
Air mass flow rate ($\dot{m}_{air}$)	100	g s^{-1}
Anode tail gas mass flow rate ($\dot{m}_{tg}$)	36	g s^{-1}
Inlet air temperature (T[1])	25	°C
Inlet air pressure (P[1])	101	kPa
Outlet compressor pressure (P[2])	320	kPa
Universal gas constant (R)	0.287	kJ kg^{-1} K^{-1}
ATG Cooler heat transfer area (ATG_{area})	5.292	m^2
Fuel temperature into ATG Cooler (T[5])	276	°C
Fuel pressure into ATG Cooler (P[5])	294	kPa
ATG Cooler width (w)	0.186	m
ATG Cooler pressing depth ($Press_{depth}$)	0.002	m
ATG Cooler length (l)	0.613	m
ATG Cooler dynamic viscosity (μ_w)	0.027	Pa s
Specific heat of fuel (Cp_{fuel})	1.701	kJ kg^{-1} K^{-1}
ATG Cooler thickness (b)	0.002	m
Pipe diameter (P_d)	0.0525018	m
Acceleration due to gravity (g)	9.81	m s^{-2}
K value for elbows (K_e)	1.5	-

K value for unions (K_u)	0.08	-
K value for ball valves (K_{bv})	0.05	-
K value for tees (K_{tee})	2.0	-
K value for control vales (K_{cv})	2.0	-
Length of piping (P_{length})	280	in
Number of elbows (N_e)	12	-
Number of unions (N_u)	4	-
Number of ball valves (N_{bv})	4	-
Number of tees (N_t)	6	-
Number of control valves (N_{cv})	2	-
Conductive heat transfer coefficient for ATG Cooler (k_{plate})	21.5	W m^{-1} K^{-1}
Correction factor (f)	2.1865	-
Anode tail gas temperature, into the ATG Cooler (T[15] and T[5])	276	°C
Air temperature, into the ATG Cooler (T[2] and T[13])	172	°C
System air temperature, within piping (T_{air})	200	°C
Ambient air temperature ($T_{ambient}$)	21.11	°C
In system pressure (P_{air})	300	kPa
Ambient air pressure ($P_{ambient}$)	84.4	kPa
Length of piping for heat loss calculation ($Length_{pipe}$)	199	in
Thickness of insulation (t_{ins})	2	in
Thickness of pipe (t_p)	0.154	in

Conductive heat transfer coefficient of pipe (k_{pipe})	22	W m^{-1} K^{-1}
Conductive heat transfer coefficient of insulation (k_{ins})	0.032	W m^{-1} K^{-1}

Table A-2. Hand calculations for validation of EES results

Parameter	Equation	Evaluated	EES Calc. Value	Hand Calc. Value	Units
Flow setting conditions					
Exhaust mass flow rate	$\dot{m}_{exhaust} = 0.9 \times \dot{m}_{air}$	$\dot{m}_{exhaust} = 0.9 \times 100$	90	90	kg s^{-1}
Compressor work	$\dot{W}_2 = \dot{m}_{air}(h_2 - h_1)$	$\dot{W}_2 = 100(438.8 - 298.4)$	14.04	14.04	kW
Compressor work, isothermal	$\dot{W}_{iso} = R \times T_{k1} \times \ln(\frac{P_2}{P_1}) \times \dot{m}_{air}$	$\dot{W}_{iso} = 0.287 \times 298.2 \ln(\frac{320}{101}) \times 100$	9.868	9.868	kW
Equivalent diameter	$D_e = 2 \times Pressing_{depth}$	$D_e = 2 \times 0.002$	0.004	0.004	m
Dynamic viscosity, air	$\mu_{air} = \nu_{air} \times \rho_{air}$	$\mu_{air} = (1.022 \times 10^{-5}) \times 2.448$	25.01	25.02	µPa s
Dynamic viscosity, anode tail gas	$\mu_{tg} = \nu_{tg} \times \rho_{tg}$	$\mu_{tg} = (1.305 \times 10^{-5}) \times 2.049$	26.73	26.74	µPa s
Reynolds number per channel, air	$Re_{ch_{air}} = \frac{\dot{m}_{air} \times D_e}{Pressing_{depth}\,(w)\,\mu_{air}}$	$Re_{ch_{air}} = \frac{0.1 \times 0.004}{0.002(0.186)25.02 \times 10^{-6}}$	42,987	42,976	-
Nusselt number, air	$Nus_{D_{air}} = 0.2913\left(Re_{ch_{air}}^{0.702}\right)\left(\frac{\mu_{air}}{\mu_w}\right)^{0.14}(Pr^{\frac{1}{3}})$	$Nus_{D_{air}} = 0.2913(42{,}976^{0.702})\left(\frac{25.02 \times 10^{-6}}{0.027}\right)^{0.14}(0.7005^{\frac{1}{3}})$	174.1	174.1	-

Convective heat transfer coefficient, air	$Nus_{D_{air}} = \frac{h_{air} \times l}{k_{air}}$	$174.1 = \frac{h_{air} \times 0.613}{0.03646}$	10.35	10.36	W K^{-1} m^{-2}
Reynolds number per channel, anode tail gas	$Re_{ch_{tg}} = \frac{\dot{m}_{tg} \times D_e}{Pressing_{depth}\,(w)\,\mu_{tg}}$	$Re_{ch_{tg}} = \frac{0.036 \times 0.004}{0.002(0.186)26.74}$	14,481	14,476	-
Nusselt number, anode tail gas	$Nus_{D_{tg}} = 0.2913\left(Re_{ch_{tg}}^{0.702}\right)\left(\frac{\mu_{tg}}{\mu_w}\right)^{0.14}(Pr^{\frac{1}{3}})$	$Nus_{D_{tg}} = 0.2913(14{,}476^{0.702})\left(\frac{26.74 \times 10^{-6}}{0.027}\right)^{0.14}(0.7005^{\frac{1}{3}})$	81.71	81.86	-
Convective heat transfer coefficient, anode tail gas	$Nus_{D_{tg}} = \frac{h_{tg} \times l}{k_{tg}}$	$81.86 = \frac{h_{tg} \times 0.613}{0.03949}$	5.294	5.291	W K^{-1} m^{-2}
Overall heat transfer coefficient, anode tail gas	$U = \frac{f}{\left[\frac{1}{h_{air}} + \frac{1}{h_{tg}} + \frac{b}{k_{plate}}\right]}$	$U = \frac{2.1865}{\left[\frac{1}{10.36} + \frac{1}{5.291} + \frac{0.02}{46.75}\right]}$	7.63	7.63	W C^{-1} m^{-2}
Heat exchanger thermodynamic analysis (one of four sections)					
Heat capacity, air	$C_{air} = \dot{m}_{air}(Cp_{air})$	$C_{air} = 0.1(1.022)$	0.1022	0.1022	kJ kg^{-1} K^{-1}
Heat capacity, anode tail gas	$C_{tg} = \dot{m}_{tg}(Cp_{tg})$	$C_{tg} = 0.036(1.701)$	0.06124	0.06123	kJ kg^{-1} K^{-1}

Heat capacity ratio, ATG Cooler	$C_r = \min[C_{air}, C_{tg}] / \max[C_{air}, C_{tg}]$	$C_r = \frac{0.06123}{0.1022}$	0.5993	0.5991	kJ kg^{-1} K^{-1}
Maximum possible HT, ATG Cooler	$q_{max} = C_{min}(T[15] - T[2])$	$q_{max} = 0.06123(276 - 172)$	1.063	1.063	kW
Number of transfer units, ATG cooler	$NTU = \frac{U \times ATG_{area}}{C_{min}}$	$NTU = \frac{.00763 \times (\frac{5.292}{4})}{0.06123}$ *Division by four for discretization	0.1649	0.1648	-
Effectiveness of HX, ATG cooler	$\varepsilon = \frac{1 - \exp[-NTU(1 - C_r)]}{1 - C_r \exp[-NTU(1 - C_r)]}$	$\varepsilon = \frac{1 - \exp[-0.1648(1 - 0.5991)]}{1 - 0.5991 \exp[-0.1648(1 - 0.5991)]}$	0.872	0.872	-
Amount of heat that was transferred	$q = q_{max} \times \varepsilon$	$q = 1.063 \times 0.872$	0.9273	0.9272	kW
Temperature calculation out of ATG cooler, air	$q = C_{air}(T[3] - T[13])$	$0.9273 = 0.1022(T[3] - 172)$	181.1	181.1	°C
Temperature calculation out of ATG cooler, anode tail gas	$q = C_{tg}(T[5] - T[16])$	$0.9272 = 0.06123(276 - T[16])$	260.9	260.8	°C
Pressure drop calculation, heat exchanger					
Friction factor for air, ATG Cooler	$f_{air} = 2.990 Re_{air}^{-0.183}$	$f_{air} = 2.990(42{,}976^{-0.183})$	0.4244	0.4244	-

Plate area calculation, ATG Cooler	$Area = b \times w$	$Area = 0.002 \times 0.186$	3.72E-4	3.72E-4	m^2
Air speed in channel, ATG Cooler	$u_{air} = \dot{m}_{air}(\frac{1}{\rho_{air}})(\frac{1}{Area})$	$u_{air} = 0.1(\frac{1}{2.217})(\frac{1}{0.000372})$	121.3	121.3	$m\ s^{-1}$
Hydraulic diameter, ATG Cooler	$D_h = \frac{4 \times l \times b}{2(l+b)}$	$D_h = \frac{4 \times 0.613 \times 0.002}{2(0.613+0.002)}$	3.987E-3	3.987E-3	m
Air pressure drop through the heat exchanger, ATG Cooler	$\Delta P_{air} = 4f_{air}(\frac{\rho_{air} \times u_{air}^2}{2})(\frac{l}{D_h})$	$\Delta P_{air} = 4(0.4244)(\frac{2.217 \times 121.3^2}{2})(\frac{0.613}{0.003987})$	3.272	3.272	kPa
Friction factor anode tail gas, ATG Cooler	$f_{tg} = 2.990 Re_{tg}^{-0.183}$	$f_{tg} = 2.990(14{,}476^{-0.183})$	0.5179	0.5179	-
Anode tail gas speed in channel, ATG Cooler	$u_{tg} = \dot{m}_{tg}(\frac{1}{\rho_{tg}})(\frac{1}{Area})$	$u_{tg} = 0.036(\frac{1}{1.67})(\frac{1}{0.000372})$	57.95	57.95	$m\ s^{-1}$
Anode tail gas pressure drop through the heat exchanger, ATG Cooler	$\Delta P_{tg} = 4f_{tg}(\frac{\rho_{tg} \times u_{tg}^2}{2})(\frac{l}{D_h})$	$\Delta P_{tg} = 4(0.5179)(\frac{1.67 \times 57.95^2}{2})(\frac{0.613}{0.003987})$	0.893	0.893	kPa

Pressure drop calculation, piping and system					
Cross sectional area, pipe	$A_p = \pi\left(\frac{P_d}{2}\right)^2$	$A_p = \pi\left(\frac{0.0525018}{2}\right)^2$	2.17E-3	2.17E-3	m^2
Major losses frictional factor, internal flow in a pipe	$f_g = \frac{64}{Re_{air}}$	$f_g = \frac{64}{42{,}976}$	1.49E-3	1.49E-3	-
Major losses, internal flow in a pipe	$h_{L_{major}} = f_g(\frac{P_{length}}{P_d})(\frac{u_{air}^2}{2g})$	$h_{L_{major}} = 0.00149(\frac{7.112}{0.0525})(\frac{121.3^2}{2 \times 9.81})$	0.1511	0.1511	m
K-value summation for pressure loss in system	$K_{tot} = (N_e k_e) + (N_u k_u) + (N_{bv} k_{bv}) + (N_t k_t) + (N_{cv} k_{cv})$	$K_{tot} = (12 \times 1.5) + (4 \times 0.08) + (4 \times 0.05) + (6 \times 2.0) + (2 \times 2.0)$	34.52	34.52	-
Minor losses calculation, full system flow	$h_{L_{minor}} = K_{tot}(\frac{u_{air}^2}{2g})$	$h_{L_{minor}} = 34.52(\frac{121.3^2}{2 \times 9.81})$	0.02587	0.02587	m
Total pressure drop from piping, full system	$\Delta P_{pipes} = (h_{L_{minor}} + h_{L_{major}})$	$\Delta P_{pipes} = (0.02587 + 0.1511)$	0.177	0.177	m

Heat loss calculation					
Outer diameter of pipe and insulation	$OD_{ins} = P_d + (2t_p) + (2t_{ins})$	$OD_{ins} = 2.067 + (2 \times 0.154) + (2 \times 2)$	6.375	6.375	in
Surface area of the pipe	$A_{s_{pipe}} = \pi P_d Length_{pipe}$	$A_{s_{pipe}} = \pi(2.067)199$	1292.2	1292.2	in
Surface area of the insulation	$A_{s_{ins}} = \pi OD_{ins} Length_{pipe}$	$A_{s_{ins}} = \pi(6.375)199$	3984.8	3984.8	in
Dynamic viscosity of air	$\mu_{air} = \rho_{air} \nu_{air}$	$\mu_{air} = 2.207 \times 0.00001827$	4.03E-5	4.03E-5	Pa s
Reynolds number of internal flow in pipe	$Re_D = (\frac{4\dot{m}_{air}}{\pi P_d \mu_{air}})$	$Re_D = (\frac{4(0.1)}{\pi(0.0525)4.03 \times 10^{-5}})$	60,160	60,160	-
Beta value calculation	$\beta = \frac{1}{T_{abs}}$	$\beta = \frac{1}{294.3}$	0.034	0.034	K^{-1}
Grashof number calculation for internal pipe flow	$Gr = \frac{g\beta(T_s - T_{ambient})OD_{ins}^3}{\nu^2}$	$Gr = \frac{9.81 \times 0.034(57 - 21.1)0.1072^3}{(1.827 \times 10^{-5})^2}$	4.43E6	4.43E6	-
Rayleigh number calculation for internal pipe flow	$Ra_D = GrPr$	$Ra_D = 4.43 \times 10^6(0.7077)$	3.138E6	3.138E6	-

Nusselt number calculation for internal pipe flow, natural convection	$Nus_D = \left[0.6 + \frac{0.387 Ra_D^{\frac{1}{6}}}{\left\{1 + \left(\frac{0.559}{Pr}\right)^{\frac{9}{16}}\right\}^{\frac{8}{27}}}\right]^2$	$Nus_D = \left[0.6 + \frac{0.387(3.138 \times 10^6)^{\frac{1}{6}}}{\left\{1 + \left(\frac{0.559}{0.7077}\right)^{\frac{9}{16}}\right\}^{\frac{8}{27}}}\right]^2$	20.13	20.13	-
Convection heat transfer coefficient, natural convection	$h_{air_{nat}} = \frac{Nus_D k_{air}}{OD_{ins}}$	$h_{air_{nat}} = \frac{20.13(0.02595)}{0.1072}$	4.872	4.872	W m^{-2} K^{-1}
Thermal resistance, conduction through pipe	$Rt_{cond_{pipe}} = \frac{t_p}{k_p A_{s_p}}$	$Rt_{cond_{pipe}} = \frac{0.003912}{22(0.8337)}$	2.13E-4	2.13E-4	K W^{-1}
Thermal resistance, conduction through insulation	$Rt_{cond_{ins}} = \frac{t_{ins}}{k_{ins} A_{s_{ins}}}$	$Rt_{cond_{ins}} = \frac{0.0254}{0.032(1.702)}$	0.4662	0.4662	K W^{-1}
Thermal resistance, natural convection on insulation	$Rt_{conv_{ins}} = \frac{1}{h_{air_{nat}} A_{s_{ins}}}$	$Rt_{conv_{ins}} = \frac{1}{4.872(1.702)}$	0.1206	0.1206	K W^{-1}
Thermal resistance, convection on pipe	$Rt_{conv_p} = \frac{1}{h_{conv} A_{s_{ins}}}$	$Rt_{conv_p} = \frac{1}{100.7(1.702)}$	0.012	0.012	K W^{-1}

Convective heat transfer coefficient, air in pipe	$h_{conv} = \frac{Nus_{conv} k_{air_{in}}}{P_d}$	$h_{conv} = \frac{138.1(0.03829)}{0.0525}$	100.7	100.7	W m^{-2} K^{-1}
Nusselt number calculation, air in pipe	$Nus_{conv} = 0.023 Re_D^{0.8} Pr^{0.3}$	$Nus_{conv} = 0.023(60{,}160)0.7077^{0.3}$	138.1	138.1	-
Equivalent thermal resistance calculation	$Rt_{eq} = Rt_{cond_{pipe}} + Rt_{cond_{ins}} + Rt_{conv_{ins}} + Rt_{conv_p}$	$Rt_{eq} = 0.000213 + 0.4662 + 0.1206 + 0.012$	0.599	0.599	K W^{-1}
Heat transfer calculation	$T_{air} - T_{ambient} = qRt_{eq}$	$200 - 21.11 = q(0.599)$	298.8	298.8	W
Temperature of surface of insulation calculation	$T_{air} - T_s = q(Rt_{conv_p} + Rt_{cond_p} + Rt_{cond_{ins}})$	$200 - T_s = 298.8(0.012 + 0.000213 + 0.4662)$	57.12	57.12	°C
Temperature at thermocouple calculation	$q = \dot{m}_{air} C_p (T_{air} - T_{tc})$	$298.8 = 0.1 \times 1.026(200 - T_{tc})$	193.3	193.3	°C

APPENDIX B. PIPING AND INSTRUMENTATION DIAGRAM

This appendix shows the piping and instrumentation diagram of the air BOP system and corresponding subsystems. These figures do not represent the full system nor are they the final version of the systems but are the P&IDs representative of the air BOP that is discussed in this paper.

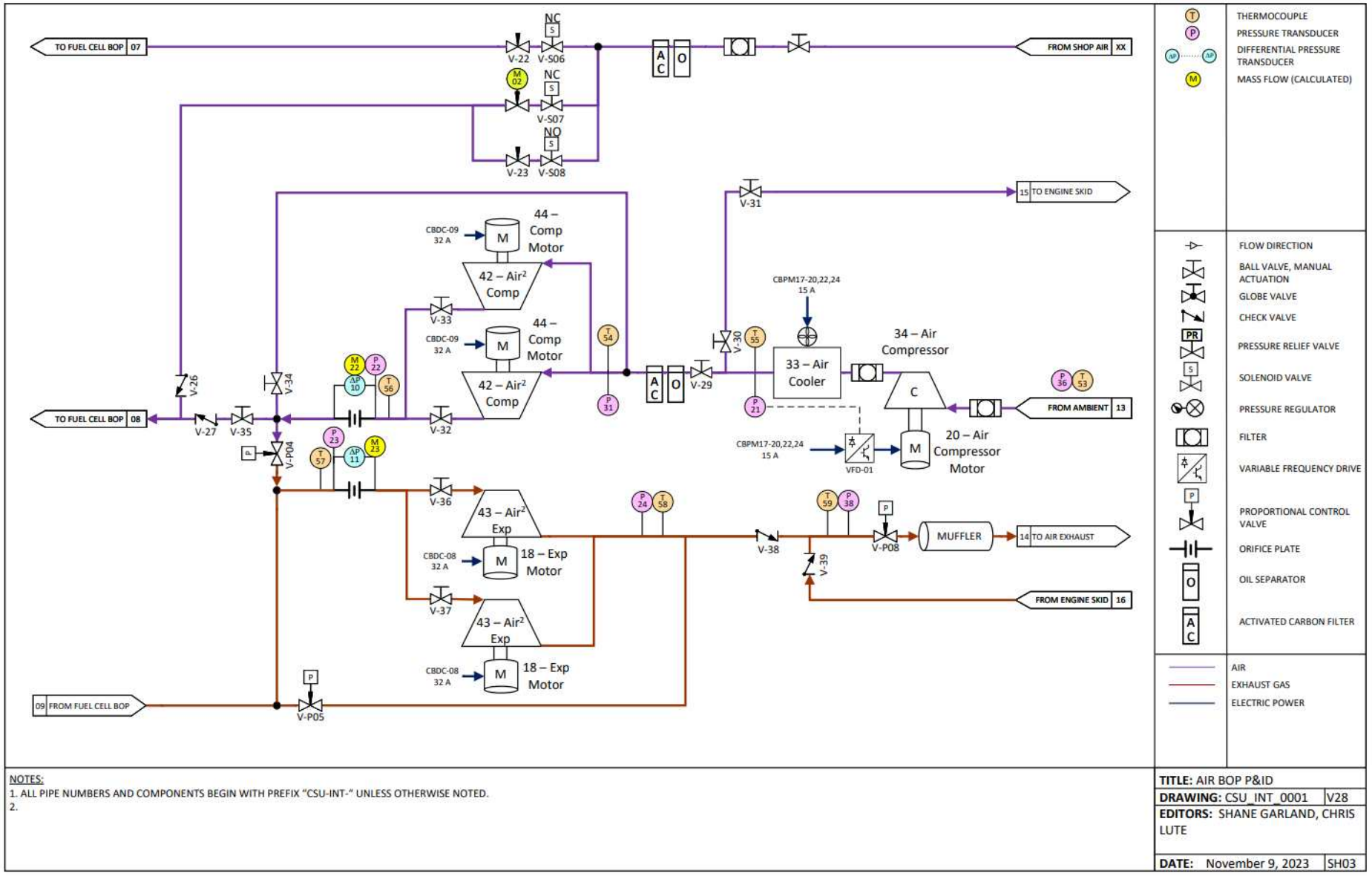

Figure B-34. Air BOP P&ID

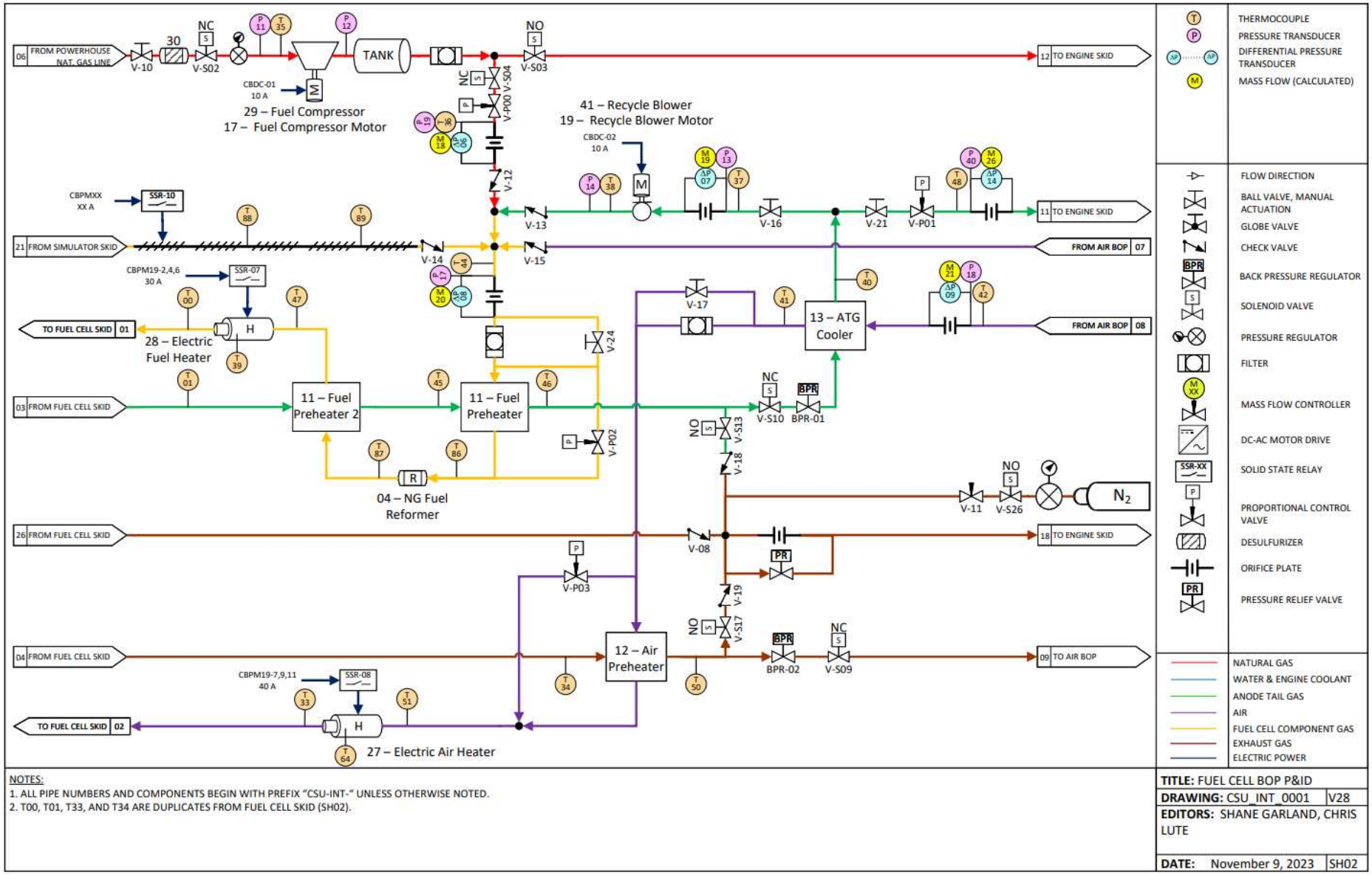

Figure B-35. Fuel Cell BOP P&ID

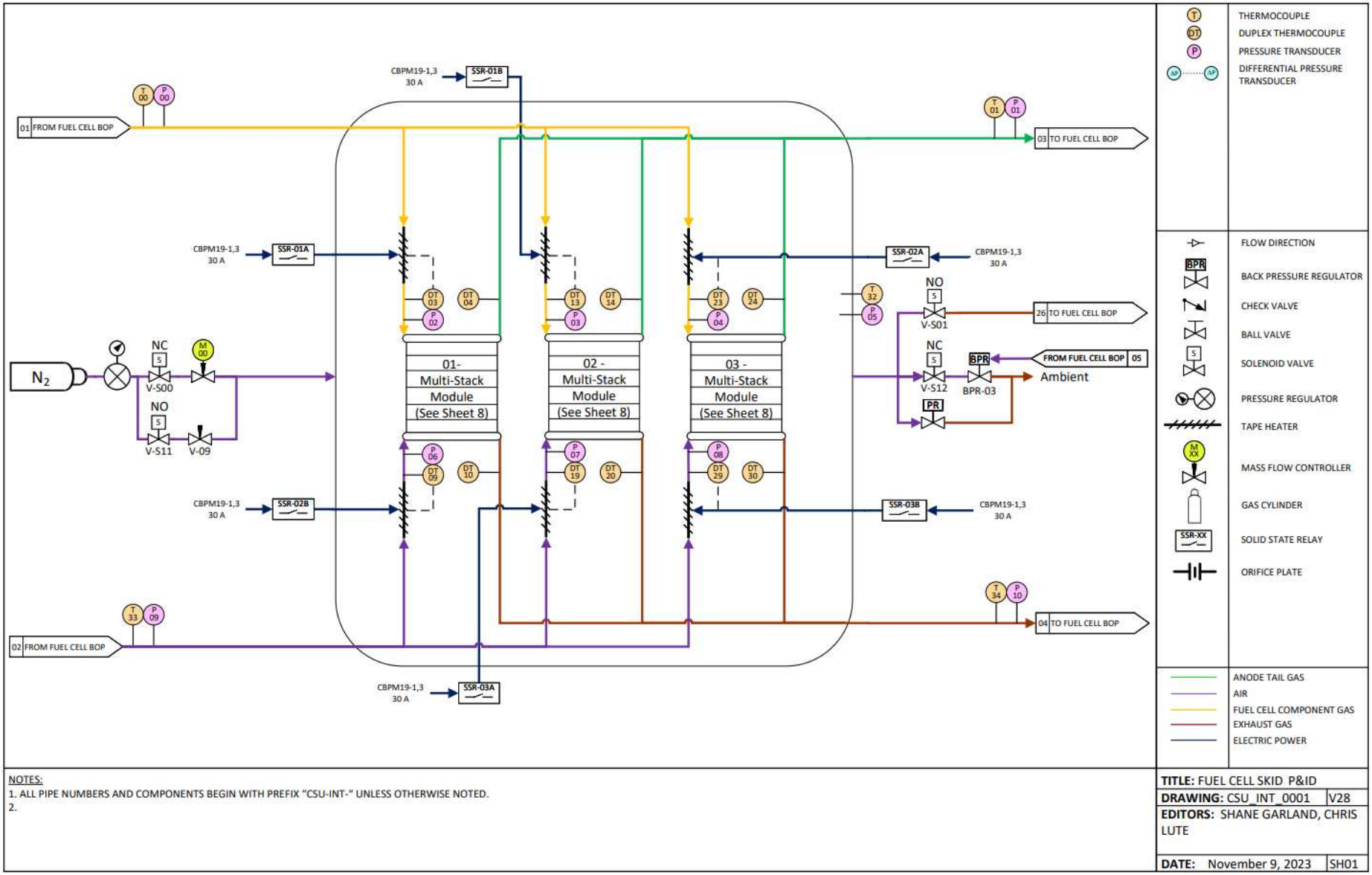

Figure B-36. Fuel Cell Skid P&ID

ABBREVIATIONS

Symbol	Description	Units
SOFC	Solid Oxide Fuel Cell	
ICE	Internal Combustion Engine	
HX	Heat Exchanger	
BOP	Balance of Plant	
GT	Gas Turbine	
GT-Suite	Gamma Technologies - Suite	
HT	Heat Transfer	
EES	Engineering Equation Solver	
ATG	Anode Tail Gas	
AP	Air Preheater	
AC	Alternating Current	
DC	Direct Current	
PEM	Proton Exchange Membrane	
PR	Pressure Ratio (Personal Record)	
BPHE	Brazed Plate and Frame Heat Exchanger	
RPM	Rotations Per Minute	
AS	Air Squared	
VFD	Variable Frequency Drive	
NPT	National Pipe Thread	
cc	Cubic Centimeters	cm^3
HP	Horsepower	
Hz	Hertz	s^{-1}
A	Amps	
P&ID	Piping and Instrumentation Diagram	
PCV	Proportional Control Valve	

BPR	Back Pressure Regulator	
LPM	Liters Per Minute	